Ragni Fjellgaard Mikalsen

Fighting flameless fires

Initiating and extinguishing self-sustained smoldering fires in wood pellets

Western Norway University of Applied Sciences

OTTO VON GUERICKE UNIVERSITÄT MAGDEBURG

RI·SE

Fighting flameless fires

Initiating and extinguishing self-sustained smoldering fires in wood pellets

Dissertation
for the award of the degree

Doktoringenieurin (Dr.-Ing.)

by   MSc Ragni Fjellgaard Mikalsen

Date of birth: 07.08.1987
in: Mo i Rana, Norway

accepted by the Faculty of Process and Systems Engineering
of the Otto-von-Guericke-University of Magdeburg

Reviewer: Prof. Dr.-Ing. habil. Ulrich Krause

                 Associate Prof. Nieves Fernandez-Anez

                 Prof. Vidar Frette

submitted on: 2. March 2018

Graduation Colloquium on: 26. June 2018

Doctoral thesis supervision by:

Main supervisor:	Prof. Dr.-Ing habil. Ulrich Krause
	Otto von Guericke University Magdeburg
Co-supervisor:	Prof. Vidar Frette
	Western Norway University of Applied Sciences
	Haugesund
Co-supervisor:	Associate Prof. Bjarne C. Hagen
	Western Norway University of Applied Sciences
	Haugesund
Co-supervisor:	Dr. Anne Steen-Hansen
	RISE Fire Research Trondheim

Abstract

Smoldering fires represent domestic, environmental and industrial hazards. This flameless form of combustion is more easily initiated than flaming, and is also more persistent and difficult to extinguish. The growing demand for non-fossil fuels has increased the use of solid biofuels such as biomass. This represents a safety challenge, as biomass self-ignition can cause smoldering fires, flaming fires or explosions.

Smoldering and extinguishment in granular biomass was studied experimentally. The set-up consisted of a cylindrical fuel container of steel with thermally insulated side walls. The container was closed at the bottom, open at the top and heated from below by a hot surface. Two types of wood pellets were used as fuel, with 0.75-1.5 kg samples.

Logistic regression was used to determine the transition region between non-smoldering and self-sustained smoldering experiments, and to determine the influence of parameters. Duration of external heating was most important for initiation of smoldering. Sample height was also significant, while the type of wood pellet was near-significant and fuel container height was not.

The susceptibility of smoldering to changes in air supply was studied. With a small gap at the bottom of the fuel bed, the increased air flow in the same direction as the initial smoldering front (forward air flow) caused a significantly more intense combustion compared to the normal set-up with opposed air flow.

Heat extraction from the combustion was studied using a water-cooled copper pipe. Challenges with direct fuel-water contact (fuel swelling, water channeling and run-off) were thus avoided. Smoldering was extinguished in 7 of 15 cases where heat extraction was in the same range as the heat production from combustion. This is the first experimental proof-of-concept of cooling as an extinguishment method for smoldering fires.

Marginal differences in heating and cooling separated smoldering from extinguished cases; the fuel bed was at a heating-cooling balance point. Lower cooling levels did not lead to extinguishment, but cooling caused more predictable smoldering, possibly delaying the most intense combustion. Also observed at the balance point were pulsating temperatures; a form of long-lived (hours), macroscopic synchronization not previously observed in smoldering fires.

For practical applications, cooling could be feasible for prevention of temperature escalation from self-heating in industrial storage units. This study provides a first step towards improved fuel storage safety for biomass.

Zusammenfassung

Schwelbrände repräsentieren Brände die eine Gefahr im häuslichen, ökologischen und industriellen Umfeld darstellen. Diese flammenlose Form eines Brandes ist leichter zu starten, stabiler im Verlauf und schwieriger zu löschen als Flammenbrände. Die wachsende Nachfrage nach nicht fossilen Brennstoffen hat die Verwendung von festen Bioenergieträgern, wie Biomasse, erhöht. Daraus resultieren neue Sicherheitsanforderungen, da die Selbstentzündung fester Biomasse einen Schwelbrand, einen Brand oder eine Explosion verursachen kann.

Schwelen und Löschen von granularer Biomasse wurde experimentell untersucht. Der experimentelle Aufbau bestand aus einem zylindrischen Brennstoffbehälter aus Stahl mit wärmeisolierten Seitenwänden. Der Behälter wurde unten geschlossen, oben offen gelassen und von unten durch eine heiße Oberfläche erhitzt. Als Brennstoff wurden zwei Arten von Holzpellets, in Proben von 0,75 kg bis 1,5 kg, verwendet.

Um den Übergang von nicht Schwelen zu selbständigem Schwelen und die beeinflussenden Parameter zu bestimmen, wurde logistische Regression verwendet. Um Schwelbrand zu erzeugen, war die Dauer der externen Erwärmung am wichtigsten. Die Probenhöhe war ebenfalls signifikant, während die Art der Holzpellets nahezu signifikant war, wobei die Höhe des Brennstoffbehälters nicht signifikant war.

Die Anfälligkeit des Schwelens gegenüber Änderungen der Luftzufuhr wurde untersucht. Mit einem kleinen Spalt am Boden des Behälters, ergab der erhöhte Luftstrom in der gleichen Richtung wie die anfängliche Schwelbrandfront (Vorwärtsluftstrom) eine signifikant intensivere Verbrennung im Vergleich zu der normalen Anordnung mit Rückwärtsluftstrom.

Die Wärmeentnahme aus der Verbrennung wurde mithilfe eines wassergekühlten Kupferrohres untersucht. Dadurch wurden Probleme in Verbindung mit direktem Brennstoff-Wasser-Kontakt (Aufquellen des Brennstoffes, Wasserkanalisierung und -abfluss) vermieden. Der Schwelbrand wurde in 7 von 15 Fällen gelöscht, wobei die Menge des Wärmeverlustes durch die Kühleinheit und die Wärmeerzeugung durch die Verbrennung im gleichen Größenbereich lagen. Dies ist der erste "Proof-of-concept" der sich mit Kühlen als Löschmethode bei Schwelbränden beschäftigt.

Geringfügige Unterschiede in der Erwärmung und Abkühlung führten zu Schwelbränden oder gelöschten Schwelbränden und zeigten das Brennstoffbett im Gleichgewicht zwischen Erhitzen und Kühlen. Niedrigere Abkühlungsniveaus führten nicht zum Erlöschen, aber das Kühlen führte zu einem vorhersagbareren Schwelen und verzögerte möglicherweise die intensivste Verbrennung. An diesem Gleichgewichtspunkt wurden pulsierende Temperaturen beobachtet; eine Form von lan-

glebiger (Stunden), makroskopischer Synchronisation, die bisher bei Schwelbränden nicht beobachtet wurde.

Denkbar als praktische Anwendung wäre eine Kühlung in industriellen Lagereinheiten zur Verhinderung einer Temperaturerhöhung durch Selbsterwärmung. Diese Studie ist ein erster Schritt in Richtung Verbesserung der Lagersicherheit von Biomasse in industriellen Lagereinheiten.

List of symbols

α		Probability function slope parameter for logistic regression
A_A	s^{-1}	Pre-exponential factor of 1.order reaction
A_{alu}	m^2	Area of 4 sides of the aluminum plate and top and bottom subtracted cylinder area
$A_{\mathrm{c,o}}$	m^2	Area of cylinder opening
$A_{\mathrm{L_1}}$	m^2	Area of the outside of the lower part of the insulated cylinder, which contains the sample
$A_{\mathrm{L_2}}$	m^2	Area of the outside of the upper part of the insulated cylinder, which contains air
$C_{\mathrm{p,air}}$	J/gK	Specific heat capacity of air
$C_{\mathrm{p,alu}}$	J/gK	Specific heat capacity of aluminum
$C_{\mathrm{p,s}}$	J/gK	Specific heat capacity of sample
$C_{\mathrm{p,w}}$	J/gK	Specific heat capacity of water
ϵ_{alu}		Emissivity of aluminum plate
$\epsilon_{\mathrm{c,o}}$		Emissivity of cylinder opening
ϵ_{surr}		Emissivity of surroundings
ϵ_{wall}		Emissivity of outside of insulated walls (clad with aluminum foil)
h_{silo}	m	Height of silo
h_{air}	W/m^{2}K	Convective heat transfer coefficient for air
H_{c}	MJ/kg	Effective heat of combustion
k_{alu}	W/mK	Thermal conductivity of aluminum
k_{ins}	W/mK	Thermal conductivity of insulation
k_{fuel}	W/mK	Thermal conductivity of wood pellets
L_{alu}	m	Shortest length from center to edge of aluminum plate
L_1	m	Height of sample in the cylinder
L_2	m	Height of cylinder above sample
$\dot{m}_{\mathrm{air}}$	g/s	Mass flow rate of air out of cylinder
m_{alu}	g	Mass of aluminum plate
m_{s}	g	Mass of sample
$\dot{m}_{\mathrm{s}}$	kg/s	Mass loss rate of sample
$\dot{m}_{\mathrm{w}}$	g/s	Water flow through cooling unit
ν_{air}	m/s	Velocity of air flow
p_{10}		Probability of smoldering 10%
p_{50}		Probability of smoldering 50%
p_{90}		Probability of smoldering 90%

p		Statistical significance level
ΔP_{air}	Pa	Air flow pressure of upward airflow
P_{amb}	Pa	Ambient pressure
P_{w}	bar	Water pressure
$\dot{q}_{\text{air}}$	W	Heat loss to air above sample
$\dot{q}_{\text{alu}}$	W	Heat loss through aluminum plate
$\dot{q}_{\text{cool}}$	W	Heat loss due to water cooling
$\dot{q}_{\text{prod}}$	W	Heat production from combustion processes in sample
$\dot{q}_{\text{heater}}$	W	Heat input from electric heater to system
$\dot{q}_{\text{L}_1}$	W	Heat loss from sample through insulated walls
$\dot{q}_{\text{L}_2}$	W	Heat loss from air above sample through insulated walls
$\dot{q}_{\text{rad}}$	W	Heat loss, sum of all radiative heat losses
$\dot{q}_{\text{rad,alu}}$	W	Heat loss from exposed areas of the aluminum plate to the surroundings (radiative)
$\dot{q}_{\text{rad,c,o}}$	W	Heat loss from cylinder opening to surroundings (radiative)
$\dot{q}_{\text{rad,L}_1}$	W	Heat loss from lower part of the outside of cylinder (radiative)
$\dot{q}_{\text{rad,L}_2}$	W	Heat loss from upper part of the outside of cylinder (radiative)
$\dot{q}_{\text{rad,surr}}$	W	Heat transfer from the surroundings to system (radiative)
$\dot{q}_{\text{st,alu}}$	W	Heat storage in aluminum plate
$\dot{q}_{\text{st,s}}$	W	Heat storage in sample
R	J/molK	Gas constant
r_{I}	m	Radius of cooling pipe in silo
r_{II}	m	Half silo radius
r_1	m	Inner radius of cylinder without insulation
r_2	m	Outer radius of cylinder without insulation
r_3	m	Outer radius of cylinder with insulation
ρ_{air}	kg/m^3	Density of air, temperature dependent
R_{gas}	J/kgK	Specific gas constant, dry air
σ	J/m^2sK^4	Stefan-Boltzman constant
T		Temperature
T_{air}	°C	Air temperature average over positions 120, 140, 330 mm (above sample, within cylinder)
T_{amb}	°C	Ambient temperature in laboratory

$T_{c,o}$	°C	Air temperature in cylinder opening (at 330 mm)
T_{fuel}	°C	Fuel temperature
t_i	s	Time during an experiment
t_{i+1}	s	Time during an experiment, one time interval after t_i
T_{IN}	°C	Water temperature into cooling unit
T_{OUT}	°C	Water temperature out of cooling unit
T_s	°C	Sample temperature, avg over positions 20-100 mm
T_{s,t_i}	°C	Sample temperature at time t_i
$T_{s,t_{i+1}}$	°C	Sample temperature at time t_{i+1}
T_{surf,L_1}	°C	Surface temperature of the lower part of the outside of the insulated cylinder
T_{surf,L_2}	°C	Surface temperature of the upper part of the outside of the insulated cylinder
T_{ualu}	°C	Temperature in center under aluminum plate
T_{ualu,t_i}	°C	Temperature in center under aluminum plate at time t_i
$T_{ualu,t_{i+1}}$	°C	Temperature in center under aluminum plate at time t_{i+1}
ΔT_w	K	Temperature difference of water entering and leaving cooling unit (T_{OUT} - T_{IN})
T_{water}	°C	Water temperature
T_x	°C	Temperature x
vol%		Volume percent
wt%		Weight percent
$\varnothing$	m	Diameter

List of abbreviations

3D	Three dimensional
aka.	Also known as
Alu	Aluminum
C	Center thermocouple position
Dpt	Department
El.	Electric
EMRIS	Emerging Risks from Smoldering Fires
et.al.	And others/ and co-workers

(g)	Gaseous state
HVL	Western Norway University of Applied Sciences
L	Left thermocouple position
MLR	Mass loss rate
N	No, negative
nS	No Smoldering
NS	Norwegian Standard
P	Probability
R	Right thermocouple position
S	Smoldering
SS	Swedish Standard
TC	Thermocouple
Tot	Total
Y	Yes, affirmative

Acknowledgements

Contents

1. Introduction

1.1. Background

Smoldering fires are flameless fires that represent domestic, environmental and industrial hazards. Smoldering is more easily initiated than flaming and is also more persistent and difficult to extinguish. [1]

Domestically, smoldering is a major cause of fires, leading to many fatalities [2,3]. Weak heat sources such as electrical appliances or a cigarette can ignite smoldering, for instance in upholstered furniture. The danger lies both in the high yields of toxic smoke and in that smoldering represents a pathway to flaming fires [1]. Fire loss statistics for smoldering is uncertain, as flaming can consume the evidence of the preceding smoldering fire [4].

Environmentally, smoldering causes concern due to large emissions of greenhouse gases from peatland fires, wildfires and coal seam fires. The long duration and vast extent of these fires cause smoke emission that corresponds to an estimated 15% of man-made greenhouse gas emissions [5,6].

Industrially, the growing demand for non-fossil fuels has increased the use of solid biofuels and thereby also the need for biofuel production, transportation and storage [7]. This represents a safety challenge, as many biofuels can self-ignite and cause smoldering fires, flaming fires or explosions [8].

Prevention and extinguishment of smoldering fires is a severe challenge for fire services. Despite the numerous problems related to smoldering fires, there are few studies on the topic.

1.2. Objectives and research questions

This doctoral thesis is written as a monography, through which the project in its entirety is presented. Smoldering and extinguishment in granular biomass was studied in small-scale experiments. The main objectives were to obtain knowledge of the

initiation and burning patterns of smoldering fires in wood pellets, and to study extinguishment of self-sustained smoldering fires by cooling.

Chapter 4 presents susceptibility of smoldering initiation and burning to changes in input parameters. This includes a method for determining a transition region from non-smoldering to self-sustained smoldering. The research questions explored in Chapter 4 were:

- Is the initiation of smoldering in bulk, granular biomass susceptible to changes in the heat input, material type, storage size or changes in air flow, and which is the most important parameter?

- How is the smoldering combustion in bulk, granular biomass affected by changing the air flow from opposed to forward mode, and will this result in increased combustion speed, increased combustion temperatures and more complete combustion with higher mass loss?

Chapter 5 presents cooling smoldering fires through heat extraction, aiming at extinguishment. Chapter 5 also covers pulsating temperature profiles observed when the system was cooled to the brink of extinguishment. The research questions explored in Chapter 5 were:

- Can heat extraction from the center of the sample significantly affect the smoldering combustion, and can this cause extinguishment?

- If extinguishment can be obtained, does cooling have to be the major contributor to the heat losses from the system, and what is the minimum cooling level needed?

The project has led to a number of conference contributions and manuscripts for peer-reviewed papers, where parts of the project have been presented. A list of these contributions is presented in appendix A.

2. The phenomenon of smoldering

In this chapter, the phenomenon of smoldering will be introduced, including factors affecting the initiation and propagation of smoldering. Different approaches to extinguishment of smoldering fires, both at bench scale and industrial scale will also be presented.

2.1. Smoke and heat production, but no flames

Smoldering is a form of combustion without flames. Heat, smoke and other combustion products are produced [1]. Common examples of smoldering are the burning of a cigarette, or underground coal seam fires. During smoldering, the fuel is consumed through reactions occurring at the surface of the fuel, resulting in slow burning with low temperatures compared to flaming fires. Heat is produced by reactions between a solid fuel and a gaseous oxidizer, making it a heterogeneous reaction due to the different phases (solid and gaseous) of the reactants [1,9]. In contrast, flaming is the result of homogenous gas phase reactions between fuel and oxidizer, emitting both heat and light, which can be observed as flames.

Ignition of smoldering can be caused either by self-heating of the material, or by external ignition sources such as burning embers. In self-heating processes in biomass, the natural continuous degradation of the biomass through bacterial activity, fungi growth and cell respiration emits heat [10]. Oxidation of unsaturated fatty acids and resin acids, are the main contributors to self-heating [10, 11].

Any heat emission from oxidation processes is strictly speaking combustion processes [12]. It can therefore be useful to distinguish between these low-temperature self-heating processes, and the later stages where heat developed overcomes heat losses, and the combustion becomes self-sustained. At this point, smoldering can propagate through a fuel bed without any external heat input and this persistent form of combustion can cause severe damage to its surroundings (details in section 2.4).

In self-sustained smoldering fires, there are countless chemical and physical reactions occurring simultaneously. These can be summarized to a few global, simplified
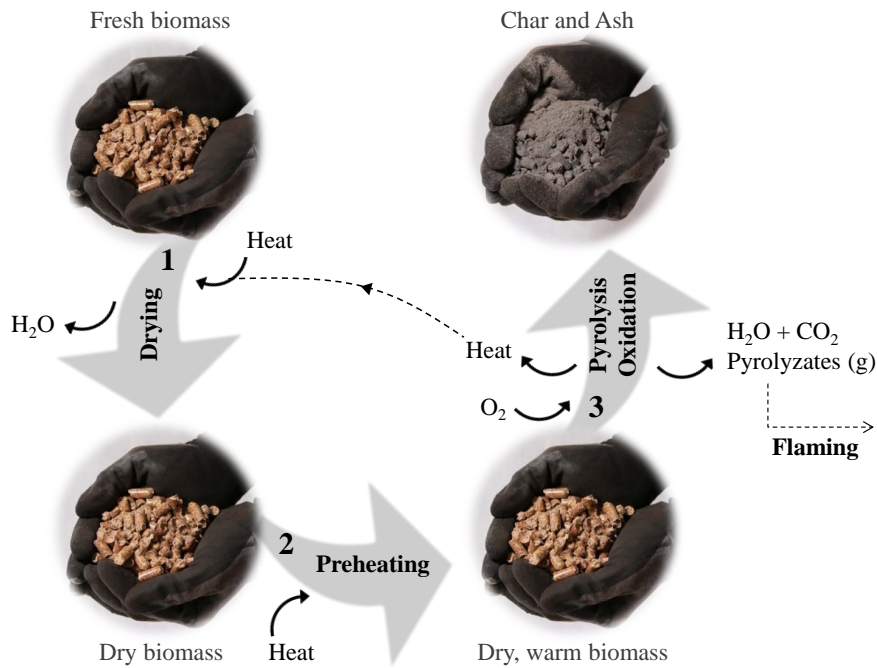
Figure 2.1.: Global, simplified reactions in self-sustained smoldering: (1) drying, (2) preheating, (3) pyrolysis and oxidation. For self-sustained smoldering, heat production is larger than heat losses combined with heat consumed during drying, preheating and pyrolysis. Heat excess is redirected into continued material degradation. Pyrolyzate gases can ignite to flaming.

reactions, namely: drying, preheating, pyrolysis and oxidation [1,5], as illustrated in Fig. 2.1.

Since smoldering occurs at the surface of the solid fuel, not merely in the gas phase, smoldering is most common in porous or granular fuels, due to a larger surface area [1,9]. Char formation upon degradation is also central for self-sustained smoldering to occur [13]. Examples of fuels that meet the criteria of porosity combined with char formation are biofuels such as wood pellets, peat, household and industrial wastes, cotton and foams in upholstered furniture, and fossil fuels such as coal [1,13,14].

2.2. Factors affecting smoldering

Smoldering fires are complex. There are a number of factors that can influence the ignition and burning behavior of smoldering fires, see overviews by Rein [1], Krause [8] and Drysdale [13]. Some factors are related to fuel properties such as material type, particle size and moisture content. Other factors are external effects such as ignition source, ventilation or fuel bed density, permeability and porosity. These contribute to govern oxygen supply to smoldering reactions, heat losses and

heat input to and from the fuel bed. Factors important for industrial applications are described in the following paragraphs.

Ignition source and heat flux:
Ignition of biomass can be caused by self-ignition (see section 2.1) or external heating sources. Conductive ignition is the heating source that can start a smoldering fire with the lowest heat flux [1]. For conductive ignition, a hot object is in direct contact with the fuel. The geometry of the hot object affects the ignition temperature for smoldering combustion, as shown for cellulosic insulation material [15]. The conductive heat transfer from the heater is important, but convection also plays a role [1]. The ignition temperature is affected by the chosen heat flux scenario. For cotton, it was found that slow, low heat influx resulted in lower ignition temperatures than strong, high heat flux input [16].

Ventilation and propagation direction:
The oxygen supply to the reaction zone is important for smoldering combustion [9]. An example of this can be found in experimental work on solid woods [17]. For self-sustained smoldering fires inside a long air flow channel, it was shown that low air flow resulted in reaction conditions for extinction, while high air flow resulted in reaction conditions for transition to flaming.

Smoldering is commonly classified into either forward or opposed (aka. reverse) mode, depending on the direction of the air flow relative to the smoldering propagation [13, 18]. In forward mode, the warm air from the reaction zone is transported in the direction of the original fuel, and thereby preheats and dry the fuel. In opposed mode, the original fuel is not exposed to the convective air flow from the warm reaction zone. Forward mode consequently results in faster and more complete smoldering combustion than opposed mode [18, 19]. Most real cases will be a combination of forward and opposed mode, as air flow direction and smoldering propagation rarely are one-dimensional [1].

For ignition from the top surface, downwards smoldering spread will occur, dominated by forward spread mode, as the smoldering spreads mainly in the same direction as the air supply [1]. Downward smoldering is for instance relevant for smoldering in peatland fires. For industrial incidents with deep seated self-ignition of biomass, the opposite can also be relevant: upwards smoldering spread, with deep seated ignition within the fuel bed, and the top as the nearest free surface [1]. For large fuel beds it can take a considerable amount of time before the smoldering front reaches the surface, for example about 2 weeks for an 85 cm pile of wood sawdust [20]. Still, the upwards spread is often faster than the downward [1] due to buoyancy-driven preheating of the original fuel by the hot gases from the reaction

zone below [21]. Although the mechanisms of upwards spread with natural convection is still not well understood, a recent study on peat fuel beds suggests that this occurs as a multi-step reaction [22]. First, the primary *upwards* smoldering front leaves behind unconsumed char, which in turn can be consumed by a *downward* secondary smoldering front. In the secondary smoldering front, there is oxidation of char, which has been shown to trigger transition to flaming in polyurethane [21] and cotton [23] fuel beds.

Fuel bed size, density and type of fuel:
For dust deposits, the thickness of the dust layer influences the ignition temperature, when ignited by a hot surface [24]. The ignition of dust layers by glowing nests depends on the dimension of the nest, as well as the sample size and dust type [25]. Ignition by pilot flame has also showed a dependency on dust type, sample size as well as particle size of the dust [20]. It has been shown that the fuel bed density affects the ignition, for cotton an increased density results in lower ignition temperatures [16, 26].

For wood pellets, there are several studies on self-heating and self-ignition [27]. Small scale basket tests can be used to predict critical ambient temperatures for safe storage of wood pellets [28]. In medium scale experiments with 1 m^3 sample sizes, it was found that gas emission and energy production was affected by the type of pellet [29]. Microscale isothermal calorimetry testing (4-5 g samples), has shown good predictability for the reactivity of wood pellets in larger scales, showing that self-heating properties are affected by the type of pellet and their age [11, 30, 31].

2.3. Wood pellets smoldering

Despite several self-heating and self-ignition studies, there are few studies on the burning behavior of self-sustained smoldering in wood pellets or other types of granular biomass, once ignited. Granular fuel beds have higher permeability than a compact fuel due to macroscopic pores between particles. This can affect smoldering, since oxygen supply is important for smoldering combustion [9].

Pellets consist of biomass particles that are compacted into pellets; wood pellets consist of compacted wood saw dust. During the pelletizing process, the physical forces cause a build-up of pressure and temperatures in the pellet mill, giving a temperature of a pellet leaving the mill typically around 70 °C [32]. This allows compacting of the wood without the use of adhesives, as the softened lignin and hemicellulose in the wood function as binding agent [7]. Each pellet is compact, but inhomogeneous, resulting in some, but very limited air diffusion into each pellet.

When undergoing pyrolysis and partial combustion, the pellets become more porous and brittle [33], allowing more air diffusion into each pellet.

2.4. Industrial storage hazard

There is currently a growth of the pellet industry and other biofuel industries to meet the demand for non-fossil fuels [7]. For biofuels that are prone to self-heating and self-ignition, such as wood pellets, this can cause increasing concern for the fire safety during production, transportation and storage.

As described in section 2.1, the continuous natural degradation of biomass cause self-heating, leading to a temperature increase in the material, which in turn accelerates the reactions. In deposits over a critical size, this self-heating will cause initiation of self-sustained smoldering fires [8]. The estimation of a critical storage size for storage units depends on which prediction theory is used. For wood pellets, the critical side length of a storage unit is suggested to be from 7 to 30 meters [28].

Smoldering in silos and deposits might seem harmless compared to flaming fires, but smoldering can inflict severe damage. Smoldering combustion consumes the product stored in a unit, while emitting toxic smoke that may be harmful to people in nearby domestic areas as well as for workers at the facility. As a smoldering fire propagates through a material, the heat from the combustion promotes pyrolysis and formation of pyrolyzate gases. These are not combusted in the smoldering process, but can mix with air and ignite. The consequent flaming fires or explosion can cause human injury as well as material damage, given sufficiently high gas volume and concentration. The conditions leading to transition to flaming or explosions are not easily predicted. [1, 18]

Smoldering fires are regularly observed in industrial facilities such as biomass silos, flat storage units, cargo ships and waste deposits [27]. An example case is a silo fire in Esbjerg, Denmark in 1998–1999 [8]. The fire started in a wood pellets storage cell, and spread to nearby cells in the multiple storage cell silo unit. The fire lasted for nine months, with an estimated cost of 8 million euro. Another example is a fire in a silo containing sawdust and wood chips in Italy, 2016 [34, 35]. During the fire brigade intervention, hatches at the top and bottom of the silo were opened simultaneously. An explosion occurred, most likely caused by an increased chimney effect through the silo. Four firefighters were injured, one of whom died. A similar incident occurred in a silo fire in Hallingdal, Norway in 2010, in which self-heating in wood pellets caused a smoldering fire, followed by a gas explosion [36]. Two

firefighters were injured and the silo was destroyed. Eckhoff provides several more case studies in which smoldering in storage units has led to explosions [37].

2.5. Extinguishment

Detecting, controlling and extinguishing smoldering fires has proven to be challenging for fire brigades, there are essentially no guaranteed or cost-effective ways of extinguishing smoldering fires in large scale industrial storage units [8].

A common method to control and extinguish smoldering fires is to remove the fuel from the storage unit, and drench it with water [8,38]. This firefighting method can result in production stop and in destruction of the fuel. For some storage units such as silos, forced manual opening of the storage unit can be necessary. Fuel removal during smoldering will often require personnel present at or near the combustion site, which can cause injury due to asphyxiation, toxic gases or explosions [8,38]. For large flat storage units, or outdoor storages like landfills, the enormous scale of the fuel bed often makes a complete extinguishment by fuel removal near impossible. Depending on the size of the smoldering fire and the fuel bed, firefighting strategy often has to be adjusted, from aiming at extinguishment to controlling the fire instead [39,40].

Two other common firefighting methods are to quench or cool the smoldering fire. Quenching has been used both in real-life industrial incidents and at laboratory scale experiments, either to control the combustion until other measures can be taken, or to completely quench the fire. Industrially, carbon dioxide and nitrogen gas are most commonly used due to availability and cost [38]. In silos, the low density of nitrogen gas enables introduction at the bottom where accessibility can be easier [38, 41]. Regardless of gas choice, if the gaseous suppression system is not pre-installed in the industrial storage unit, penetration of the gas into the fuel bed can be insufficient for complete extinguishment. Holding times for complete quenching of smoldering is very long compared to flaming, at days or months instead of minutes or hours [5,42]. Re-ignition is common both at the industrial and at the laboratory scale [8,41,43,44]. For all inerting gas systems, suffocation and toxic effect for humans present in the facility represent hazards. Also, rapid injection of gases can cause hazardous dust clouds [38].

Cooling the reaction zone using water is the most widely used extinguishing method. However, water in a large fuel bed will tend to find the path of least flow resistance; the consequent channeling cause uneven water distribution, which will not necessarily reach the combustion zone [1, 42]. In the laboratory scale, the amount of water needed is in the range 1-6 liters of water per kilogram fuel, for coal and peat [42,43].

Industrially, the additional weight of the water can damage the structural integrity of the storage unit. Rupture of the storage unit may also be caused by swelling of compressed fuels, such as pellets, when in contact with water [8, 38]. To limit the amount of water, sprays [42] and water mists [44] have been used with limited success. Water sprays, mists and showers can even cause scattering of glowing embers or dispersion of dust, which can lead to dust explosions [38]. Foams can be used to increase the wetting of the fuel, but it is still not an effective extinguishing method [41]. Foams are often used only as an explosion prevention measure applied at the top of the biomass [8]. At a large scale, water and foam run-off to nearby rivers and lakes can be harmful to the environment [45, 46].

Cooling the fuel bed without direct contact between water and fuel can be a way to avoid channeling, swelling, scattering and water run-off. This approach is currently being tested at large scale in St.Louis, USA, where an underground smoldering fire in a landfill is approaching nuclear waste. Cool liquid is pumped through pipes sunken into the ground to absorb heat [39, 40]. The outcome of this case study has not been published yet. A numerical study of a similar system, not yet published, showed that the spacial extent of the cooling was limited, suggesting that local cooling around a cooling pipe would have a very limited impact on a smoldering fire [47]. For smoldering fires, no experimental studies on cooling without direct fuel-water contact have been found.

3. Materials and methods

The materials and methods used in this study are presented in this chapter. An introduction to the use of logistic regression for fire science studies is given in section 3.5. A discussion of the wood pellet fuel, the experimental set-up and experimental procedure is presented in section 3.6.

3.1. Wood pellets

Wood pellets were used as sample material in this study, as a model material for granular biomass. Two types of wood pellets were used, denoted Pellet A and Pellet B, see pictures in Fig. 3.1. Material properties are given in Table 3.1. The pellet types differed in production site, wood and bark content, and some material properties. The pellets were produced according to Norwegian (NS 3165) [48] and Swedish (SS 187120) [49] standards, as Class 1 pellets. Both pellet types consisted of mixtures of pine and spruce, a combination that has been found to be reactive and prone to self-heating [30].

Pellet A was sampled 3 months after production by the producer. The pellets were stored in closed 10 kg bags at -25 °C to ensure unchanged reactivity of the pellets for all experiments in the series, as recommended by Larsson et.al. [11]. Pellets were defrosted at room temperature 1-2 days prior to each experiment. Sampling was made to reflect the content of the 10 kg bags, containing approximately < 1 wt% fine particles (< 4 mm x 4 mm).

Pellet B was purchased from a commercial hardware store. Sampling, storage time and storage conditions before purchase is not known. Pellet B was stored in ambient conditions in the laboratory before the experiments.

3.2. Focus of experiments

An overview of the focus and governing parameters of the different parts of this study is given in Table 3.2 as a brief guide for the reader.

Table 3.1.: Material properties of wood pellets and measurement methods used.

Material properties	Pellet A	Pellet B
Type of material	Wood	Wood
	(incl. bark)	(not incl. bark)
Pine content [%]	20-50	60
Spruce content [%]	50-80	40
Country of production	Norway	Sweden
Unit density [kg/m^3]	1020	1050
Bulk density [kg/m^3]	710	730
Porosity [%]$^\alpha$	30.4	30.5
Diameter [mm]	8	8
Activation energy [kJ/mol] $^\beta$	91.4	107.1
Upper calorific value [kJ/kg]$^\gamma$	18 834	17 453
Lower calorific value [kJ/kg]$^\delta$	17 433	15 931
Permeability [m^2]$^{\epsilon*}$	$\leq 2.4 \cdot 10^{-8}$	$\leq 2.1 \cdot 10^{-8}$
Moisture content [%]$^{\zeta*}$	6.3 (6.8)	7.7 (9.2)
Volatile compounds [%]$^{\eta*}$	77 (82)	78 (85)
Ash content [%]$^{\eta*}$	0.46 (0.49)	0.21 (0.23)
Elemental composition [%]$^{\theta*}$		
Carbon (C)	48 (48) [52]	48 (47) [52]
Hydrogen (H)	6 (6) [6]	6 (6) [7]
Nitrogen (N)	0 (0) [0]	0 (0) [0]
Oxygen (O) & Others	39 (39) [42]	38 (37) [41]

*Given as: As received (Air dried) [Water and ash free].

$^\alpha$ Given by 1-(Bulk density/ Unit density).

$^\beta$ Adiabatic test [50].

$^\gamma$ Bomb calorimeter (IKA C200). Measured including evaporation
of water (aka. gross or total heat of combustion).

$^\delta$ Bomb calorimeter (IKA C200). Calculated without evaporation
of water (aka. net heat of combustion).

$^\epsilon$ Determined using a self-made set-up, $\varnothing 0.16$ m x length 0.6 m,
with constant flow rate.

$^\zeta$ Thermogravimetric Analyzer and Moisture Analyzer (Leco TGA 701).

$^\eta$ Thermogravimetric Analyzer (Leco TGA 701). Defined as the amount of
the material that undergoes pyrolysis and primary oxidation to form char.

$^\theta$ Thermogravimetric Analyzer (Leco TGA 701) and
Carbon/Hydrogen/Nitrogen Determinator (Leco CHN 1000 and Leco CS230).
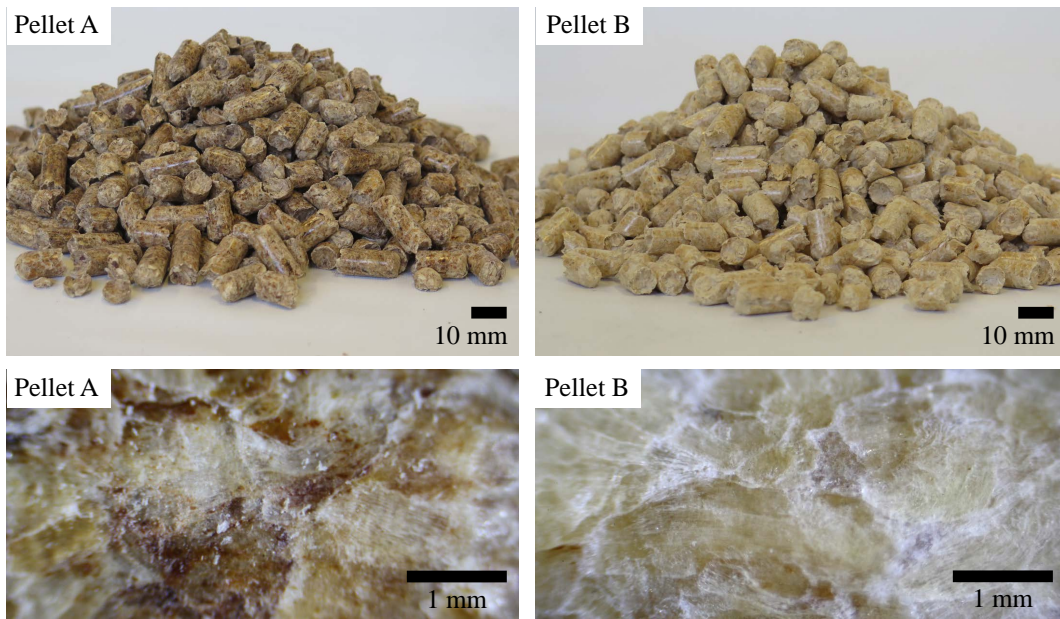
Figure 3.1.: Pictures of wood pellets A and B. The bulk mass is granular (top) with high permeability (see Table 3.1). Each individual pellet is inhomogeneous (bottom), consisting of compacted wood saw dust, dark areas show bark content in Pellet A.

In section 4.1, initiation of smoldering was studied with regard to the susceptibility to changes in input parameters. In section 4.2 the impact of changes in the air flow inlet to the bottom of the sample was studied. In chapter 5, cooling of the fuel bed by heat extraction was studied, for one background scenario without cooling and three scenarios with cooling.

Table 3.2.: Focus areas of the study, with governing parameters.

	Chapter 4, section 4.1:
Focus:	Susceptibility of smoldering initiation
Parameters:	Sample height, cylinder height, pellet type, external heating
	Chapter 4, section 4.2:
Focus:	Susceptibility to changes in air flow (opposed versus forward)
Parameters:	Set-up with and without opening at the bottom
	Chapter 5:
Focus:	Cooling of the fuel bed
Parameters:	Set-up with and without cooling unit
	Varying degree of cooling by changing start time of water flow

3.3. Experimental set-up

3.3.1. Base set-up

The experimental set-up consisted of a cylindrical fuel container of steel with thermally insulated side walls. The container was closed at the bottom, open to free air convection at the top and heated from below by a hot surface.

The base set-up described in this section was used in all experiments. Additional equipment was added when needed as described in sections 3.3.2 - 3.3.4. The base set-up was modified from that used by Hagen et.al. [16, 26, 51], which in turn was based on the set-up used by Torero et.al. [52]. The modification to the current set-up was to use closed and insulated side walls, in order to limit mass and heat exchange through the vertical sides of the sample.

The experimental equipment was positioned on a flat surface in a ventilation hood, where the air extraction was kept constant for all experiments. Data was collected every 5 seconds using a data acquisition unit. The ambient room temperature was 22 ± 1 °C.

The base set-up was assembled as illustrated in Fig. 3.2 and Fig. 3.3 and consisted of five main components: an insulated steel cylinder, an aluminum plate, a heating unit, a scale and a thermocouple attachment unit.

The stainless **steel cylinder** was 330 mm high, diameter 150 mm, with wall thickness 1 mm. The side walls were insulated to avoid heat loss, by 60 mm mineral wool with thermal conductivity 0.041 W/mK at 50 °C, 0.085 W/mK at 300 °C, the average over the relevant temperature range of 50-400 °C was 0.068 W/mK. The outside of the mineral wool insulation was clad with aluminum foil. The steel cylinder was placed on onto the flat aluminum plate with no sealing applied, giving a near closed bottom of the fuel container.

The **aluminum plate** measured 280 mm x 280 mm, thickness 30 mm. The topside of the aluminum had a 2 mm wide, 2 mm deep slit from the edge to the center for insertion of a thermocouple. The underside of the aluminum plate also had such a thermocouple slit, in addition to a circular carving fitted to the ceramic disc of the electric heating unit below. The aluminum plate provided an even heat distribution to the bottom of the sample. The aluminum plate thereby represents a hot surface in direct contact with the fuel, giving conductive ignition.

The **electric heating unit** was a Wilfa CP1 hotplate with a maximum power of 2000 W. The top was a 185 mm diameter ceramic disc. The electric heating unit had an internal thermostat to avoid over-heating that could not be monitored
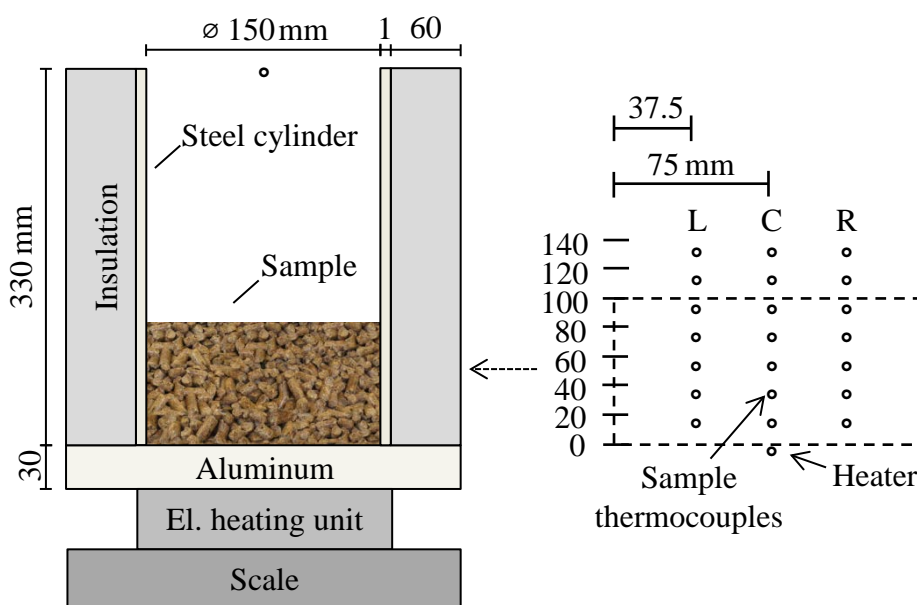
Figure 3.2.: Diagram of the base experimental set-up (left) with insulated steel cylinder, aluminum plate, electric heating unit, scale and sample. Thermocouple positions (right) are given by (o). Thermocouples were positioned along a plane in the center, one at 0 mm (heater), three en each height 20-140 mm, and one at 330 mm (near cylinder opening). Horizontal position is denoted as left (L), center (C) and right (R). Dimensions are given in mm, the illustration is not to scale.

or removed. The electric heating unit was connected to a Jumo B70.1050.0 digital thermostat, with regulatory interval of 0.2 °C. The thermostat was set to a fixed setpoint temperature, and regulated power supply to the electric heating unit, using a thermocouple located in the slit between the electric heating unit and the aluminum plate. The temperature measured by a thermocouple located in a slit at the top of the aluminum plate (at 0 mm in Fig. 3.2) is hereby referred to as the "heater".

The **scale** was a Kern 30 kg IP65 weighing platform connected to Systech IT 1000 4-20 MAMP digital scale, with precision 1 g.

Temperatures were measured using encapsulated 0.5 mm K-type **thermocouples**. The thermocouples (TC) were attached to a stainless steel unit in the shape of a ladder ("TC ladder"). The purpose of the TC ladder was to maintain the vertical position of thermocouples despite sample collapse during combustion. The TC ladder consisted of two vertical 0.4 mm thick, 12.7 mm wide stainless steel bands, and horizontal 0.2 mm thick, 2 mm wide stainless steel bands. The horizontal bands were positioned with 20 mm vertical spacing. The thin steel bands could flex (±10 mm) in the horizontal direction. Thermocouples were positioned by inserting the thermocouple tip through holes in the horizontal bands, ensuring no contact between
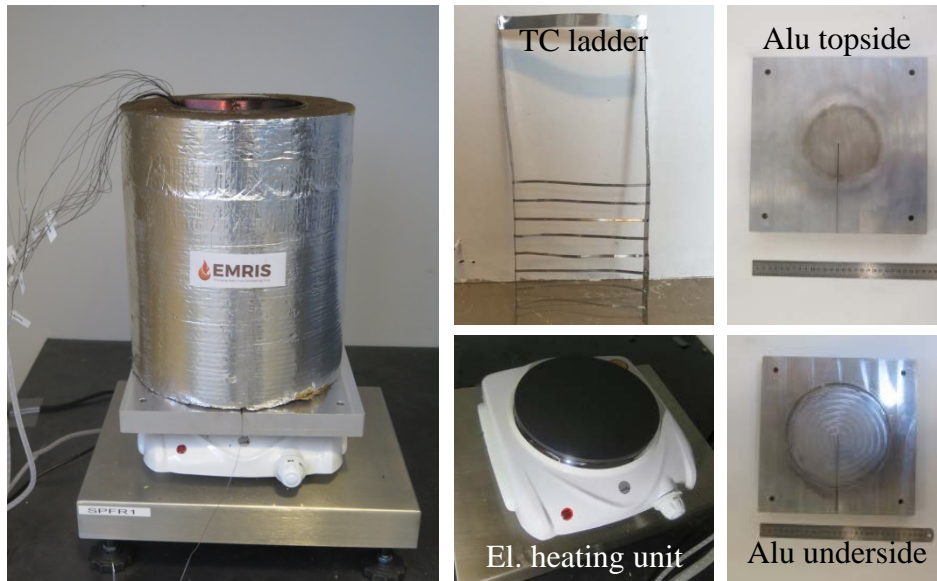
Figure 3.3.: Photos of the base experimental set up. Details of components: Thermocouple (TC) ladder, electric heating unit, the top and underside of the aluminum plate.

steel band and thermocouple tip. There were three thermocouples in each height above the heater, as illustrated in Fig. 3.2, three in each height, height levels spaced 20 mm apart. The TC ladder was positioned in the center of the steel cylinder.

3.3.2. Additional equipment: susceptibility of smoldering initiation

This section presents equipment that enabled the study of the susceptibility of smoldering initiation to changes in the set-up geometry, in section 4.1.

Two heights of the stainless steel cylinder were used. The first, denoted as *Low pipe* was as described in section 3.3.1, 330 mm high. The second, denoted as *High pipe*, consisted of two such stainless steel cylinders mounted on top of each other, see Fig. 3.4a and Fig. 3.5a. The total height of the High cylinder was 580 and 630 mm, the difference was caused by slightly different shapes of the individual cylinders. The high cylinder was assumed to give an increased buoyancy to the hot air in the cylinder. The aim was to study if any changes in air flow from this increased chimney-like-effect would influence the combustion.

The other parameters varied in section 4.1 were sample height and pellet type, which did not include any equipment change.
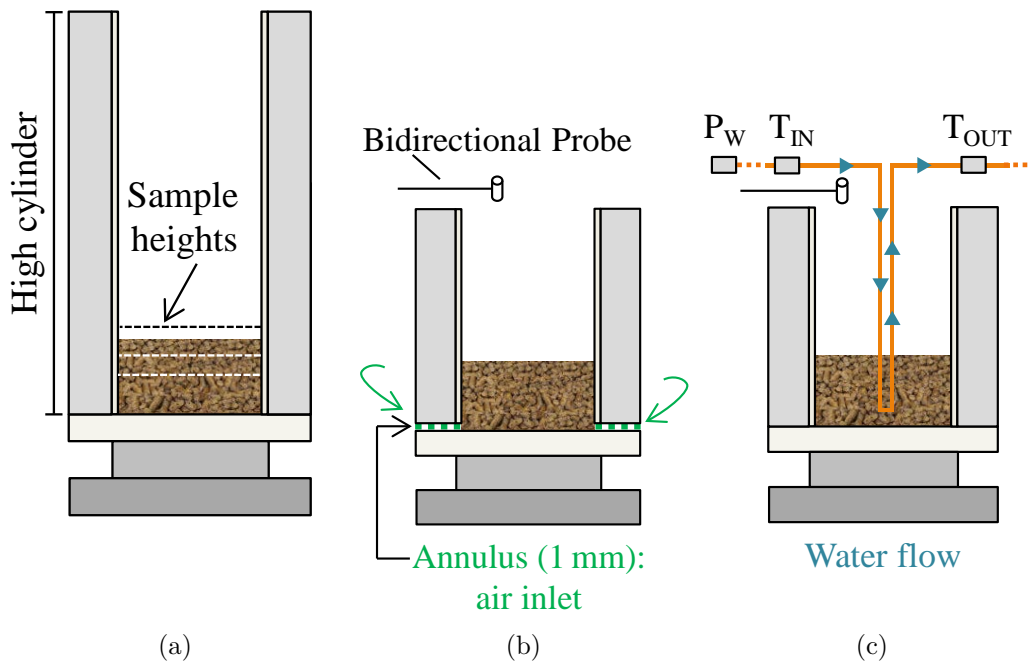
Figure 3.4.: Diagrams of experimental set-up with additional equipment. (a) Increased cylinder height and four sample heights. (b) Bidirectional probe positioned near cylinder opening, a perforated annulus positioned between cylinder and aluminum plate. (c) Cooling unit positioned in the sample center. Water temperature (T_{IN} and T_{OUT}) and pressure (P_W) measurement positions are indicated, as well as water flow direction.
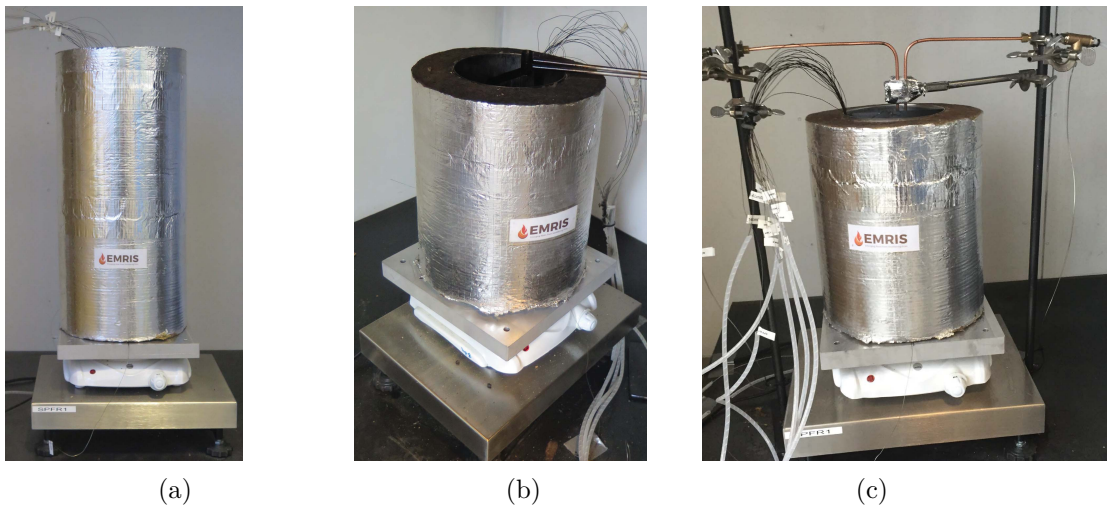
Figure 3.5.: Photos of the experimental set-up with additional equipment.

3.3.3. Additional equipment: susceptibility to changes in air flow

This section presents equipment that enabled the study of how a change from opposed to forward air flow mode affected the combustion, in section 4.2. Air was introduced to the bottom of the fuel bed, see Fig. 3.4b and Fig. 3.5b.

A perforated stainless steel annulus was used (Fig. 3.6b), with outer $\varnothing$240 mm, inner $\varnothing$135 mm, thickness 1 mm, perforation holes $\varnothing$3 mm, This was positioned between the aluminum plate and the insulated steel cylinder. This allowed air to enter the lower parts of the sample, without escape of fuel or pyrolysis products (illustrated in Fig. 3.6a). A bidirectional probe [53] attached to a Setra model 267 pressure transmitter 0-25 Pa was positioned vertically at the top of the steel cylinder, 10 mm above the opening, to measure the air flow out of the cylinder (Fig 3.6c).
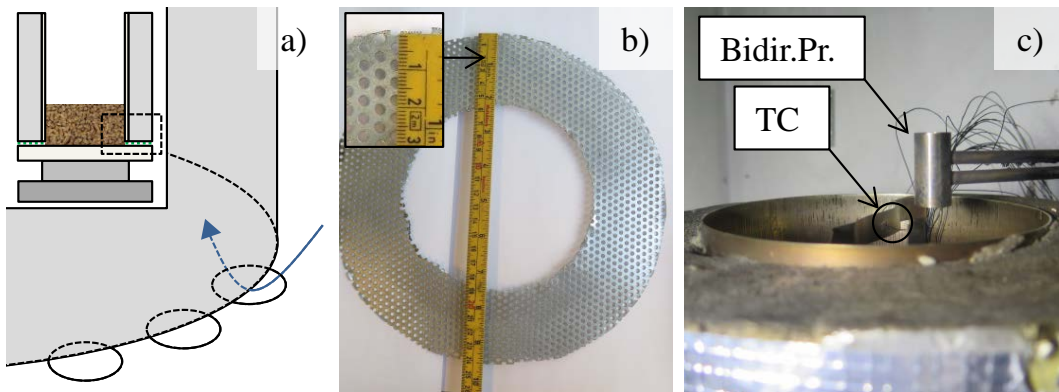
Figure 3.6.: (a) Illustration of the air inlet to the bottom of the cylinder via the holes in the perforated annulus. (b) Photos of annulus. (c) Position of the bidirectional probe (Bidir.Pr.) and thermocouple (TC) position at 330 mm, near the cylinder opening.

3.3.4. Additional equipment: Cooling of smoldering

This section presents equipment that enabled the study of cooling of smoldering by heat extraction from the center of the fuel bed, in chapter 5. Equipment that enabled a study of 3D temperature profiles in the fuel bed in chapter 5 will also be presented.

A cooling unit was positioned near the center of the steel cylinder with no contact between cooling unit and thermocouple mounting rack (Fig. 3.4c, Fig. 3.5c and Fig. 3.7a). The cooling unit consisted of a copper pipe (outer $\varnothing$4.76 mm) bent into a U-shape with outer distance 24.6 mm and inner distance 16.4 mm between the two tube branches (Fig. 3.7c). The total volume of the cooling unit within the sample was $4.5 \cdot 10^{-6}$ m^3, or 0.3 vol% of the sample volume. The lower tip of the cooling unit
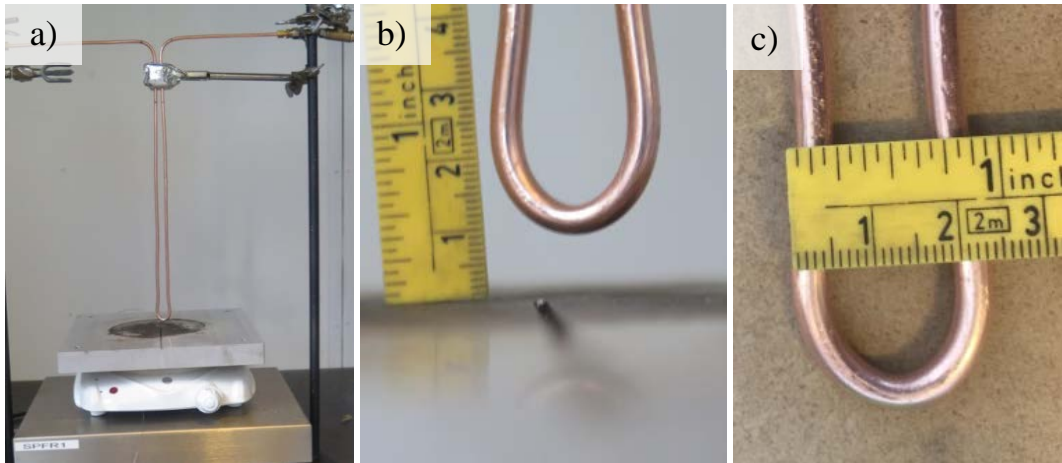
Figure 3.7.: Detail photos of cooling unit. (a) The U-shaped cooling unit with no surrounding cylinder. (b) Distance between cooling unit and aluminum plate was 10 mm. (c) Detail of the size of the U-curve and distance between the two tube branches.

was positioned 10 mm above the aluminum plate to avoid conductive heat transfer (Fig. 3.7b).
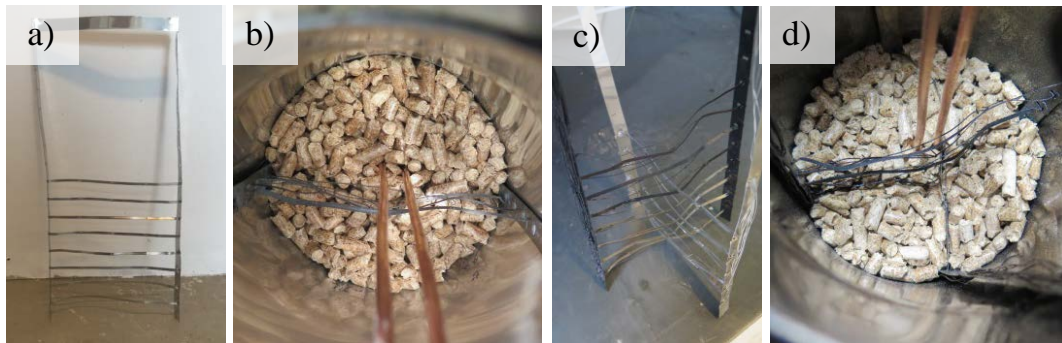
Figure 3.8.: Thermocouple ladder (a) side view and (b) top view, for the base set-up. Double thermocouple ladder (c) side view and (d) top view, with two perpendicular planes for 3D temperature info.

Water inlet was connected to the municipal water supply, with some variations in water flow and temperature. A pressure regulator was used to control the water flow to around 0.65 L/min. Water pressure was measured about 2 meters from the experimental set-up, using a 0-25 bar Keller piezoresistive pressure transmitter PA-23SY. Water outlet was connected to tubes leading to the drain. The inlet and outlet of the copper pipe were supported by a rack. The water temperature was on average 16 ± 2 °C. Water temperatures were measured near the center of the cooling pipe, using 1.5 mm encapsulated type K thermocouples.

In the base set-up, temperatures were measured along a vertical plane in the fuel bed (Fig. 3.8a and 3.8b). To obtain information of the 3D temperature profiles in the fuel bed, experiments with extra thermocouples in the fuel bed were also performed. An additional TC ladder with thermocouples mounted along a plane perpendicular to that of the base set-up was used (Fig. 3.8c and 3.8d).

3.4. Experimental procedure

The experimental set-up was assembled as described in section 3.3. For each experiment, a sample was weighed using a Mettler Toledo ML 3002/01 scale with 0.01 g precision. The mass of the sample and the wood pellets bulk density gives the initial sample heights. Sample mass of 0.75 kg, 1.0 kg, 1.25 kg and 1.5 kg was used to give initial sample heights of 60, 80, 100 or 120 mm, respectively. Multiple sample heights were explored in section 4.1, and only one sample height of 100 mm (1.25 kg) was used in the other part of the study. The sample was poured into the cylinder to allow random stacking. The sample height was validated by manual measurements before each experiment.

Data logging was started 2 minutes before the electric heating unit was switched on, to verify ambient starting conditions. The heater was set to its maximum power of 2000 W, resulting in a temperature increase of about 3-4 K/min. The heater ramped up to a given set-point temperature of 370 °C, chosen based on preliminary experiments. Upon reaching the set-point temperature, power supply to the electric heating unit was regulated to maintain this temperature. The power supply was on about 43% of the time, giving an average power input around 860 W. The heater temperature was regulated by a thermocouple located on top of the electric heating unit, below the aluminum plate. The surface in contact with the sample was the top of the aluminum plate, reaching a temperature of 348 ± 7 °C. This was lower than the set-point temperature due to heat loss from the exposed 30 mm thick aluminum plate.

The following procedure was used to determine the duration of the external heating period: In section 4.1, the duration of the external heating was determined by fuel bed temperatures. The heater was switched off when 2 of 3 thermocouples located at 20 mm above the aluminum plate had reached a predetermined temperature, denoted as the "Cut-off temperature". This procedure was chosen based on observations in preliminary experiments, where the heating of the fuel bed was not symmetric horizontally and the same heating duration could give different temperatures in the lower part of the sample. The procedure of setting a given cut-off temperature was therefore chosen to obtain the same starting temperature in the lower part of the

fuel, to provide a similar starting point for the smoldering to propagate. As will be shown in section 4.1, the duration of the external heating was in fact the most important factor for the initiation of smoldering. Therefore, a fixed duration of the external heating was used in the other parts of the study (6 h and 13 h). These durations were based on preliminary experiments determining the duration needed to obtain self-sustained smoldering.

After the heater was switched off, the system was left undisturbed. Temperature profiles in the fuel bed, total mass loss and appearance of the residue after the experiments were used to distinguish self-sustained smoldering from non-smoldering cases. The experiment ended when all temperatures in the fuel bed had decreased below 30 °C with a continuing decreasing trend. Data logging continued for a minimum of 1 h after the end of the experiment, to observe any re-ignition.

After the experiment, the sample height was measured manually. The sample was removed from the set-up and sorted by physical appearance. No equipment cleaning was done in the smoldering initiation study (section 4.1). Any build-up of residue on the equipment during the experimental series was not found to have an impact on the initiation of smoldering, as no trend in time-dependency of the outcome was found. The procedure was nevertheless changed after this series, to provide more reproducible starting conditions. In the other parts of the study (section 4.2 and chapter 5) the test equipment was cleaned, removing tar and other residue sticking to the inside of the cylinder, the top of the aluminum plate and the cooling unit.

3.5. Statistical methods

Statistical analysis was used in this study to evaluate if there was a significant difference between results in two groups, and to quantify the impact of variations in input parameters on the experimental outcome.

The data sets of this study consisted of a relatively small number of repetitions. A Shapiro-Wilk W test for normality [54] showed that in most cases the data was not normally distributed. A two-tailed Mann-Whitney U test [55] was therefore used for comparing the means of two groups in chapters 4 and 5. Statistica software, version 13 [56] was used for these analyses. A significance level of $p < 0.05$ was used for all statistical analysis in this study.

Logistic regression was used in section 4.1 to quantify the influence of parameters on the outcome of experiments with two possible results: non-smoldering and smoldering. A basic introduction to the method will be described here, to encourage an

increased use of the method in the fire science community. Hypothetical example cases from smoldering experiments will be used.

The diagrams in Fig. 3.9 shows the results from 11 hypothetical experiments where only one parameter is varied - the temperature, T. The red curve gives the probability of smoldering as a function of temperature, for a given combination of experimental outcomes.

(a) Clear distinction   (b) Gradual transition
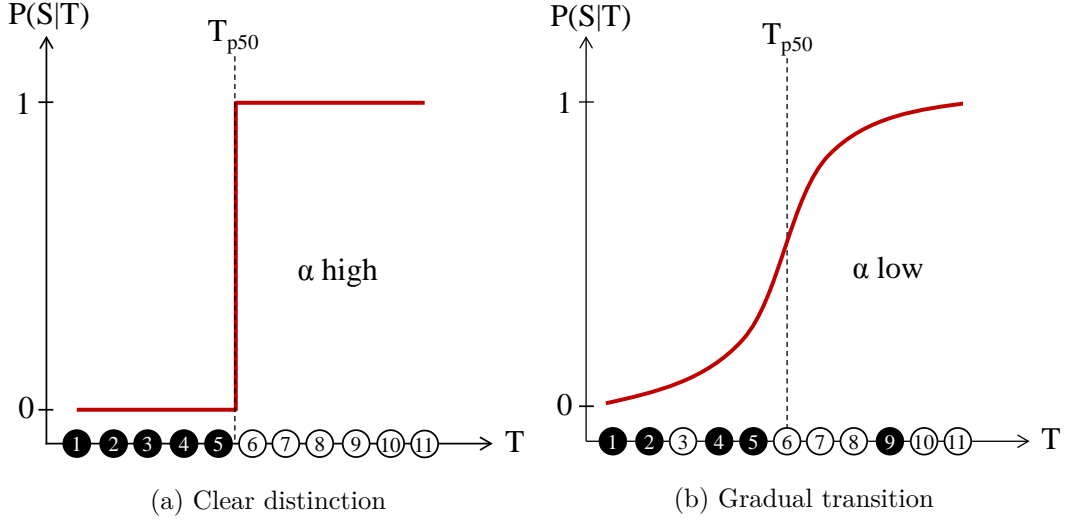
Figure 3.9.: Diagram of the probability of smoldering, P(S|T), as a function of temperature for 11 example experiments, for cases with (a) a clear distinction between non-smoldering (filled circles) and smoldering (empty circles) and (b) a gradual transition from non-smoldering to smoldering. Details on T_{p50} line and α in the main text.

In Fig. 3.9a, experiments at T = 1-5 resulted in non-smoldering (filled circles), while experiments at T = 6-11 resulted in smoldering (empty circles). The probability function set for smoldering at a given temperature, $P(S|T)$, is given by Eq. 3.1 and for non-smoldering, $P(nS|T)$, by Eq. 3.2.

$$P(S|T) = \frac{e^{\alpha_1(T_x - T_{p50})}}{1 + e^{\alpha_1(T_x - T_{p50})}} \tag{3.1}$$

$$P(nS|T) = 1 - P(S|T) \tag{3.2}$$

Since there is a distinct separation between the two outcomes in Fig. 3.9a, it is easy to locate the T_{p50} line, which gives the temperature where the probability of initiation of smoldering is 50%. Combined with α, which gives the slope, a probability function for each experiment can be determined. The optimal combination of T_{p50} and α for

a set of experiments is found by a maximum likelihood estimation of the probability product, $P(Tot)$, of all individual experiments, see Eq. 3.3.

$$
\begin{aligned}
P(Tot) &= P(nS|T = 1) \cdot P(nS|T = 2) \cdot P(S|T = 3)... \\
&= 1.00 \cdot 1.00 \cdot 1.00...
\end{aligned}
\tag{3.3}
$$

In Eq. 3.3, example values from Fig. 3.9a are displayed. In this simple case, choosing a high α (steep slope) and a T_{p50} between T_5 and T_6 gives a maximized $P(Tot)$. This gives a $P(S|T) = 1$ for all smoldering cases, while for the non-smoldering cases, $P(S|T) = 0$, which gives $P(nS|T) = 1$, see Eq. 3.2.

For the more complex case in Fig. 3.9b, the outlier experiments at $T = 3$ and $T = 9$ would have given a very poor probability product ($P(tot) \rightarrow 0$) if the slope from Fig. 3.9a had been used, since both P(S|T=3) and P(nS|T=9) would have been 0. Instead, the α can be altered to give a less steep slope of the probability function, as illustrated in Fig. 3.9b. The T_{p50} line should also in this case be shifted towards a higher temperature, to accommodate the non-smoldering case observed at high temperatures in experiment $T = 9$. An example of an optimal choice of α and T_{p50} for Fig. 3.9b is given in Eq. 3.4, giving a non-zero probability product.

$$
\begin{aligned}
P(Tot) &= P(nS|T = 1) \cdot P(nS|T = 2) \cdot P(S|T = 3)... \\
&= 1.00 \cdot 0.95 \cdot 0.10...
\end{aligned}
\tag{3.4}
$$

Expanding to include more than one parameter, the probability function for each experiment is given by Eq. 3.5, with an α_i for each of the two example parameters A and B.

$$
P = \frac{e^{\alpha_A(A_i - A_{p50}) + \alpha_B(B_i - B_{p50})}}{1 + e^{\alpha_A(A_i - A_{p50}) + \alpha_B(B_i - B_{p50})}} = \frac{e^{\alpha_0 + (\alpha_A A_i) + (\alpha_B B_i)}}{1 + e^{\alpha_0 + (\alpha_A A_i) + (\alpha_B B_i)}}
\tag{3.5}
$$

Constants can be gathered to a "lumped" α_0, see right side of Eq. 3.5. The transition from non-smoldering to smoldering can be displayed by a transition region as illustrated in Fig. 3.10. At the p_{50} line, the probability for initiation of smoldering is 50%, and hence, P is set to 0.5. Corresponding lines for 10% probability of smoldering (T_{p10}), 20% probability of smoldering (T_{p20}) etc. can be determined accordingly. In this example, the transition region constitutes of p_{10}, p_{50} and p_{90} lines, for 10%, 50% and 90% probability of smoldering. Notice that it is assumed that the parameters are independent. Non-linear transition regions can also occur.

The procedure for determining whether a model with a certain set of parameters is suitable, is first to estimate α_i, then use a statistical tool (for instance R) to evaluate
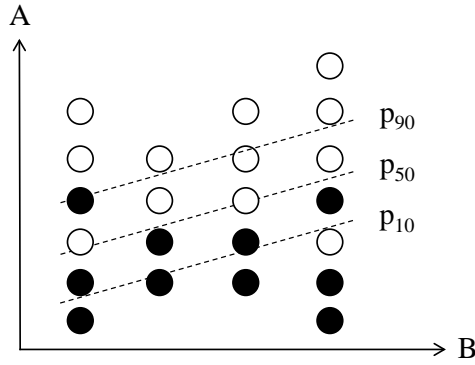
Figure 3.10.: Diagram of experiments where parameters A and B are varied. The transition region between non-smoldering (filled circles) and smoldering (empty circles) is illustrated by p_{10}, p_{50} and p_{90} lines, see main text.

the significance of that parameter. The output p-value of each parameter determines if that parameter is significant ($p < 0.05$) for the outcome of the experiment or not. For non-significant parameters, α_i is set to 0, and thus the parameter will not affect the quantified transition region. Different combination of dependence between parameters give different models.

The Akaike information criterion [57] and Bayesian information criterion [58] can be used to quantify the relative quality of the different models. The criteria do not provide information of the absolute model quality, but gives a comparison of the relative quality of the studied models, based on the goodness of fit for all observed data. In general, as few parameters as possible should be included in a model not to over-fit the data, in particular when the number of experiments is small. Models with many parameters are therefore given a penalty. The criteria are calculated from maximum likelihood estimations of the probability product (Eq. 3.3), combined with a parameter penalty, which is stronger for the Bayesian compared to the Akaike information criterion.

An advantage of using logistic regression is that an iterative process can be used to estimate the transition zone from non-smoldering to smoldering, even with few experiments. The accuracy of the method will increase with experiment repetitions.

3.6. Evaluation of materials and methods

In this section, the chosen material, experimental set-up and experimental procedure will be evaluated.

3.6.1. Material evaluation

The wood pellets used in this study were commercially available, inhomogeneous pellets, not produced specifically for this study. The wood content composition stated by the producer was approximate. There could have been uncontrolled variations between batches, due to variations in wood content, production or storage conditions. Several batches of pellets were used during this study. To limit the impact of sampling, only pellets from the same batch were used in the same experimental series. The benefit of the choice of pellets is that this is a relevant commercial product.

Pellet A was fresh and Pellet B was aged. Fresh wood pellets are more reactive than old ones [11, 31, 59], and their reactivity change upon ambient storage. Pellet A was therefore stored in a freezer to preserve its reactivity as significant changes in reactivity during the experimental period could potentially have affected the experimental results. This procedure is as recommended by Larsson et.al. [11], who do not report any changes in the sample quality or properties due to the process of freezing and defrosting. Ideally both pellet types could have been stored in a freezer, but it is assumed that the reactivity decay of the aged Pellet B was limited during the experimental period.

3.6.2. Experimental set-up evaluation

If the main main purpose of the study of the initiation of smoldering (section 4.1) had been merely to determine the self-ignition temperature for the fuel, a standardized hot-surface ignition test method [60] could have been used. However, the sample size of the hot-surface ignition method (12.7 mm depth, 100 mm diameter) makes it suitable for dusts and powders. For granular fuels, larger sample size is needed. Our experimental set-up resembled a vertically elongated version of the hot-surface ignition method, in that, the sample was contained within a cylinder, which was located on top of a heated metal plate. The insulated side walls of the cylinder enabled a study of self-sustained smoldering and extinguishment in bulk fuel beds, with limited mass and heat exchange through the sides.

A challenge with the experimental set-up was fuel collapse during combustion. The set-up was based on studies on cotton and polyurethane foam, materials for which vertical collapse during combustion was not an issue [16,26,51,52]. For wood pellets, however, the upwards smoldering spread occurred simultaneously as mass consumption caused height decrease due to the granular nature of the pellets. This complicated determination of the location of smoldering fronts, but could at the same

time give a better understanding of the upwards smoldering spread in granular fuel beds.

The water supply was somewhat unstable. The municipal water supply had some small water pressure variations with time of day. There were also some random larger water flow fluctuations, which for the set average of 0.65 L/min, could vary in the range 0.48-0.85 L/min during short periods of time. Sudden flow rate variations could give a recoil impact on the mass loss data, due to the added weight of the water. To limit the influence of changes in water flow on the mass data, the water supply tubes were supported by a rack mounted on top of the scale. Peaks in water pressure could not only have had an indirect impact on the measured mass data, but could also have had a direct influence on the combustion, as will be discussed in section 5.3.6. The water temperature of the inlet also varied slightly, on average 16 °C, with temperature variations in the range 13-21 °C. Seasonal variations of the water temperature were found to be insignificant, as there was no significant dependency of test month on the outcome of an experiment. A closed water supply system would have resulted in better control of the water pressure and temperatures.

The electric heating unit was also unstable, with some variation in temperature ramping and stabilization between experiments. During the air flow experimental series, the electric heating unit had to be replaced due to failure, which could have affected the results, as will be discussed in section 4.2.

The number of thermocouples was limited to minimize the volume of foreign objects within the fuel bed. The foreign objects were both the thermocouples and TC ladder used to position the thermocouples (see Fig. 3.3). More thermocouples could have provided a more detailed view of the temperature profiles in the fuel bed, but this could also have affected the combustion in heat transport to and from the sample, and between hot zones within the sample. Different mounting approaches were considered, such as inserting thermocouples through holes in the side walls of the cylinder, or dangling thermocouples from the top. The TC ladder was chosen to prioritize rigid vertical positioning also during sample collapse, without making alterations to the walls of the sample container. Ceramic materials or other materials with lower conductivity could have been used, but steel was chosen due to robustness and design flexibility.

3.6.3. Experimental procedure evaluation

The long duration of the experiments (several days) means that compromises had to be made between data collection and data storage capacity. The logging interval

was therefore set to 5 seconds and only selected experiments were videotaped. The consequence is that short-lived reactions will not have been registered.

Experiments exploring initiation of smoldering (section 4.1) were performed at two different locations, at Western Norway University of Applied Sciences in Haugesund and at RISE Fire Research in Trondheim. The same procedure and experimental set-up was used in both locations, and control experiments showed that the heating process was reproducible. There could still have been differences in site-specific conditions that were not monitored, which may have affected the experiments.

Given the stochastic nature of smoldering fires, the number of experiments in this study should be mentioned. Repetition of experiments was prioritized over variation of parameters. This limits the number of parameters studied, but enhances the statistical significance of the findings.

4. Smoldering susceptibility

In this chapter, studies of the susceptibility of smoldering in granular biomass will be presented. First, the initiation (ignition) of smoldering is explored, focusing on the susceptibility of variations in input parameters in section 4.1. Second, smoldering with opposed air flow is compared to forward air flow in section 4.2. An overall discussion of smoldering susceptibility is given in section 4.3.

4.1. Susceptibility of smoldering initiation

The main results from the study of initiation of self-sustained smoldering in wood pellets will be presented in this section. Here, initiation is used instead of ignition, as the latter is often associated with the ignition of flaming combustion. Such sudden transitions between states do not apply to the slow phenomenon of smoldering fires. The study focuses on initiation of self-sustained smoldering as a result of the temperature build-up in the sample, imposed by an external heater. This part of the study is based on work presented in Villacorta et.al. [61].

The selected parameters represent input that could affect smoldering in different ways: material properties, storage size, and change in air flow due to changes in the geometry of the set-up. The parameters were pellet type (Pellet A and B), sample height (60, 80, 100, 120 mm) and height of the cylinder containing the sample (Low and High), as described in chapter 3.

For each parameter combination, an iterative process was used to find the temperature region between non-smoldering and self-sustained smoldering cases. The two cases were very different in terms of temperature profiles and mass loss rates, as shown in Fig. 4.1. Non-smoldering (Fig. 4.1a and 4.1c) was characterized by sample temperatures remaining well below the heater temperature for the entire duration of the experiment, and low total mass loss (around 15-30 wt%). Self-sustained smoldering (Fig. 4.1b and 4.1d) was characterized by temperatures that decreased during the first hours after the external heater was switched off, followed by an increase to elevated temperatures. This was combined with high total mass loss (around 80-90 wt%). For the self-sustained smoldering cases, the heat producing processes were sufficiently strong to balance heat losses.
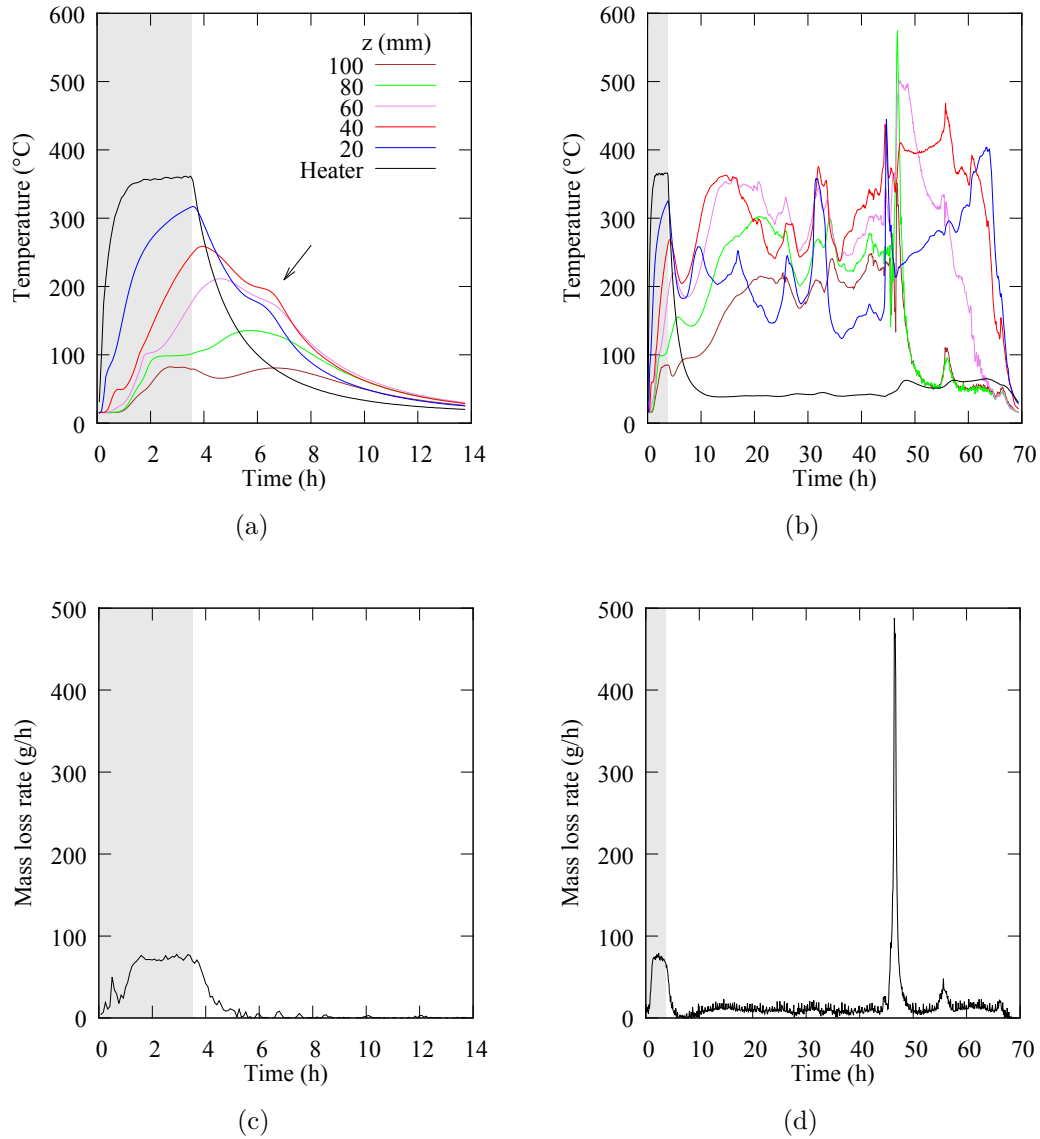
Figure 4.1.: Temperature and mass loss rate as functions of time. Two representative experiments are presented, both with pellet A, 120 mm sample height, low pipe height. Notice the different x-scales. (a) and (c) Non-smoldering with cut-off temperature of 310 °C. (b) and (d) Self-sustained smoldering with cut-off temperature of 320 °C. External heating is indicated by gray shading. The legend gives the vertical temperature measurement positions in the sample (20-100 mm). For clarity, only center temperatures are shown (C in Fig. 3.2). Mass loss rate is given as 5 min averages. Arrow in (a) indicates deviation from cooling.

There were also heat producing processes in the non-smoldering cases. This can be seen in the temperatures in Fig. 4.1a by deviation from pure cooling, as indicated by an arrow. Also, the total mass loss for the non-smoldering cases was larger than the moisture content, indicating mass consumption processes such as pyrolysis and partial combustion. This was also evident from the residue after the experiments, with a substantial amount of brown and black/charred pellets (details in Madsen et.al. [62]).

In this part of the study, 47 experiments were performed. The results from the iterative process to determine the transition zone between non-smoldering and self-sustained smoldering are summarized in Fig. 4.2 and Fig. 4.3. The results are presented first as a function of the cut-off temperature (described in section 3.4), then as a function of the duration of external heating. Notice that the iterative process was done based on Cut-off temperatures, for instance by stepwise increasing from 300, 310, 320 to 350 °C. Duration of external heating was a mere consequence of the time to obtain this sample temperature, explaining the more irregular step pattern separating the different experiments in Fig. 4.3.

In Fig. 4.2 and Fig. 4.3, the transition region from non-smoldering to self-sustained smoldering is given by three lines. The p50-line gives the estimated 50% probability of non-smoldering and self-sustained smoldering for the given combination of sample height, pellet type, cylinder height and cut-off temperature or heating duration. To show the span of the transition region, the corresponding 10% and 90% probabilities are given by the p10- and p90-lines. Quantification of this transition region was done by logistic regression using the binary outcome in this study, namely non-smoldering and self-sustained smoldering, to determine which parameters have the strongest impact on the results. An introduction to the method and how to select the best model is given in section 3.5. Cut-off temperature and duration of external heating can not be significant in the same model, as they are strongly correlated.

Initial analysis using cut-off temperatures showed that all included parameters were significant (cut-off temperature, sample height, pellet type and cylinder pipe height). However, this resulted in very narrow transition regions, as shown in Fig. 4.2. This indicates over-fitting of the data, considering the relatively small number of experiments. This is a consequence of the iterative experimental method, chosen to limit the total number of experiments, but still be able to determine the transition from non-smoldering to self-sustained smoldering. Therefore, including all experiments from Fig. 4.2 into one model as shown in Fig. 4.4, gives a better basis for the model. Here, only the cut-off temperature was significant, while sample height was near significant, and the transition region was wider, as is expected with this number of experiments.
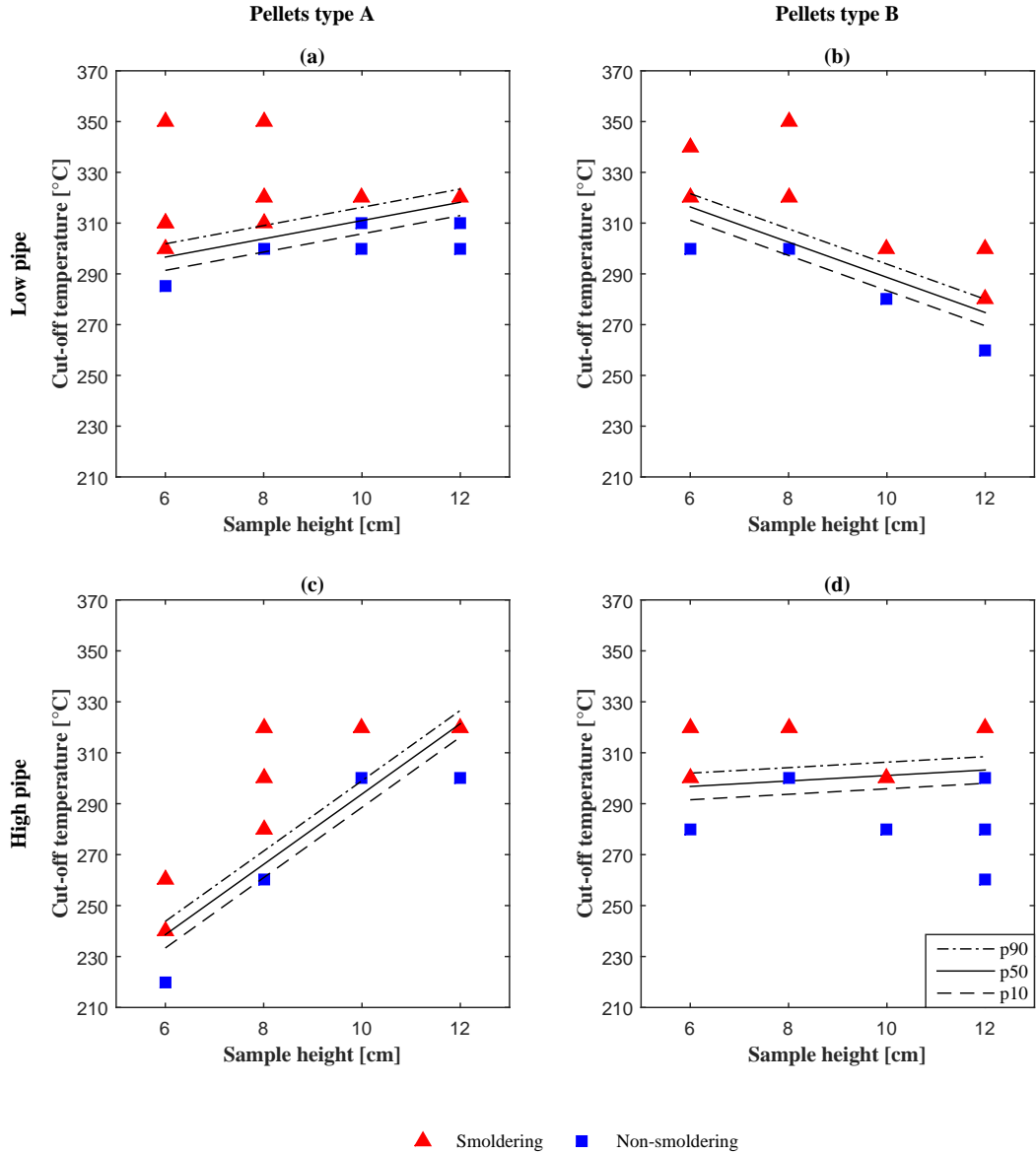
Figure 4.2.: Cut-off temperature as functions of sample height, for high and low pipe height and for pellet type A and B. Non-smoldering experiments are given by squares, self-sustained smoldering experiments by triangles. The transition region from non-smoldering to smoldering is given by probability lines representing 10%, 50% and 90% probability of smoldering (p10, p50 and p90). The figure is reused with permission from Villacorta et.al. [61].
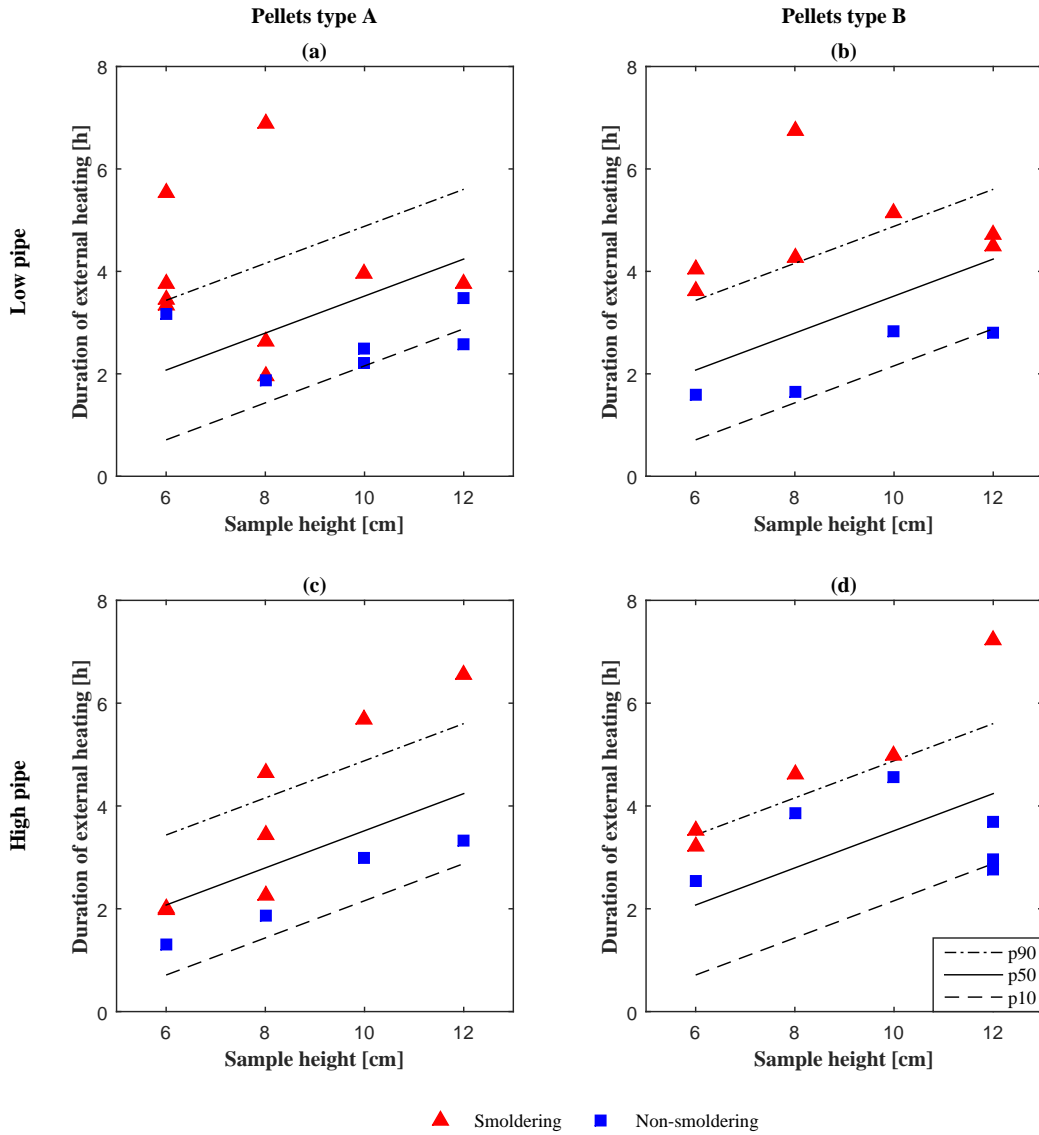
Figure 4.3.: Heating duration as functions of sample height, for high and low pipe height and for pellet type A and B. Non-smoldering experiments are given by squares, self-sustained smoldering experiments by triangles. The transition region from non-smoldering to smoldering is given by probability lines representing 10%, 50% and 90% probability of smoldering (p10, p50 and p90). The figure is reused with permission from Villacorta et.al. [61].
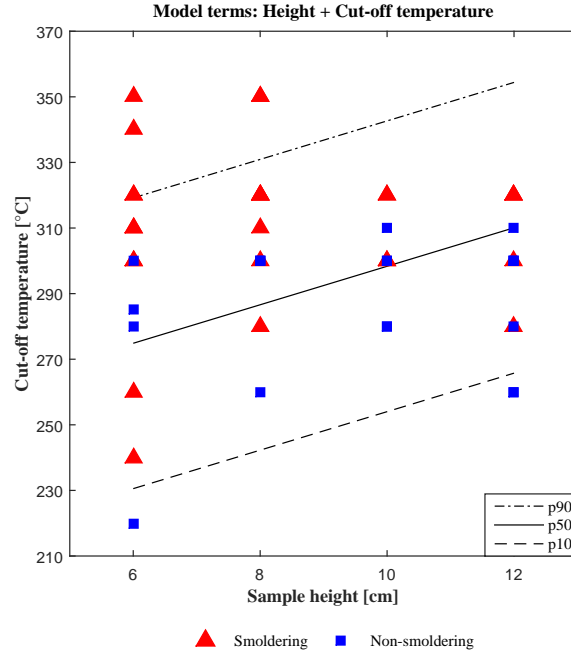
Figure 4.4.: Best fit for logistic regression based on Cut-off temperatures. The figure is reused with permission from Villacorta et.al. [61].

Table 4.1.: Model terms with combinations of sample height (Height), Cut-off temperature, cylinder height (Pipe), pellet type (Pellet) and duration of external heating (Duration). Akaike and Bayesian information criteria and relevant figures are given. Data over-fitting is indicated by italic font.

Model terms	Height + Cut-off temp + Pipe + Pellet	Height + Cut-off temp	Height + Duration	Height + Height · Duration
Akaike	*35*	56	44	43
Bayesian	*52*	61	50	49
Fig.	4.2	4.4	4.3 and 4.5a	4.5b

Using the duration of external heating instead of the cut-off temperature, resulted in a model with a better fit to the experimental data. A good fit is given by a low Akaike and Bayesian information criteria (Table 4.1), based on high maximum likelihood estimation of the probability product, as described in section 3.5. This parameter change was done to study the validity of an observation made during the experimental work - namely that the heating duration seemed to have a bigger impact on the outcome than the exact temperature in the fuel bed did.

All experimental results for sample size as a function of duration of external heating from Fig. 4.3 are included in Fig. 4.5a. In this model, both duration of heating and sample height were found to be significant, while the pellet type was found to be near significant and the cylinder height (*Low pipe* versus *High pipe*) was not.
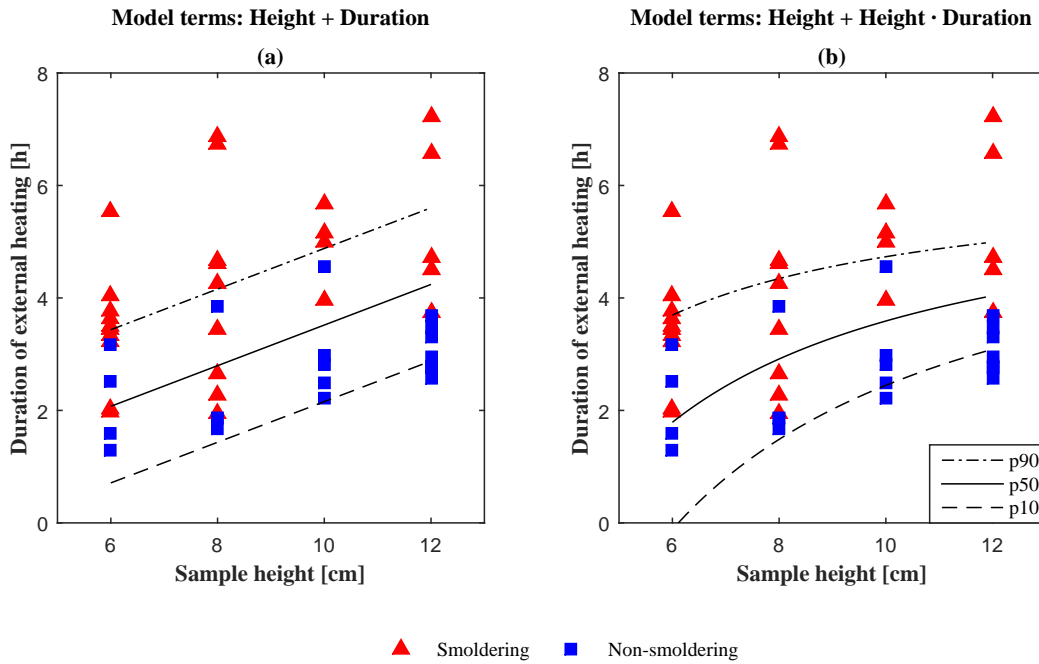
Figure 4.5.: Best fit for logistic regression based on duration of external heating. The figure is reused with permission from Villacorta et.al. [61].

Using a different model of dependence between height and duration of heating, the best fit to the observed data out of all studied models was found, presented in Fig. 4.5b. The two parameters in the model are sample height and duration of heating coupled with sample height. The resulting transition region had a higher dependency on sample height at low sample heights. When the sample height was increased from 60 to 80 mm, the duration of heating must be increased by 1 h, while for an increase in sample height from 100 to 120 mm the difference was only 0.5 h.

4.2. Susceptibility to changes in air flow

In section 4.1, it was found that the cylinder height (*Low pipe* versus *High pipe*, as described in section 3.3.2) did not have any significant effect on the initiation of smoldering. This indicated insufficient air flow change from this geometry alteration. To study susceptibility to changes in air flow, a 1 mm gap was introduced between the cylinder and aluminum plate (equipment description in section 3.3.3 and Fig. 3.4b) to impose increased air flow to the bottom of the fuel bed. This part of the study is based on the master thesis of Rebaque-Valdés [63] as well as Rebaque-Valdés et.al. [64].

The smoldering was initiated by a heater at the bottom of the fuel bed. The gap allowed direct air flow to the bottom of the cylinder, with air flow in the same

direction as the upwards moving smoldering front (forward). Without the gap, the air supply was from the top, the opposite side of the fuel bed compared to the heater (opposed). In total 21 experiments were performed in this part of the study: 11 with gap (denoted forward) and 10 without gap (denoted opposed).

Notice that both with and without gap, there will be a combination of upwards and downwards drafts in the cylinder, as there was no forced air flow (for instance by a fan), and since the top of the sample was an open surface. This variation in upward and downward air draft during an experiment was measured by the bidirectional probe positioned in the cylinder opening. This single measurement position showed both upward and downward air draft during an experiment. This does not provide a complete picture of the air flow movements to and from the sample, but it is reasonable to assume a complex air flow pattern in both cases, although with a stronger upward air flow for forward mode. The complexity reflects that, as for most real cases, air flow direction and smoldering propagation rarely are one-dimensional [1]. The cases in this study could therefore have been denoted semi-forward and semi-opposed.

In preliminary experiments, it was found that 4 h heating duration was sufficient to obtain self-sustained smoldering in all forward-cases, but not in all opposed cases. The heating duration for the main study was therefore set to 6 h, to ensure initiation of self-sustained smoldering in all cases.

The overall temperature pattern was different for experiment with opposed air flow compared to forward air flow, see Fig. 4.6. All 10 opposed cases displayed a similar temperature profile to that presented in Fig. 4.6a. In the forward cases, two different temperature profiles were observed. There were 9 cases where the most intense combustion occurred before the external heating period was finished (Fig. 4.6c) and 2 cases where the most intense combustion occurred a few hours after the external heating was switched off (Fig. 4.6b).

The increased air supply to the bottom of the fuel bed resulted in a more intense smoldering. Statistically significant differences between forward and opposed cases were found using a two-tailed Mann-Whitney U test (method description in section 3.5) for the following data. The most intense combustion during the experiments had higher peak temperatures, with averages ∼740 °C for forward and ∼570 °C for opposed, shown in Fig. 4.7a. The peak temperature occurred earlier for forward cases compared to opposed cases (at t = 8 h versus 29 h), shown in Fig. 4.7b. The increased intensity of the combustion led to burn-out after a shorter total combustion time (23 h versus 61 h), shown in Fig. 4.7c. The more intense combustion also resulted in a higher total consumption of the fuel, with total mass losses on average 91 wt% for the forward cases and 85 wt% for the opposed cases, shown in Fig. 4.7d.
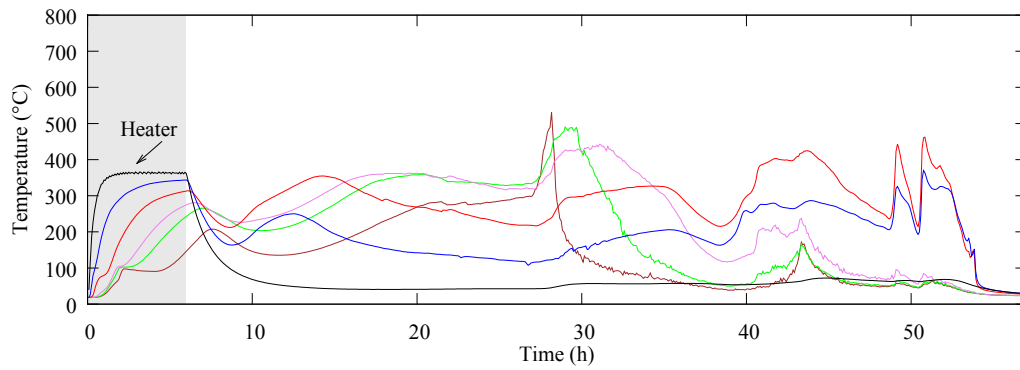
(a) Opposed, 10 observed cases
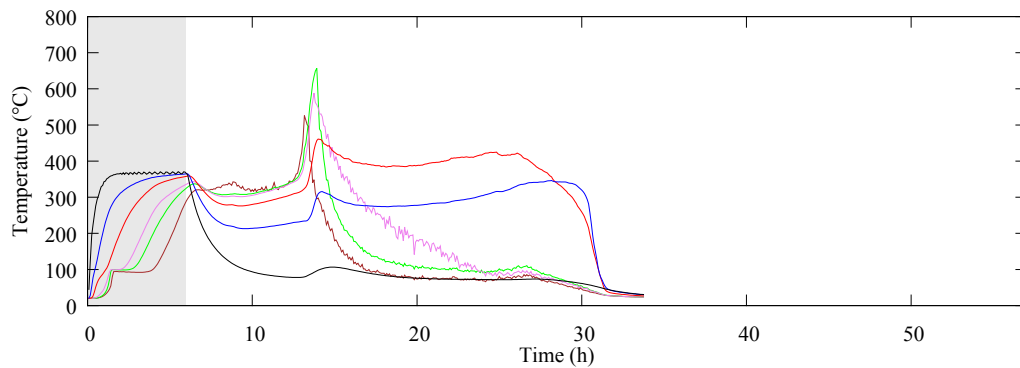
(b) Forward, 2 observed cases
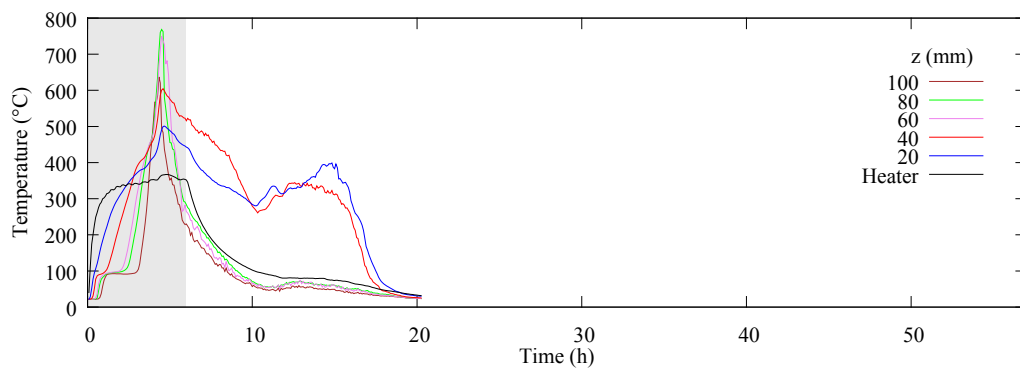
(c) Forward, 9 observed cases (1 with flaming)

Figure 4.6.: Temperature as functions of time. (a) Opposed experiment. (b) and (c) Forward experiments. The most intense combustion occurred either before the external heating period was finished (c) or after a period of slow and steady combustion (a) and (b). After the most intense combustion followed a period with slow and steady combustion, with occasional temperature peaks, before sample temperatures decreased to ambient. External heating is indicated by gray shading. The legend gives the vertical temperature measurement positions in the sample (20-100 mm). For clarity, only center temperatures are shown (C in Fig. 3.2).
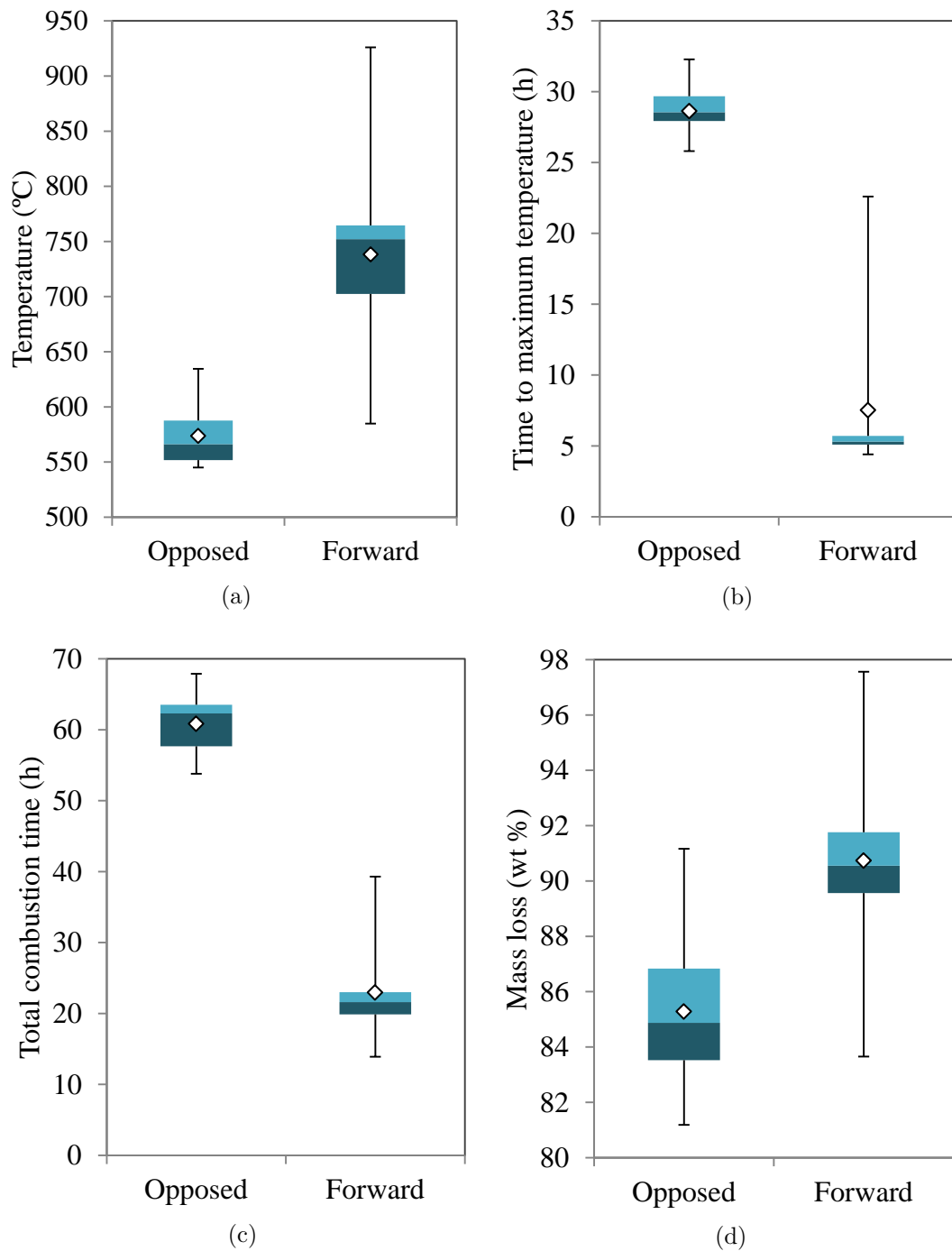
Figure 4.7.: Box and whiskers plots displaying data distribution for all opposed cases compared to all forward cases. (a) Maximum temperature (b) Time to reach maximum temperature. (c) Total combustion time from experiment start till burn-out. (d) Total mass loss. Boxes show lower and upper quartiles of data set, rhombus represents average value and whiskers show maximum and minimum values of data set. The figures are adapted with permission from Rebaque-Valdés [63].

Maximum temperatures at each temperature measurement height 0-120 mm are given in Fig. 4.8. The spread in the temperature data between experiments was larger for forward than opposed air flow (broader boxes, wider whiskers in Fig. 4.8). This shows that opposed smoldering was more steady and predictable than forward smoldering. The higher intensity and lower predictability of the forward air flow mode was also reflected in one case of transition to flaming fire observed in this mode. Flaming was documented by temperature readings above the fuel. Temperatures in the opening of the fuel containing cylinder (at 330 mm in Fig. 3.2) peaked at 720 °C. This was significantly higher than peak values at the same position, around 120 °C, for all other experiments. Flaming lasted for a short duration (minutes), compared to the total test duration (hours). The peak temperature measured in the fuel bed for this experiment was 926 °C, which was the highest measured sample temperature (Fig. 4.7a).
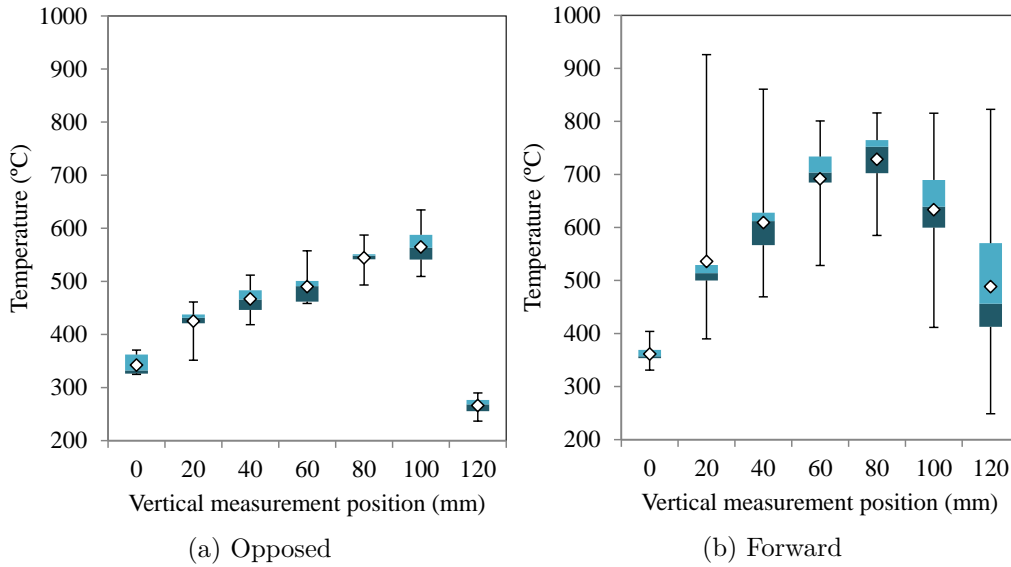
(a) Opposed (b) Forward

Figure 4.8.: Maximum temperature during experiments at each vertical measurement position for all (a) opposed and (b) forward cases. Boxes show lower and upper quartiles of data set, rhombus represents average value and whiskers show maximum and minimum values of data set. The figures are adapted with permission from Rebaque-Valdés [63].

During this experimental series, the electric heating unit was replaced due to failure (as mentioned in section 3.6.2). Different electric heating units gave similar, but not identical heating. The two different electric heating units were used for experiments in both forward and opposed mode. For forward mode, experiments resulted in two different temperature profiles before and after the unit replacement, as shown in Fig. 4.6b and Fig. 4.6c. This indicates that the replacement could have affected the results, due to changes in the initial heating. On the other hand, there was little variation in the temperature profiles for opposed cases, even though these experi-

ments also included the use of the two electric heating units. Also, in preliminary experiments, both types of forward temperature profiles (Fig. 4.6b and Fig. 4.6c) were observed using one heating unit. It would still have been preferable to use the same electric heating unit for all experiments, as smoldering can be susceptible to changes in the initial heating.

4.3. Discussion: Smoldering susceptibility

Initiation of smoldering:
The duration of the external heating was the most significant parameter for initiation of self-sustained smoldering, as shown in section 4.1. Sample height also affected initiation and increasing sample height extended the necessary heating duration for initiation of smoldering. This is in accordance with findings by Torero and Fernandez-Pello [21], in which longer heating duration of polyurethane foam was necessary to initiate smoldering as the sample length was increased. They suggest that this could be due to the reduced air flow through the whole fuel bed as the sample size increased, thus providing insufficient oxidizer to sustain the smoldering. Higher heat capacity of large fuel beds could also explain this increase. The model with the best fit to our data (Fig. 4.5b) suggests that the relation between duration of heating and sample height is non-linear. An increase in sample height from 60 to 80 mm required 1 h longer heating duration, while the difference was only 0.5 h from 100 to 120 mm. The smaller spread in the data for high sample heights indicate a more steady and predictable system, possibly due to a more insulated fuel bed with lower free surface to volume ratio. It could also be speculated that random, small variations between inhomogeneous pellets could affect the sampling in small sample sizes more than large sample sizes.

The pellet type was found to be near significant for the initiation of smoldering. Based on previous studies on self-heating of wood pellets [11, 29–31], it could have been expected that the type of pellet should have had a larger impact on the results. However, the two pellet types chosen for this study were relatively similar, compared to the wide range of pellets available on the market (see an example in Larsson et.al. [30]). A larger variation in material properties between the pellet types could potentially have revealed a larger impact of pellet type on the experimental outcome. A study including a wider range of pellet types is recommended for future research.

These results from section 4.1 were used in the other parts of this study, in that, initiation of self-sustained smoldering from this point was based on the duration of external heating instead of the fuel bed temperature (cut-off temperature). Also, a sample height of 100 mm was chosen; Lower sample heights were not used to limit

heat losses and sampling susceptibility; Higher sample heights were not used to limit the total combustion time to a few days, from start till burn-out. The pellet type was found to be near significant for the initiation of self-sustained smoldering, so only one type of pellet was used in the other parts of this study (section 4.2 and chapter 5).

Logistic regression:
The method for distinguishing between non-smoldering and self-sustained smoldering was based on logistic regression, presented in section 3.5. This is a versatile method that can be used also for other experimental fire studies with binary outcomes to determine the impact of various parameters on the results, particularly when there is a limited number of experiments. The value of using such a method is that, even though the absolute value of the ignition temperatures are set-up dependent [15], it enables a relative comparison of the impact of parameters.

Air flow:
The air flow to the fuel bed was studied in sections 4.1 and 4.2. First, the cylinder height was increased under the assumption that this would cause an increased chimney effect, due to increased buoyancy of hot air in the cylinder. Any change in air flow pattern was, however, too small to have a significant effect on the initiation of smoldering. This motivated the continued study of air flow, as it is expected that natural (buoyant) convection should dominate over diffusion for fuel beds with large particles [1]. An alteration in the air supply to the bottom of the cylinder was made to study the impact of increased upward air flow in the same direction as the smoldering (forward) compared to opposed mode. This had a large impact on the combustion. Firstly, the initiation of smoldering was affected. The increased air supply to the fuel bed in the forward air flow mode resulted in shorter heating duration needed to obtain self-sustained smoldering, as was shown in preliminary experiments. Once ignited, the increased air flow also greatly affected the smoldering pattern, with higher maximum temperatures reached in shorter time, higher mass consumption and shorter time till burn-out. This supports literature reports of forward air flow resulting in a more intense combustion than opposed mode, due to the increased drying and preheating of the fuel [1, 20]. This study indicates that these mechanisms are valid also for granular fuel beds with no forced air flow. The study also demonstrates how air flow can be adjusted without the use of forced air flow, by introducing a gap resulting in a boyancy-driven chimney effect through the fuel bed.

Smoldering propagation:
The top of our fuel bed remained unaffected by the deep-seated smoldering until around the time of the most intense combustion. At this point, charring of the pellets

at the top could be observed. For 100 mm sample height in the base set-up (opposed mode), the time to reach the most intense combustion period was around 29 h, while for the forward mode it was around 8 h, see Fig. 4.7b. This is in the same time scale as that found by Palmer for upwards smoldering in wood sawdust, in which charring at the top surface of a 100 mm fuel heap was visible at around 4-7 h, and for a 300 mm sample at 40 h [20]. In that study, smoldering was initiated in a small pile of wood sawdust, after which more dust was added on top, and time till the charring reached the top surface was measured. It has previously been suggested that in a vertical fuel bed, there is a primary smoldering front moving upwards that consumes the fresh fuel and leaves char behind, followed by a secondary smoldering front moving downward consuming the char [22]. Any occurrence of such a *primary* front can not be observed in the temperature profiles in our study. During the external heating period, the lower parts of the sample were heated first, and in that regard, there was a warm front moving upwards in the sample. However, once the external heating was switched off, there was a long period of stable self-sustained smoldering in the fuel bed, without a distinct smoldering front movement, see Fig. 4.1b, Fig. 4.6a and Fig. 4.6b. But, based on visual observation of charring on the top surface, it could be speculated a primary smoldering front had reached the top surface at that time. Once the most intense combustion occurred, the highest temperatures were reached in locations close to the free surface, where there was ample oxygen supply. As the fuel was consumed, and the sample height decreased, the highest temperatures were successively observed in lower heights of the fuel bed, which at this point were closer to the free surface. This supports the observation of a second downward smoldering front as reported by Huang and Rein [22].

Unsymmetric spread and transition to flaming:
Lastly, two observations regarding the smoldering spread and transition to flaming will be mentioned, as they could be of interest for further work. In this study, the propagation of the smoldering fire was initially upwards, as a consequence of the heater position below the fuel bed. For this propagation mode, a smoldering spread shape in the form of an elongated bell is expected [1]. However, the smoldering spread in the granular fuel bed of this study was more irregular than what can be expected for non-granular fuel beds. If the spread of smoldering had been symmetric, the trends with sample height of Fig. 4.2 and 4.3 would have been similar. Also, the thermocouples located in the same height level would have reached a given temperature at the same time. This was not the case, indicating a more complex heat propagation during the external heating period than that of horizontal iso-temperature planes. The temperature difference between the warm heater below the initially cold fuel bed gave unstable air flows throughout the granular fuel bed. This can promote a more intense combustion in some locations compared to others. A

further study of the air flow patterns to and from the combustion zone would provide more insight into the mechanisms of upwards smoldering spread.

Transition from smoldering to flaming fire was observed in one case of the forward air flow mode in section 4.2 as well as in one case with cooling of the fuel bed, which will be presented in chapter 5. Both occurred during the most intense combustion period of an experiment. In the first case, flaming occurred at an early stage during smoldering, when the fuel bed consisted mainly of dried and heated original fuel. Forward air flow mode gives increased air flow to the reaction zone. This has previously been found to promote transition from smoldering to flaming in solid wood [65] and to promote a more intense combustion in pine needle fuel beds [66]. The second case occurred during a late stage of an experiment, at which time the fuel bed most likely consisted mainly of charred pellets. Char oxidation has previously been linked to transition to flaming in vertical fuel beds, for polyurethane [21] and cotton [23, 51]. Our study thereby provides examples to support the suggested links between transition to flaming and increased air flow as well as char oxidation. Interestingly, our fuel bed (100 mm) is lower than fuel beds in which transition to flaming has previously been observed. For polyurethane foam, Torero and Fernandez-Pello suggest that a minimum height of 250 mm was needed for transition to occur [21], while for cotton the minimum height used in experiments by Hagen et.al. was 150 mm [23, 51]. Mechanisms causing transition to flaming in granular fuel beds would benefit from further studies.

5. Extinguishing smoldering by cooling

In the previous chapter, susceptibility of smoldering initiation and burning to changes in input parameters was studied. This serves as a background reference for the extinguishment study presented in chapter. The same base set-up was used to study the potential of using cooling as a preventive or active extinguishing method. Extinguishment was obtained in one of the four studied cooling scenarios, see section 5.1. Differences in the combustion between scenarios were also found for non-extinguished cases, see section 5.2. Heat transfer calculations were used to evaluate the cause of extinguishment (section 5.3) and to evaluate the feasibility of upscaling to industrial scale (section 5.4). In addition to complete extinguishment, an exciting feature was the observation of pulsating temperatures. This gave rise to new research questions and new experiments. The pulsating phenomenon is explored in section 5.5. An overall discussion of the impact of cooling on smoldering is given in section 5.6.

5.1. Scenarios and results overview

Extinguishing self-sustained smoldering fires using heat extraction from the fuel bed with a cooling unit was the main goal of this part of the study. Four scenarios were studied, one background scenario without cooling and three scenarios with increasing level of cooling from A to B to C:

- Background: No cooling unit in fuel bed. 6 h heating.

- Scenario A (minimum cooling): Cooling unit in fuel bed, no water. 13 h heating.

- Scenario B (medium cooling): Cooling unit in fuel bed, water flow started halfway through the external heating period (at t = 6.5 h). 13 h heating.

- Scenario C (maximum cooling): Cooling unit in fuel bed, water flow started at the beginning of the experiment (at t = 0 h). 13 h heating.

An overview of the scenarios is given in Table 5.1. The choice of scenarios and heating duration was based on preliminary experiments. With no cooling unit in the fuel bed (Background scenario), self-sustained smoldering was obtained after 6 h heating. When the cooling unit was located in the fuel bed (even without water

Table 5.1.: Overview of the studied scenarios and results. The number of repetitions within each scenario is given. Set-up with (Y) and without (N) cooling unit is specified. Water in the cooling unit is given as hours after test start, or as (N) for no water. The number of experiments that did not extinguish, that did extinguish and that had no initiation of self-sustained smoldering is given. It is also indicated if pulsating temperatures were observed during the experiments (with/no pulses).

| Scenario | Experiments | | | Resulting outcome | | | |
	Repetitions	Cooling unit	Water start (h)	Non-extinguished no pulses	Non-extinguished with pulses	Extinguished with pulses	No self-sustained smoldering
Background	10	N	N	10/10	0/10	0/10	0/10
Scenario A	6	Y	N	3/6	3/6	0/6	0/6
Scenario B	6	Y	6.5	5/6	1/6*	0/6	0/6
Scenario C	15	Y	0	0/15	7/15**	7/15	1/15
Scenario C:3D	6	Y	0	1/6	2/6	2/6	1/6

* Pulses *after* the most intense combustion
** One experiment with transition to flaming

flow), the same heating duration did not result in self-sustained smoldering. This shows that the heat losses to the cooling unit affected the initiation of smoldering. To enable a study of extinguishment of self-sustained smoldering, the heating duration was increased to 13 h, which resulted in self-sustained smoldering.

Preliminary experiments also explored possible effects of starting the water flow after initiation of self-sustained smoldering, that is, after 13 h. The result was a combustion in which the temperature and mass loss appeared unaffected by the introduction of water flow. This indicated that the cooling effect from the cooling unit was too low to quench a fully developed smoldering fire. In the selected scenarios described in the list above and in Table 5.1, the water flow was therefore started at an earlier stage in the experiments. The Background scenario was included as a reference without cooling unit, and scenario A was included as a reference without water flow in the cooling unit (empty pipe, drained between experiments).

For scenario C, experiments were carried out both with the base set-up of thermocouples (shown in Fig. 3.2, Fig. 3.8a and 3.8b) and with additional thermocouples in the fuel bed (shown in Fig. 3.8c and 3.8d). The additional thermocouples were added to provide information of the 3D temperature profiles in the fuel bed (scenario denoted *Scenario C:3D* in Table 5.1). These results are given in section 5.5.2.

In total 43 experiments were performed in this part of the study. Extinguishment of self-sustained smoldering was observed in 7 of 15 cases for scenario C and never in the Background scenario or for scenarios A and B. Extinguishment was also observed in 2 of 6 cases in *Scenario C:3D*. In two cases, in scenario C and *Scenario C:3D*, there was no initiation of self-sustained smoldering, despite 13 h heating. Temperature profiles for these two cases are not displayed in section 5.2, as the fuel bed temperatures simply cooled down to ambient temperatures after the external heating was switched off.

In addition to extinguishment, an interesting phenomenon of pulsating temperatures was observed both in extinguished and non-extinguished cases. The pulsations were observed after the external heating was switched off, and before the most intense combustion occurred (with one exception), as given in Table 5.1. This phenomenon will be detailed in section 5.5.

5.2. Temperature and mass loss results

In this section, the temperature and mass loss data from extinguished experiments will first be presented (Fig. 5.1a), followed by temperature and mass loss data from experiments where extinguishment was not obtained (Fig. 5.1b). For the non-extinguished experiments, differences in data as a consequence of the impact of different cooling levels between scenarios will be highlighted.

Extinguished experiments:
Temperature and mass loss data for experiments where complete extinguishment was obtained is shown in Fig. 5.1a. Extinguishment was only obtained in scenario C. During the 13 h external heating period the temperatures in the sample increased and the fuel was dried. After the external heating was switched off, the sample temperatures decreased, followed by one or two temperature pulsations. This increase in sample temperatures with no external heating shows self-sustained smoldering, where heat producing processes exceeds heat losses. The temperatures of the pulses were around 200-400 °C, in the same range as for the same time period of the non-extinguished experiments (Fig. 5.1b). The mass loss rate of the first pulse was about 10 g/h, for the second pulse 20 g/h. After the pulsations, the fuel bed temperatures decreased to ambient, without any additional extinguishing measures.

Extinguishment was obtained at an early stage, with no intense combustion peaks at the same level as that observed in the non-extinguished (smoldering) experiments. This is evident when comparing extinguished experiments to non-extinguished experiments in the same scenario C. Peak temperatures were lower (397 ± 44 °C versus

(a) Extinguished

(b) Non-extinguished (smoldering)
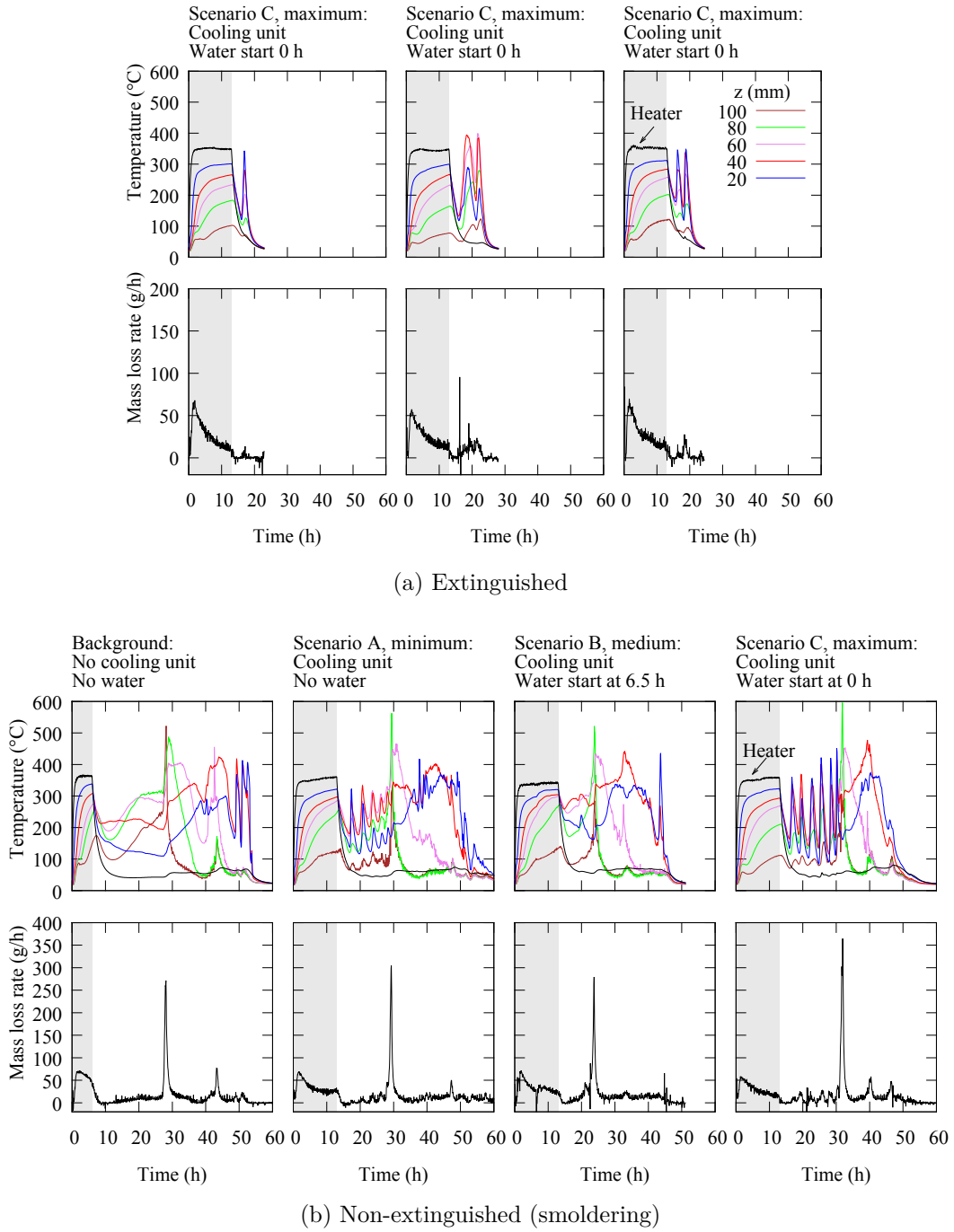
Figure 5.1.: Temperature and mass loss rate as functions of time. (a) Non-extinguished (smoldering) experiments. (b) Extinguished experiments. External heating is indicated by gray shading. The legend gives the vertical temperature measurement positions in the sample (20-100 mm). For clarity, only one temperature per height level is shown (L in Fig. 3.2). Mass loss rate is given as 5 min averages, notice the different y-scales. The figure is adapted with permission from Mikalsen et.al. [67].

599 ± 33 °C), as was mass loss rate peak (74 ± 13 g/h versus 302 ± 139 g/h) and mass loss rate average (16 ± 1 g/h versus 20 ± 1 g/h), see Fig. 5.1.

The early-stage extinguishment was also observed in the total mass loss of the extinguished experiments of ∼30 wt%, significantly lower than ∼86 wt% for non-extinguished experiments. The remaining fuel (70 wt%) after the extinguished experiments were distributed as ∼27 wt% non-charred and ∼43 wt% brown or charred pellets. This residue composition resembled the residue after experiments of 60 mm sample height presented in section 4.1 (details in Madsen et.al. [62]). The similarity reflect the high heat losses in both cases, to a large free surface to volume ratio in section 4.1, and to the cooling unit in this section.

Non-extinguished (smoldering) experiments:
Complete extinguishment was not obtained in any experiment of the Background scenario and scenarios A and B, nor in 7 of 15 cases in scenario C, see Table 5.1. In these non-extinguished experiments, the self-sustained smoldering continued till burn-out, as shown by temperature and mass loss data in Fig. 5.1b. The external heating duration was 6 h and 13 h, after which the heating unit was switched off. The self-sustained smoldering proceeded either with slow and steady temperature profiles (Background and scenario B in Fig. 5.1b), or with pulsating temperature profiles (scenarios A and C in Fig. 5.1b). Temperatures during this period were typically in the order of 200-400 °C. Following this period was the most intense combustion of the experiment, both in terms of peak temperatures (around 570-600 °C) and mass loss rates (around 200-400 g/h), significantly higher than the mass loss rate average (around 18-20 g/h). The first most intense combustion was followed by a new period of slow and steady temperatures. In most experiments, there was one or more temperature peaks towards the end also with elevated mass loss rates. Finally, the fuel bed temperatures decreased to ambient. The total mass loss was around 86 wt%, and the residue after the experiments consisted of black, charred pellets and ash.

The impact of the cooling can be seen in the slower temperature increase in the fuel bed and lower mass loss rate during the external heating period of scenarios A-C (with cooling) compared to the Background scenario (without cooling), see Fig. 5.2a and Fig. 5.2b. The effect of water flow through the cooling unit can also be seen in scenario B, where both sample temperatures and mass loss rates were affected by the start of water flow at t = 6.5 h, see Fig. 5.2c.

The impact of different cooling levels in scenarios A-C on experimental results will be presented in the following paragraphs. In general, there were variations in the overall smoldering pattern between the repetitions within each scenario with the same initial parameters, evident by spread in both temperature and mass loss data. This reflects
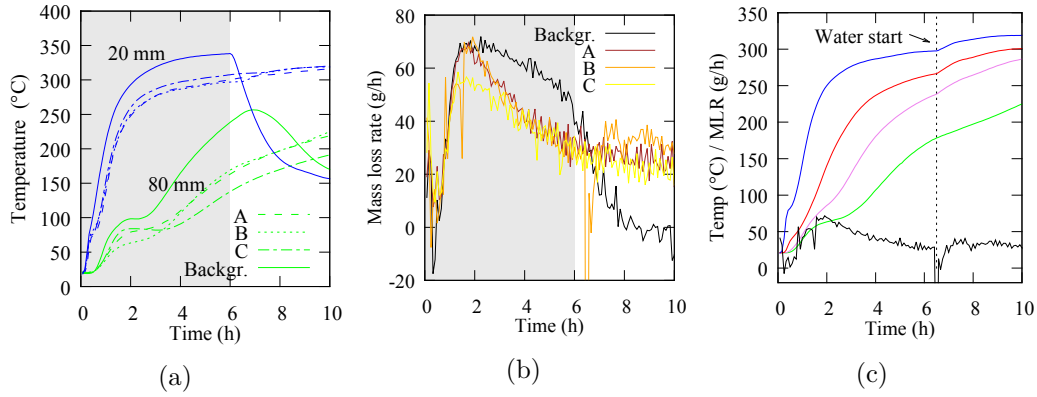
Figure 5.2.: Examples of the impact of cooling. (a) Temperature as functions of time at 20 mm and 80 mm height for one experiment of each scenario. (b) Mass loss rate as functions of time for one experiment of each scenario. (c) Temperatures (legend given in Fig. 5.1a) and mass loss rate (black) as functions of time for scenario B, where water flow was started at 6.5 h. The full experiments are given in Fig. 5.1b. External heating for Background scenario was 6 h (indicated by gray shading), the others had 13 h heating.

the stochastic nature of smoldering fires. Comparison of data was evaluated using a two-tailed Mann-Whitney U test (see section 3.5) to determine significance.

There were no statistically significant differences in the maximum temperatures between scenarios. When increasing the cooling, peak temperatures were 580 ± 36 °C, 575 ± 37 °C and 599 ± 33 °C for scenarios A, B and C, respectively, as shown in Fig. 5.3a.

The time to reach the most intense combustion was 24 ± 10 h for scenario A, 23 ± 4 h for scenario B and 34 ± 6 h for scenario C, as shown in Fig. 5.3b. For scenario A, the large spread in the data reflects that in 3 of 6 experiments, the most intense combustion occurred directly after the heater was switched off. An example can be found in Mikalsen et.al. [68], similar to temperature profiles shown in Fig. 4.6b. For the remaining 3 of 6 experiments in scenario A, the intense smoldering occurred later (shown in Fig. 5.1b). Increasing the cooling, the early-stage intense combustion was only observed in 1 of 6 cases of scenario B and never in scenario C. There was a significant difference in the time to reach the most intense combustion between scenarios B and C, it could therefore be speculated that strong cooling could delay the intense combustion. Also, the smaller spread in the time to reach the most intense combustion for scenarios B and C, compared to scenario A, shows a higher predictability for scenarios with water flow through the cooling unit. Increased predictability is advantageous from a risk perspective, but it is worth noting that
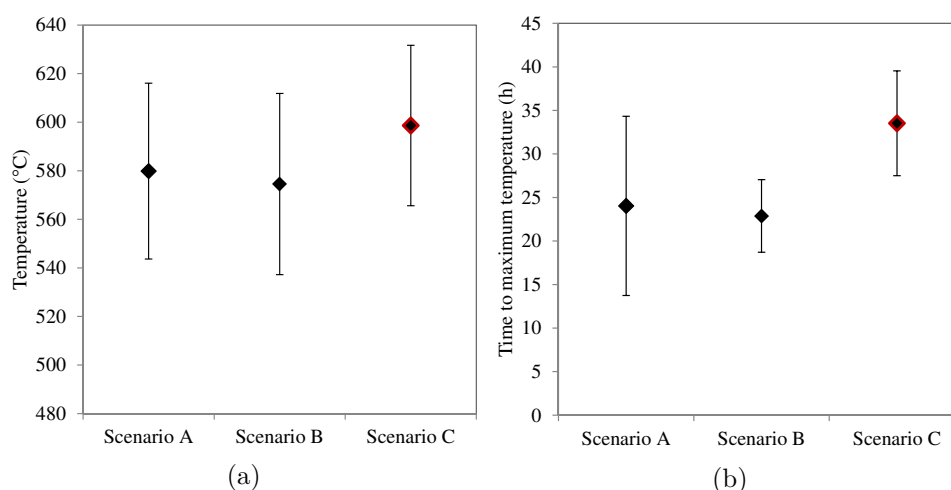
Figure 5.3.: Maximum temperature and time to reach maximum temperature for non-extinguished (smoldering) experiments in scenarios A-C, averages with standard deviations. Red marker indicates one experiment with transition to flaming in scenario C.

delaying the most intense combustion could cause fuel beds to be more prone to transition to flaming, as was observed in one experiment of scenario C.

5.3. Heat transfer calculations

The overall heat transfers to and from the system have been calculated, to identify the mechanisms causing experiments to smolder, pulsate and extinguish. The system considered is the insulated cylinder combined with the aluminum plate. Details on calculations with assumptions will be given in sections 5.3.1-5.3.3. Data from a representative experiment is presented. Distances used in the calculations are given in Fig. 5.4, nomenclature is explained only at first mention (an overview is provided in the list of symbols on page IV). These calculations are approximations of heat production and cooling power, based on measured data. Heat loss to the cooling unit is compared to the total heat losses and to the the heat production for the time period relevant for extinguishment in sections 5.3.5 and 5.3.6. Scalability to industrial scale is estimated presented in section 5.4.

5.3.1. Heat gain: Heat production, Heater input and Radiative input

In this section, the heat production and heat input to the system is presented. The sum of all these contributions is denoted as heat gain to the system.

Figure 5.4.: Distances used in heat transfer calculations. The lower part of the cylin-der (L_1, 0.1 m) contains sample, while the upper part (L_2, 0.23 m) does not. The cylinder opening is denoted as *c,o*. The shortest length from center to edge of aluminum plate is denoted as L_{alu} (0.14 m). The inner and outer radius of the steel cylinder is given as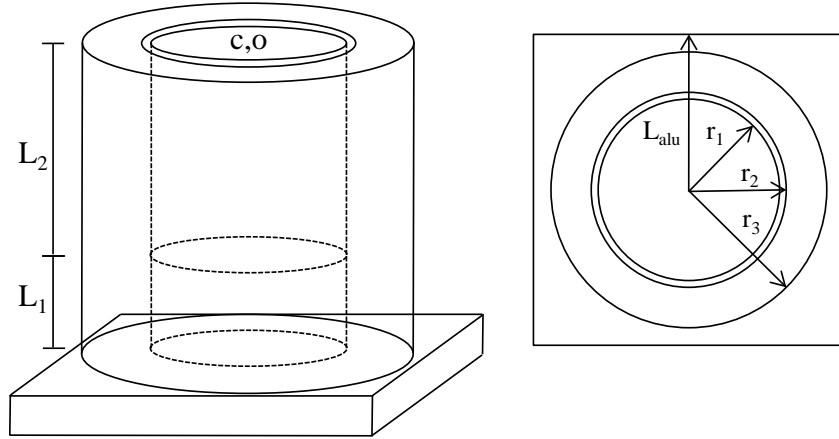 r_1 (0.075 m) and r_2 (0.076 m), the outer radius of steel cylinder with insulation as r_3 (0.136 m). The illustration is not to scale.

The **heat production** ($\dot{q}_{\mathrm{prod}}$) is given by Eq. 5.1.

$$\dot{q}_{\mathrm{prod}} = \dot{m}_{\mathrm{s}} \, H_{\mathrm{c}} \tag{5.1}$$

Here $\dot{m}_{\mathrm{s}}$ is the sample mass loss rate, H_{c} the effective heat of combustion for smol-dering of wood pellets (6 MJ/kg, see discussion below), which includes the factor χ commonly used to account for incomplete combustion [12]. The drying of the fuel is not separated from the heat production (all mass loss is assumed to be due to combustion), as the evaporation rate is unknown. Assuming that all drying occurred during the external heating period, using the heat of vaporization for water of 2500 kJ/kg, the vaporization of (1.25 kg · 6.3 wt%) 0.08 kg water requires about 4 W over 13 h heating. Compared to the heat input to the system during the external heating period of 860-2000 W (see section 5.3.1), this is negligible. Also, notice that the measured mass loss could have been affected by sudden water flow rate variations, which could have a recoil impact on the mass loss data, due to the added weight of the water.

The effective heat of combustion was set to 6 MJ/kg, but there is a large uncertainty attached to this value. Firstly, while the *net* and *gross* or *total* heat of combustion can be measured, the *effective* heat of combustion for smoldering is very uncertain. The few available reports include some spread in the data without apparent explanations for the spread [69,70]. The effective heat of combustion (H_{c}) for smoldering in various
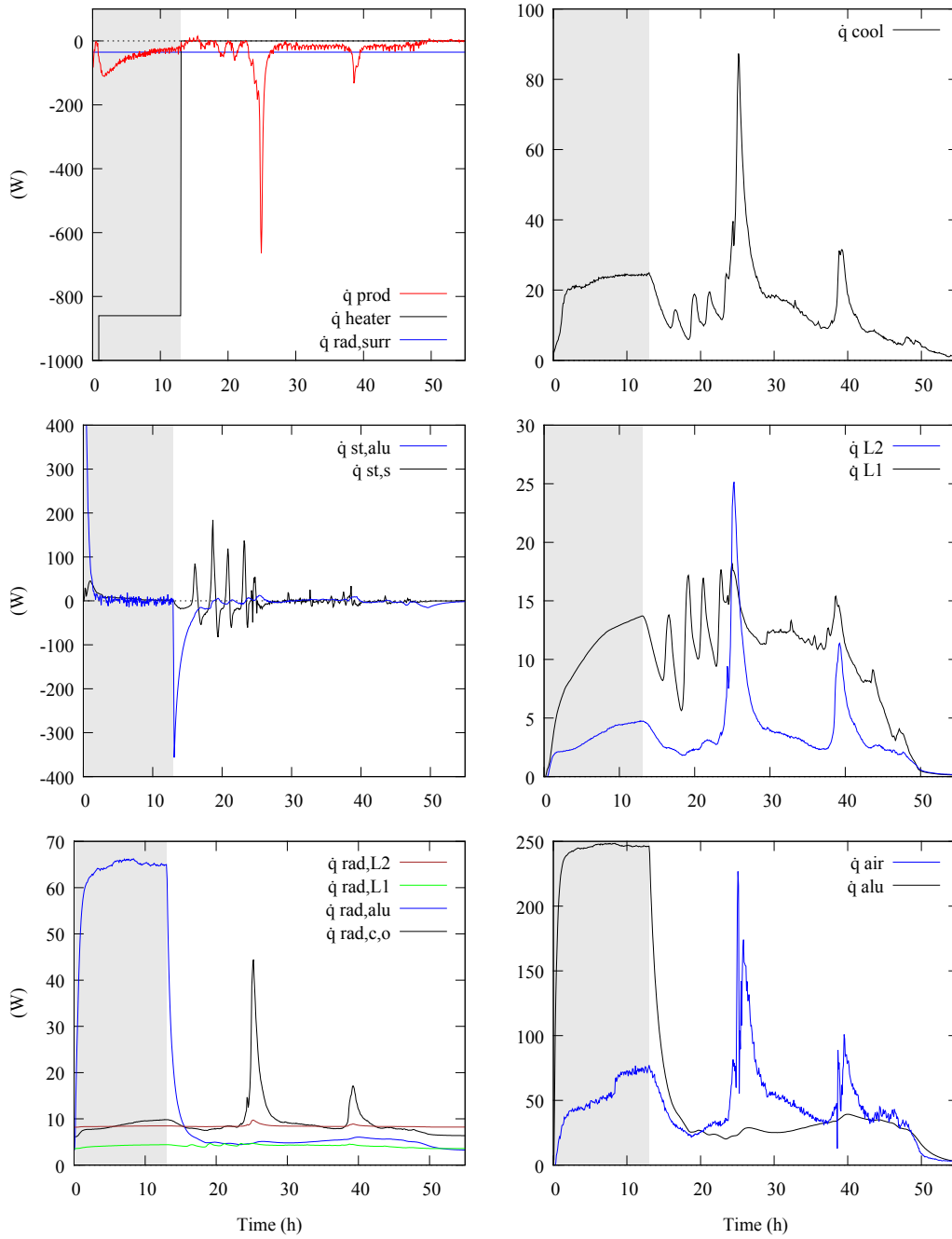
Figure 5.5.: Heat gain, heat storage and heat loss for a representative example experiment, details in sections 5.3.1-5.3.3. Notice the different y-axis scales. Net < 0 denotes heat gain, > 0 denotes heat loss. External heating is indicated by gray shading. The sum is given in Fig. 5.6.

materials is reported as 1-2 MJ/kg up to 12 MJ/kg, with increased forced air flow giving increased effective heat of combustion [1,17,71,72]. The lowest reported value for wood, 6 MJ/kg [1, 17], was chosen as the most representative for this study, as there was no forced air flow, only natural convection. Another important uncertainty is the composition of the fuel at the various stages of an experiment, changing from fresh fuel to dried, to partially or completely combusted. This causes its material properties to change as well. Despite this, the heat of combustion was kept constant as the exact composition at a given time in an experiment is not known. For the example in Fig. 5.5, the heat gain to the system from the heat production was in the range 0 to -680 W.

The **heater input** ($\dot{q}_{\text{heater}}$) is given by the power of the electric heating unit . During the 1 h ramping up to set-point temperature, it is assumed that the heater input is the maximum power of the electric heating unit, 2000 W. During the set-point temperature regulation period, the heater was on 43% of the time, giving 860 W heat input (heating procedure details in section 3.4). After the electric heating unit was switched off, the heater input is set to 0 W. The stepwise heater input is shown in Fig. 5.5.

This heater input assumes no heat losses. The consequence is that the estimated heat input is much higher than the heat losses during the external heating period, with a heating excess of about -600 W (see section 5.3.4). To identify possible origins of this heating excess, additional measurements were made of the surface temperature of the electric heating unit while it was switched on. The surface temperature was around 115-140 °C during the external heating period, corresponding to a maximum net radiative heat loss of about 50 W. This still does not account for the full heating excess. An alternative is to estimate the input power based on the temperature difference between the bottom and the top of the aluminum plate, instead of the given power of the electric heating unit. This was on average 5.5 K, corresponding to an average effect of 656 W for the entire external heating period, or 619 W for the period after the initial ramping. The challenge using these values is that the aluminum plate is defined as a part of the system, and this will therefore not reflect heat input *to* the system. In total, an adjustment of the estimated heater input from around 860 W to 619/656 W, combined with the additional 50 W radiative loss from the warm heater surface results in a maximum reduction in the heater input excess of around 150-200 W. The remaining observed excess could perhaps be linked to the internal thermostat in the electric heating unit, which was there to prevent overheating, though this could not be removed or monitored.

The **radiative heat input** from the surroundings ($\dot{q}_{\text{rad,surr}}$) is given by Eq. 5.2.

$$\dot{q}_{\text{rad,surr}} = \epsilon_{\text{surr}}\, \sigma\, (A_{\text{alu}} + A_{\text{c,o}} + A_{\text{L}_1} + A_{\text{L}_2})\, T_{\text{amb}}^4 \tag{5.2}$$

Here ϵ_{surr} is the emissivity of the surroundings (set to 0.9 [73,74]), σ the Boltzman constant, T_{amb} the ambient room temperature, A_{alu} the exposed area of the aluminum plate (0.074 m^2), $A_{\text{c,o}}$ the area of the cylinder opening (0.018 m^2), A_{L_1} the area of the lower part (L$_1$ in Fig. 5.4) of the insulated cylinder (0.085 m^2) and A_{L_2} the area of the upper part (L$_2$ in Fig. 5.4) of the insulated cylinder (0.20 m^2). For all experiments, a constant ambient temperature of 20 °C gave a constant radiative heat input to the system at -35 W.

5.3.2. Heat storage: Sample and Aluminum plate

In this section, heat storage in the system will be presented.

The **heat storage in the sample** ($\dot{q}_{\text{st,s}}$) is given by Eq. 5.3.

$$\dot{q}_{\text{st,s}} = \frac{T_{\text{s,t}_{i+1}} - T_{\text{s,t}_i}}{t_{i+1} - t_i}\, C_{\text{p,s}}\, m_{\text{s}} \tag{5.3}$$

Here $T_{\text{s,t}_i}$ is the average of all sample temperatures at time t_i, m_{s} the mass of the sample at time t_i and $C_{\text{p,s}}$ the specific heat capacity of the sample (1.8 J/gK). Reported values for $C_{\text{p,s}}$ for fresh wood, dry wood, wood pellets and wooden products are in the range 1.2-2.8 J/gK, lowest values for processed woods such as plywood, highest across the grain in whole wood [73,75,76]. The granular nature of whole wood pellets complicates direct measurement of $C_{\text{p,s}}$. In these calculations, the reported $C_{\text{p,s}}$ value of 1.8 J/gK [75] for dry spruce and pine wood was therefore used. This was kept constant as the exact composition of the fuel bed during an experiment is unknown.

The calculated heat storage in the sample was around 0 W for most of the experiment duration, reflecting the slow and steady temperature evolution during a smoldering fire. Large changes in fuel bed temperature lead to heat storage peaks, as can be seen in the pulsating period of the example experiment in Fig. 5.5, for t = 16-24 h. Instantaneous heat transfer within the bulk of the sample is assumed, although heating is a gradual process, with gradual heat diffusion into each pellet. For the example in Fig. 5.5, the heat storage in the sample was in the range -80 to 190 W.

The **heat storage in the aluminum plate** ($\dot{q}_{\text{st,alu}}$) is given by Eq. 5.4.

$$\dot{q}_{\mathrm{st,alu}} = \frac{T_{\mathrm{ualu,t_{i+1}}} - T_{\mathrm{ualu,t_i}}}{t_{i+1} - t_i} \, C_{\mathrm{p,alu}} \, m_{\mathrm{alu}} \tag{5.4}$$

Here $T_{\mathrm{ualu,t_i}}$ is the temperature in the center under the aluminum plate at time t_i, $C_{\mathrm{p,alu}}$ the specific heat capacity of aluminum (0.903 J/gK [73]) and m_{alu} the mass of the aluminum plate (5781 g). The largest changes in heat storage was when the aluminum plate rapidly heated up and cooled down, as a consequence of the heater below being switched on (t = 0) and switched off (t = 13 h). Later in an experiment, there was no abrupt change in the aluminum temperatures, leading to an approximate constant heat storage around 0 W. Instantaneous heat storage is assumed. For the example in Fig. 5.5, the heat storage in the aluminum plate was in the range -360 to 1300 W.

5.3.3. Heat loss: To cooling unit, Through insulated wall, Through aluminum plate, To air above sample and Radiative

In this section, heat losses from the system will be presented.

The **heat loss to the cooling unit** ($\dot{q}_{\mathrm{cool}}$) is given by Eq. 5.5.

$$\dot{q}_{\mathrm{cool}} = \dot{m}_{\mathrm{w}} \, \Delta T_{\mathrm{w}} \, C_{\mathrm{p,w}} \tag{5.5}$$

Here $\dot{m}_{\mathrm{w}}$ is the water flow rate, ΔT_{w} the temperature difference of the water entering and leaving the cooling unit (around 0.4 K) and $C_{\mathrm{p,w}}$ the specific heat capacity of water (4.18 J/gK [73]). The water cooling reduced the temperature of the sample, and also cooled the air above the sample, as the copper cooling unit was uninsulated. The cooling from the cooling unit peaked at the same time as the average temperature maximums in the sample. For the example in Fig. 5.5, the heat loss to the cooling unit was in the range 5 to 90 W.

The **heat losses through the insulated wall** of the cylinder are given by $\dot{q}_{\mathrm{L_1}}$ in Eq. 5.6 for the lower part of the cylinder, containing the sample (L_1 in Fig. 5.4), and by $\dot{q}_{\mathrm{L_2}}$ in Eq. 5.7 for the upper part of the cylinder containing air (L_2 in Fig. 5.4).

$$\dot{q}_{\mathrm{L_1}} = \frac{1}{\frac{ln(r_3/r_2)}{2\pi k_{\mathrm{ins}} L_1} + \frac{1}{h_{\mathrm{air}} 2\pi r_3 L_1}} (T_{\mathrm{s}} - T_{\mathrm{amb}}) \tag{5.6}$$

$$\dot{q}_{\mathrm{L_2}} = \frac{1}{\frac{1}{h_{\mathrm{air}} 2\pi r_1 L_2} + \frac{ln(r_3/r_2)}{2\pi k_{\mathrm{ins}} L_2} + \frac{1}{h_{\mathrm{air}} 2\pi r_3 L_2}} (T_{\mathrm{air}} - T_{\mathrm{amb}}) \tag{5.7}$$

Here k_{ins} is the thermal conductivity of the insulation (0.068 W/mK), h_{air} the convective heat transfer coefficient for air (10 W/m²K [77]), T_s the average sample temperature at measurement positions 20-100 mm, and T_{air} the average temperature of the air above the sample within the cylinder (measurement positions 120, 140, 330 mm in Fig. 3.2). The distances r_1, r_2, r_3, L_1, L_2 are given in Fig. 5.4. A constant insulation thermal conductivity for the given temperature range was used. The chosen heat transfer coefficient for air, 10 W/m²K, has been suggested by Holman [77] as an approximate value for free-convection problems.

The sum of thermal resistances are given in the denominators of Eq. 5.6 and Eq. 5.7. For the lower part of the cylinder (Eq. 5.6) the conductive resistance through the insulation and the convective resistance of the outer insulation/air interface were included. For the upper part of the cylinder (Eq. 5.7), the convective resistance of the air/steel interface inside the cylinder was also included. The conductive resistance through the steel cylinder was not included, as this was negligible ($< 0.1\%$ of the total thermal resistance). The thermal resistance of the sample/steel interface and the steel/insulation interfaces were not included, as these heat transfer coefficients are not known. It is thus assumed that the sample temperature equals the steel temperature at the contact point, and likewise for the contact point between steel and insulation. The consequence of omitting thermal resistances is that heat loss contribution from the walls could have been overestimated.

For the example in Fig. 5.5, the heat loss through the lower part of the cylinder wall ($\dot{q}_{\mathrm{L}_1}$) was in the range 0 to 20 W, the heat loss through the upper part of the cylinder wall ($\dot{q}_{\mathrm{L}_2}$) was in the range 0 to 25 W.

The **heat loss through the aluminum plate** ($\dot{q}_{\mathrm{alu}}$) is given by Eq. 5.8.

$$\dot{q}_{\mathrm{alu}} = \frac{1}{\frac{L_{\mathrm{alu}}}{k_{\mathrm{alu}} A_{\mathrm{alu}}} + \frac{1}{h_{\mathrm{air}} A_{\mathrm{alu}}}} \left(T_{\mathrm{ualu}} - T_{\mathrm{amb}} \right) \tag{5.8}$$

Here L_{alu} is the shortest distance from center to edge of the aluminum plate (see Fig. 5.4), k_{alu} the thermal conductivity of aluminum (237 W/mK [73]) and T_{ualu} the center temperature under the aluminum plate. T_{ualu} was measured by a thermocouple located in a slot in the center of the underside of the aluminum plate (see section 3.3). The thermocouple was not attached to the plate, but it is assumed that the measured temperatures represent the highest temperature of the aluminum plate. The dominant thermal resistance was the convective resistance of the air/aluminum interface, while the conductive resistance through the aluminum plate was small ($<$ 1% of the total). The thermal conductivity for aluminum was kept constant. The length and area of the aluminum plate assumes heat loss only from exposed surfaces

and through the shortest available distance. The heat loss through the aluminum plate was large, especially during the external heating period. This could have been avoided by insulating the aluminum plate. The aluminum plate was nevertheless kept uninsulated to enable a quick temperature decrease after the external heating was switched off. With insulation, the aluminum plate would have functioned as a thermal reservoir, which could have affected the smoldering.

For the example in Fig. 5.5, the heat loss through the aluminum plate was in the range 25 to 250 W.

The **heat loss to the air above the sample** ($\dot{q}_{\text{air}}$) is given by Eq. 5.9.

$$\dot{q}_{\text{air}} = C_{\text{p,air}} \, \dot{m}_{\text{air}} \, (T_{\text{c,o}} - T_{\text{amb}}) \tag{5.9}$$

$$\dot{m}_{\text{air}} = \frac{1}{2} \, A_{\text{c,o}} \, \rho_{\text{air}} \, \nu_{\text{air}} = \frac{1}{2} A_{\text{c,o}} \sqrt{2 \rho_{\text{air}} \Delta P_{\text{air}}} \tag{5.10}$$

$$\rho_{\text{air}} = \frac{P_{\text{amb}}}{R_{\text{gas}} T_{\text{c,o}}} \Rightarrow \frac{353}{T_{\text{c,o}}} \tag{5.11}$$

Here $C_{\text{p,air}}$ is the specific heat capacity of air (1.01 J/gK [73]), $\dot{m}_{\text{air}}$ the mass flow rate of air out of the cylinder and $T_{\text{c,o}}$ the air temperature in the opening of the cylinder (at measurement position 330 mm in Fig. 3.2). The mass flow rate of the air was estimated based on the Bernoulli equation as given in Eq. 5.10 [53, 78]. Here $\frac{1}{2} \, A_{\text{c,o}}$ is the area of the upwards air flow, ρ_{air} the density of air, ν_{air} the velocity of the air and ΔP_{air} the measured pressure difference across the bidirectional probe for the air flow. The density of air is temperature dependent as given in Eq. 5.11. Here P_{amb} is the ambient pressure in the room and R_{gas} the specific gas constant for dry air.

It is assumed that the area of the upward air draft equals the downward air draft, that is, half the cylinder opening. This presupposes that the density of the upwards and downwards air flow was equal, and that the bottom of the cylinder was air tight (although it was placed on a flat surface, it was not sealed). It is assumed that the Bernoulli equation is valid, although during the short periods with the most intense combustion, the smoke production could visually be seen to be turbulent. It is assumed that the properties of dry air (density and specific heat capacity) are valid also for smoke, due to low fuel combustion rate. The room pressure was not monitored, but assumed to be ambient (101325 Pa). It is assumed that the temperature measured in the cylinder opening is representative for the bidirectional probe position, despite the 10 mm vertical and about 20 mm horizontal distance between them, see Fig. 3.6. The bidirectional probe was mounted vertically, and it was assumed that the pressure difference caused by the vertical mounting of the bidirectional probe (lateral difference of measurement positions 7.3 mm) was

negligible compared to ΔP_{air}. This was verified with measurements. For the example in Fig. 5.5, the heat loss to the air above the sample was in the range 25 to 230 W.

The **radiative heat losses** from the cylinder opening ($\dot{q}_{rad,c,o}$), from the aluminum plate ($\dot{q}_{rad,alu}$), from the lower part of the cylinder ($\dot{q}_{rad,L_1}$) and from the upper part of the cylinder ($\dot{q}_{rad,L_2}$) are given respectively in Eq. 5.12-5.14.

$$\dot{q}_{\text{rad,c,o}} = \epsilon_{\text{c,o}} \, \sigma \, A_{\text{c,o}} \, T_{\text{air}}^4 \tag{5.12}$$

$$\dot{q}_{\text{rad,alu}} = \epsilon_{\text{alu}} \, \sigma \, A_{\text{alu}} \, T_{\text{ualu}}^4 \tag{5.13}$$

$$\dot{q}_{\text{rad,L}_1} = \epsilon_{\text{wall}} \, \sigma \, A_{\text{L}_1} \, T_{\text{surf,L}_1}^4 \tag{5.14}$$

$$\dot{q}_{\text{rad,L}_2} = \epsilon_{\text{wall}} \, \sigma \, A_{\text{L}_2} \, T_{\text{surf,L}_2}^4 \tag{5.15}$$

Here $\epsilon_{\text{c,o}}$ (0.9), ϵ_{alu} (0.1) and ϵ_{wall} (0.1) is the emissivity of respectively the cylinder opening, the aluminum plate and the outside of the insulated walls (the surface of which was clad with aluminum foil) [73, 74], and $T_{\text{surf,L}_1}$ and $T_{\text{surf,L}_2}$ the surface temperature of the lower and upper part of the outside of the insulated cylinder. The surface temperature of the outside of the insulated cylinder wall was not measured for all experiments, but estimated based on sample and air temperatures combined with thermal resistances. These estimations were validated by control measurements of wall surface temperatures, showing that the maximum difference between measured and estimated surface temperatures corresponds to an error up to 7 W during the external heating period and between 0-2 W after t = 13 h. The surface temperature of the aluminum plate sides was not measured, but assumed to be the same as T_{ualu}, due to the low thermal resistance of aluminum. For the example in Fig. 5.5, the radiative heat loss from the cylinder opening was in the range 5 to 45 W, from the aluminum plate 5 to 65 W, from the lower part of the cylinder around 5 W and from the upper part of the cylinder around 10 W.

5.3.4. Heat balance

The sum of heat gain, heat storage and heat loss gives the heat balance in the system, see Fig. 5.6. The calculations in the previous sections provide a rough estimation of the relative sizes of the different contributions. A non-zero heat balance shows that there are heat gains or heat losses that are not fully accounted for.

During the external heating period at t = 0-13 h (period **I** in Fig. 5.6), the heat balance was dominated by the heat input from the heater and heat losses through the aluminum plate. The net negative value around -600 W shows an underestimation
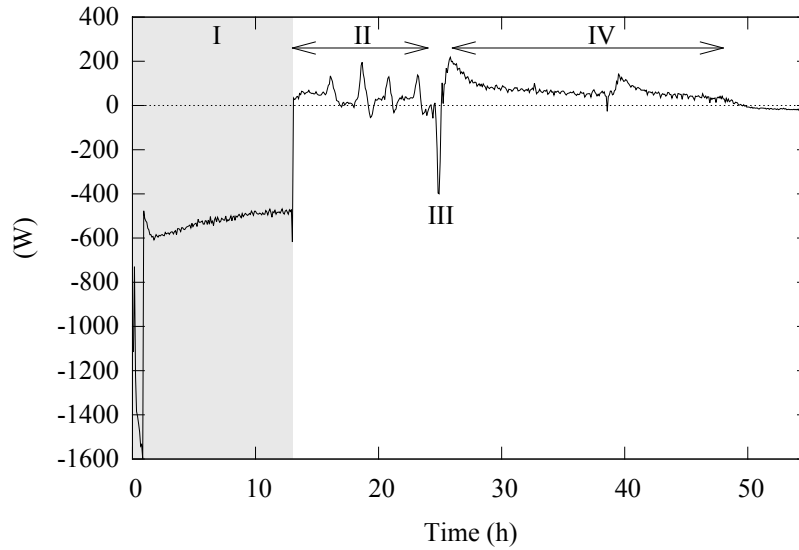
Figure 5.6.: Heat balance: the sum of all contributions shown in Fig. 5.5, detailed in sections 5.3.1-5.3.3. External heating is indicated by gray shading. Details on periods I-IV are presented in the main text.

of heat losses or an overestimation of the heat input. As explained in section 5.3.1 on page 51, only about 150-200 W of the heating excess could be identified.

After the heater was switched off at 13 h (period **II** in Fig. 5.6), the net heat balance oscillated around zero until around t = 24 h. During this period, there were pulsating temperatures in the example experiment shown here, and the dominating contribution to the heat balance was the heat storage in the sample (see section 5.3.2). This is a consequence of the large, synchronized temperature changes in the fuel bed during the pulsations.

During the most intense combustion of the experiment (period **III** in Fig. 5.6), the heat transfer balance was dominated by the heat production from the combustion of the sample. The net negative heat balance during this period indicate an underestimation of heat losses.

In the period after the most intense combustion (period **IV** in Fig. 5.6), the sum of all heat losses were larger than the heat production, with a net positive heat balance around +100 W. This could be due to the choice of using a constant heat of combustion throughout the experiments (as discussed in section 5.3.1 on page 49). Charred pellets have higher calorific values than fresh pellets. It can be assumed that the largest change in fuel composition (from mainly fresh to mainly charred pellets) coincided with the most intense combustion period (period **III** in Fig. 5.6). By consequence, if the chosen heat of combustion was correct at the beginning of

the experiment, it becomes increasingly underestimated as the fuel chars, with the most pronounced shift seen before and after the most intense combustion.

5.3.5. Cooling compared to sum of heat losses

In section 5.3.3, heat losses for the entire duration of an experiment were presented (see Fig. 5.5). In this section, the heat loss to the cooling unit will be compared to the sum of heat losses for the time period relevant for extinguishment. Since the external heating of the sample was the same for all experiments, the time period relevant for extinguishment is the period after the heater was switched off starting at t = 13 h, until complete extinguishment was obtained.

During this pre-extinguishment period, the relative sizes of the different contributions compared to the sum of all heat losses are shown in Fig. 5.7. The largest heat loss was the heat loss through the aluminum plate at ∼32%. The cooling effect from the cooling unit represented ∼18% of the total heat losses. The heat loss due to the buoyant smoke emission at the top of the sample was ∼17% and the thermal radiation heat losses from the system were in total ∼17%. The heat loss through the lower and upper part of the cylinder walls were respectively ∼14% and ∼3%.
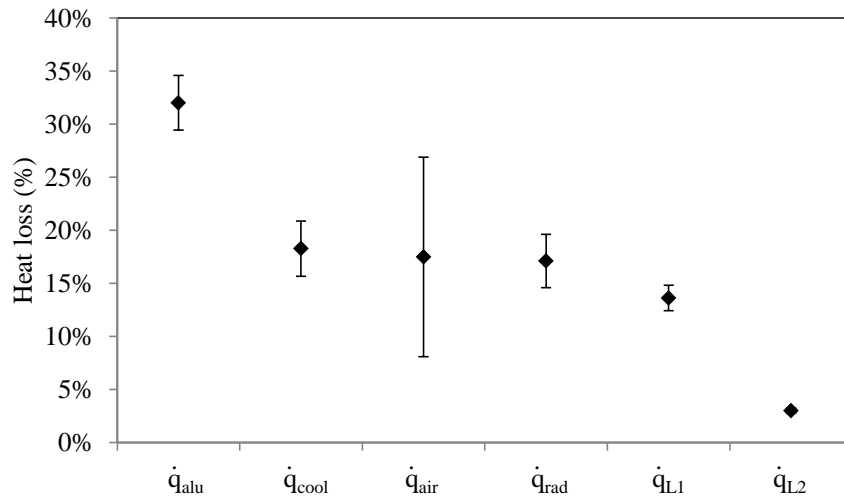

Figure 5.7.: Heat loss contributions (details in section 5.3.3), relative to the sum of heat losses for pre-extinguishment period. Averages with standard deviations.

The heat loss to the cooling unit was one of the major contributors to heat losses, but relatively low compared to the sum of heat losses.

5.3.6. Cooling compared to heat production

In this section, the heat loss to the cooling unit (Eq. 5.5) will be compared to the heat production (Eq. 5.1) for the time period relevant for extinguishment. Representative extinguished experiments and non-extinguished experiments in for the maximum cooling scenario C are given in Fig. 5.8. The time period given corresponds to the entire duration of the extinguished experiments, and the same time span is presented for the non-extinguished, even though these experiments lasted longer.

Extinguished, scenario C   Non-extinguished, scenario C
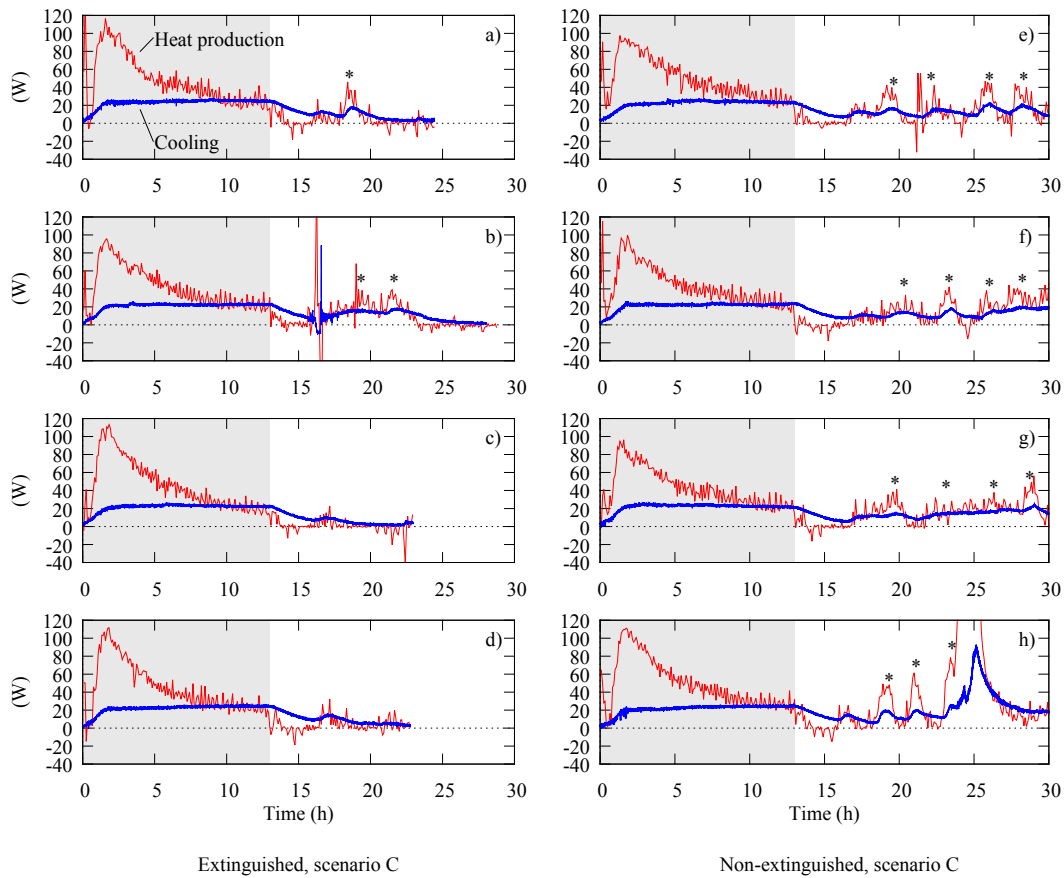
Figure 5.8.: The heat production (Eq. 5.1) and heat loss to the cooling unit (Eq. 5.5), for four extinguished experiments (a-d) and four non-extinguished experiments (e-h). Heat excess is indicated by asterisks (*). External heating is indicated by gray shading. The figure is adapted with permission from Mikalsen et.al. [67].

During this time period, the heat production was in the range 0-60 W, while the heat loss to the cooling unit was in the range 5-20 W. In Fig. 5.8, periods of heat excess are indicated by asterisks (*) as a visual guide for the reader. There were more periods of heat excess for the non-extinguished experiments, but the difference between heating and cooling for non-extinguished and extinguished cases was marginal. The choice of the effective heat of combustion in the calculations, discussed in section 5.3.1 on

page 49, could increase or decrease the difference between heat production and heat losses. A higher effective heat of combustion would "stretch" the heat production compared to the heat loss to the cooling unit in Fig. 5.8. This would result in higher heating excess in the non-extinguished cases compared to the extinguished cases, making it easier to distinguish between the two outcomes. A lower effective heat of combustion would mean a lower heat production compared to cooling unit heat loss, meaning that the heat excess in Fig. 5.8 is overestimated, and the cooling unit could in fact extract a larger share of the heat produced from the fuel bed.

Regardless of the exact choice for the effective heat of combustion, the resulting extinguishment in half the cases shows that the system is at a balance point between extinguishment and continued combustion. This balance point was only observed in scenario C, with the strongest cooling.

It could be speculated that small, random differences in the combustion could have been sufficient to flip the balance one way or the other. Variations in cooling due to variations in the water temperature or pressure (see example at 17 h in Fig. 5.8b) could also have influenced this balance point.

For scenarios A and B, there were no extinguished experiments. Pulsations *did* occur, in 3 of 6 experiments in scenario A, and in 1 of 6 experiments in scenario B. In the remaining experiments, smoldering with no pulsations was observed. This balance point between pulsations and normal smoldering shows that even moderate cooling could extract sufficient heat from the system to cause the emergence of pulsations, but never sufficient to cause extinguishment. Details on the pulsating phenomenon is presented in section 5.5.

5.4. Scalability and application

This section presents an estimation of the water flow needed to use cooling at an industrial scale for smoldering prevention.

A silo similar to a case study of a silo fire in Esbjerg, Denmark in 1998-99 [8] is used. Silo cell diameter 3 meters and height 85 meters were used, see Fig. 5.9. A centrally located cooling unit with diameter 0.2 m is used as an example. The cooling from the cooling unit ($\dot{q}_{\text{cool}}$) is given by Fourier's law in Eq 5.16.

$$\dot{q}_{\text{cool}} = 2\,\pi\,k_{\text{fuel}}\,h_{\text{silo}}\,\frac{T_{\text{fuel}} - T_{\text{water}}}{ln(r_{\text{I}}/r_{\text{II}})} \tag{5.16}$$
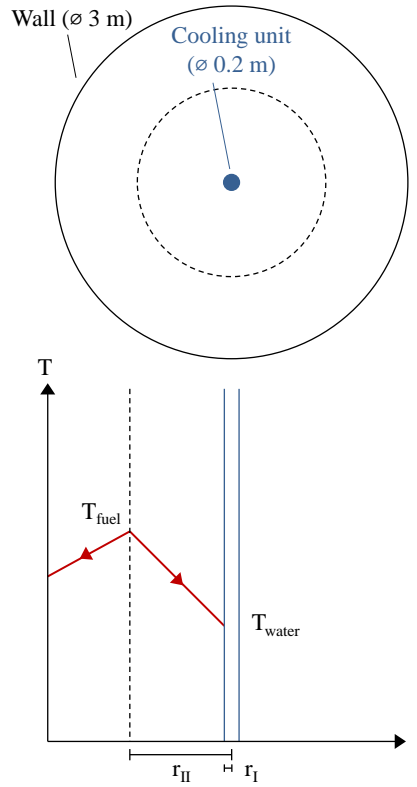
Figure 5.9.: Illustration of the cross section of 3 meter diameter example silo with a centrally positioned water-cooled pipe, top view (top). Temperature as function of radial distance (bottom). Dotted line represents the maximum fuel bed temperature. The figure is adapted with permission from Mikalsen et.al. [67].

Here, k_{fuel} is the thermal conductivity of the wood pellets (0.15 W/mK), h_{silo} the height of the silo (85 m), T_{fuel} the fuel bed temperature, T_{water} the water temperature, r_{I} the cooling pipe radius (0.1 m) and r_{II} half the silo radius (0.75 m). The thermal conductivity of our pellets was set to 0.15 W/mK, which was the lowest measured thermal conductivity for our grinded wood pellets, comparable to values found for similar and ungrounded wood pellets measured by Guo et al (0.146-0.192 W/mK) [79]. A given situation with constant temperatures in the fuel bed is studied. Stationary conditions with linear temperature decrease from the area with maximum temperature (dotted line in Fig. 5.9) to the cooling unit and heat transfer dominated by conduction is assumed.

With typical self-heating temperature of bulk storage of wood pellets [11, 79] of $T_{\text{fuel}} = 50°C$, and water temperature $T_{\text{water}} = 16 °C$ (as measured in this study), the required cooling is around 1300 W. The necessary water flow through a cooling unit would be around 800 g/s (50 L/min), based on eq 5.5, using the specific heat capacity of water and a typical water temperature difference measured in this study

61

(ΔT_w around 0.4 K). On the other hand, with a fuel bed temperature for self-sustained smoldering 400 °C (as measured in this study), the necessary water flow is around 9000 g/s (550 L/min).

5.5. Pulsating smoldering

The pulsating phenomenon observed in this study is new for smoldering combustion, in that, it occurs globally in the sample. Pulsating mode is maintained for long periods of time (up to 25 h). In sections 5.5.1-5.5.4, details on the observed phenomenon of pulsating smoldering will be presented, exploring the following research questions:

- Can the transition from pulsating mode to either extinguishment or intense combustion be predicted?

- Is this a global or local phenomenon?

- What are the propagation characteristics of the pulsations?

- What are the mechanisms causing pulsations?

5.5.1. Pulsation temperature and frequency

In experiments where pulsations were observed, these became apparent 2-3 h after the heater was switched off. Four example experiments with pulsating are shown in Fig. 5.10, displaying the temperature profiles in the sample during pulsations. During a pulse, temperatures across the sample increased in a synchronized manner, reaching maximum temperatures around 300-500 °C, the period of a single pulse was around 2-4 h. After reaching peak temperatures, the sample cooled down and remained at low temperatures (100-200 °C) for several hours. The lowest measured turnaround temperature was 94 °C, which can be seen after the first pulse in Fig. 5.10b. After the minimum point temperatures, the temperatures started to increase again, in concert.

For the extinguished experiments, there were one or two such pulses, before the temperatures in the fuel bed cooled down to ambient. For the experiments with multiple pulsations, between 4 (Fig. 5.10a) and 9 (Fig. 5.10d) consecutive pulsations were observed. The pulsating mode lasted up to 25 h.

After up to 9 consecutive pulsations, the system spontaneously transitioned from synchronized pulsations, to normal, disordered smoldering with intense combustion.
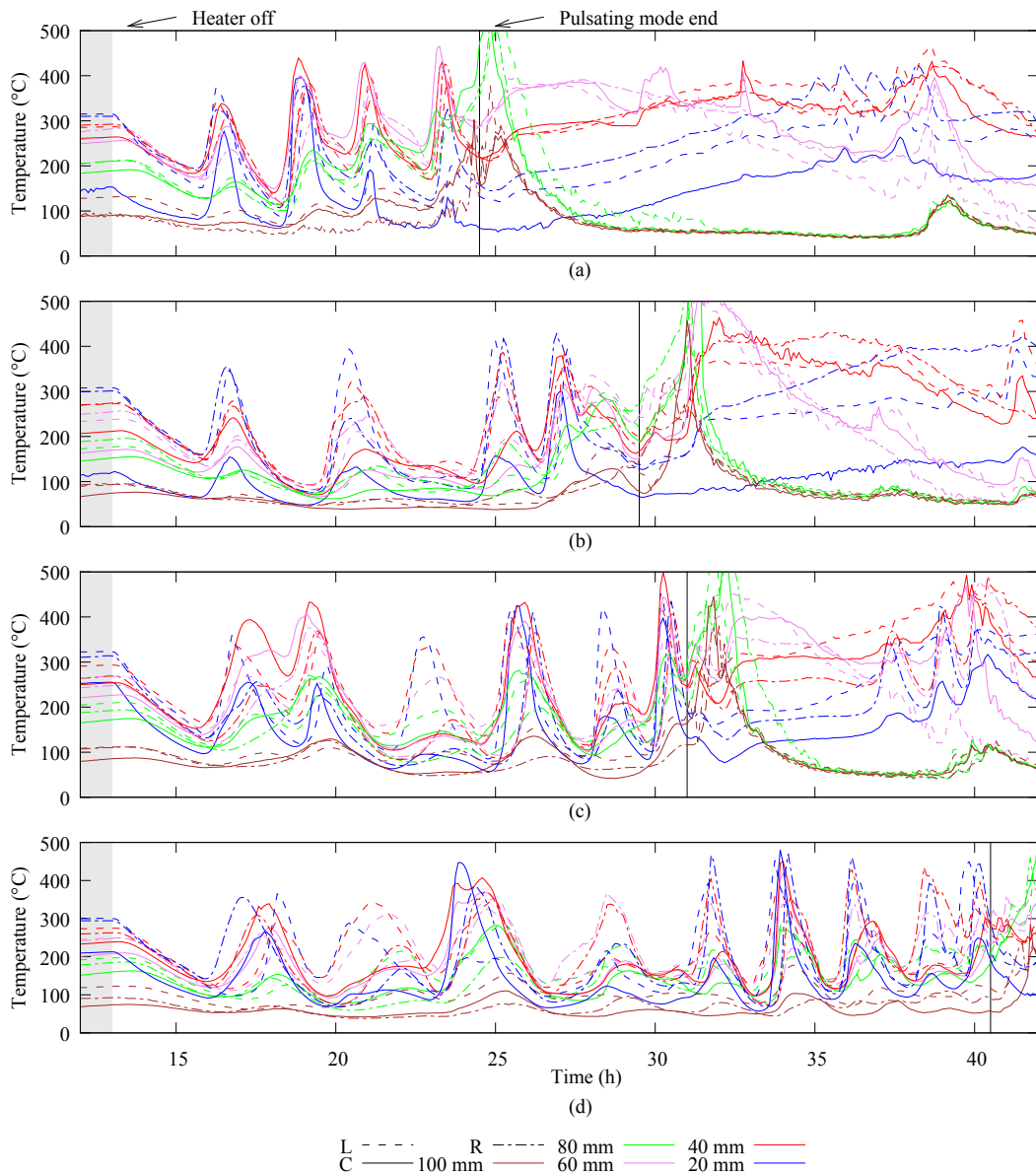
Figure 5.10.: Temperatures as functions of time for four experiments with pulsations. Full, vertical lines indicate the end of the pulsating period, after which there was normal, disordered smoldering. The legend (below bottom graph) gives the vertical temperature measurement positions in the sample (20-100 mm) and horizontal positions L, C and R (see Fig. 3.2). External heating is indicated by gray shading. The displayed the period is t = 12-42 h. The full experiment (c) is given under Scenario C in Fig. 5.1b.

The pulsations represent a low-intensity form of combustion compared with the most intense combustion during the experiments, with lower typical mass loss rates (25-45 g/h versus 140-600 g/h) and lower maximum temperatures (379 ± 55 °C versus 599 ± 33 °C).

The transition from pulsating mode to normal disordered combustion (breakdown of pulsating mode), could to some degree be predicted based on the temperature and frequency of the pulses. Linear regression showed that the temperature maximum and frequency of the pulses increased as the system approached disorder. The very last pulse before disorder of all experiments occurred at statistically significant higher temperatures and frequencies (413 ± 44 °C and 0.53 ± 0.2 pulses per hour) compared to the pulses followed by a new pulse (367 ± 55 °C and 0.34 ± 0.1 pulses per hour).

Notice that extinguishment could not be predicted in the same way, as the temperatures of the pulses before extinguishment was in the same range as the first pulsations of the non-extinguished cases, although often at the lower end. As there were only one or two pulsations before extinguishment, no significant increase in frequency could be found.

5.5.2. Global pulsations

Sample temperatures were measured by thermocouples located along a vertical plane near the sample center. It could therefore be speculated that the observed pulsations only occurred locally. There are three observations supporting global pulsations. Firstly, temperature measurements at different locations in the fuel all displayed temperatures pulsations at regular intervals.

Secondly, the measured mass loss was compared to the observed sample height reduction during pulsation. The sample height reduction during pulsations was less than 20 mm. At this point most of the sample was dried, and it is assumed that mass loss corresponds to volume decrease. If the measured mass loss during pulsations of about 200 g (initial mass was 1.25 kg) should result in a sample height reduction below 20 mm in the ⌀150 mm cylinder, a minimum of 40 vol% of the sample would have to be involved in the combustion. This estimation shows that a large share of the sample had to have been involved in the pulsating combustion.

Thirdly, experiments were also made with additional thermocouples located on a vertical plane perpendicular to the base set-up thermocouple plane. Information on 3D temperature profiles in the fuel bed was obtained. The thermocouple ladder configuration is shown in Fig. 3.8. All other conditions were kept the same as in scenario C. As given in Table 5.1, pulsations were observed also in these experiments. Both pulsations followed by non-extinguishment and followed by extinguishment were observed, similarly to in the basic scenario C. This supports the notion of global pulsations.

5.5.3. Pulsation propagation

For each pulse, a hot region initiated at a seemingly random position in the lower part of the sample and propagated through the fuel bed, as illustrated in Fig. 5.11. This was followed by a long period of low temperatures in the entire fuel bed, before a new hot region appeared.
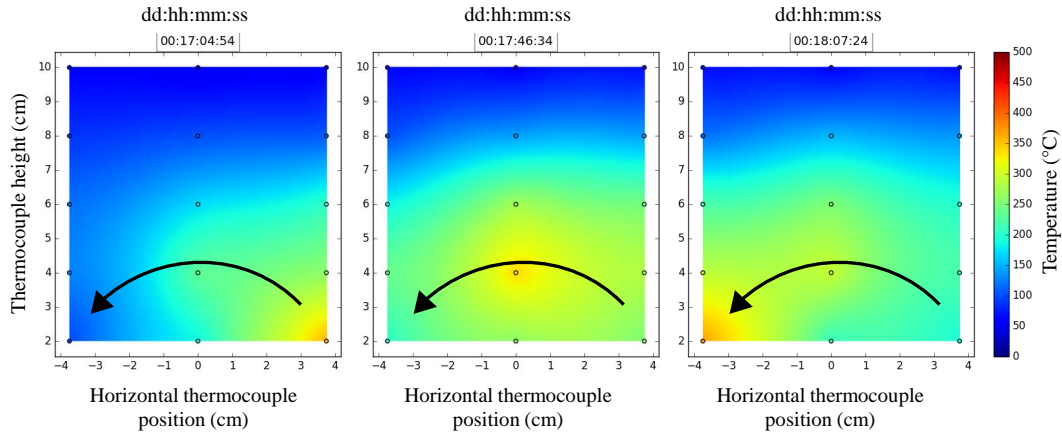

Figure 5.11.: Contour plot of temperatures along the vertical thermocouple plane near the sample center. Thermocouple positions are indicated by (o), linear interpolation between points. Extrapolation is not made to locations with no measurements, that is, below 20 mm or between the outmost thermocouples (at ± 3.75 cm) and the cylinder walls. This particular hot region traveled from the lower right corner, to the center, to the lower left corner, over a time period of around 1 h (shown in Fig. 5.12b at t = 17-18 h).

This is more clearly seen in the space-time plot of temperatures within the sample given in Fig. 5.12. A normal combustion case is provided for comparison in Fig. 5.12a, in addition to two experiments with pulsations followed by non-extinguishment (Fig. 5.12b,c) and one with pulsations followed by extinguishment (Fig. 5.12d).

For the normal combustion case, there were no comparable traveling hot regions, only slow and steady combustion where the warmest region remained near the surface. In the experiments with pulsations, the traveling speed of the hot regions was in the range 0.5-7.5 mm/min, median 2.1 mm/min. Interestingly, the propagation rate of the hot regions in our system resemble initial smoldering *fronts* moving through horizontal fuel beds with natural convection, which are typically in the range 0.1-45 mm/min, median 1.8 mm/min [1].
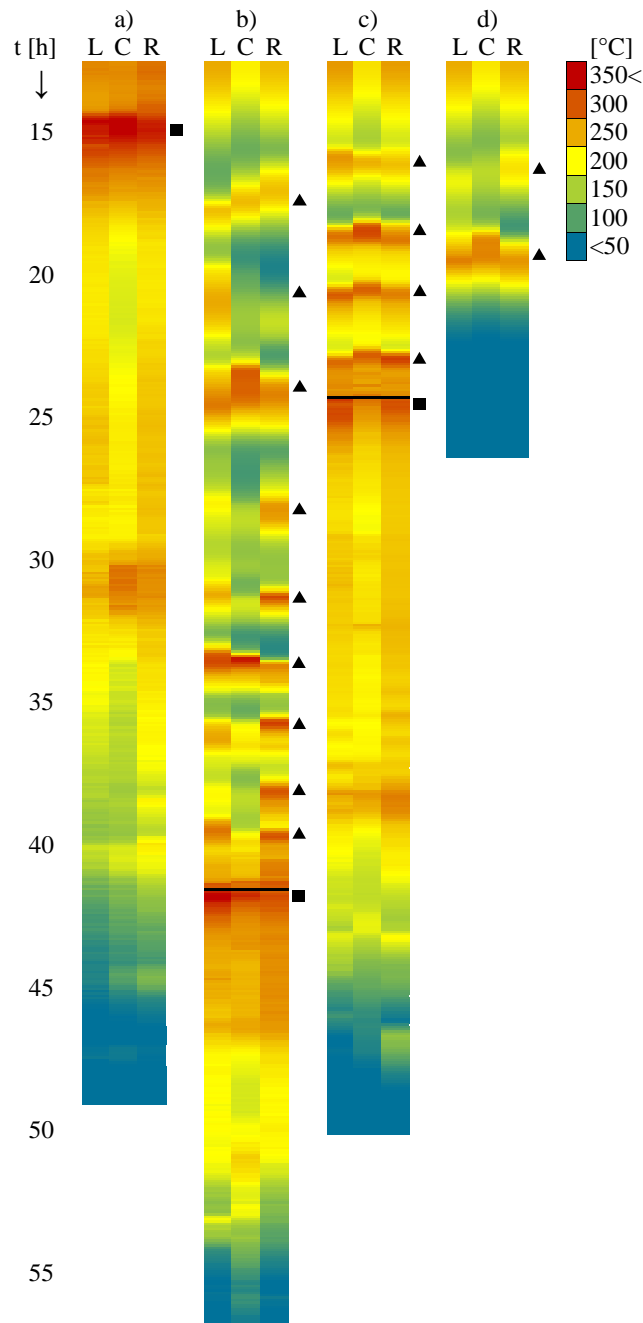
Figure 5.12.: Space-time plot, in which each time step gives the temperature averages (°C) over all vertical sample positions 20-100 mm above the heater for L (left), C (center), R (right) horizontal positions in the sample (see Fig. 3.2). The given time period is from the heater was switched off, till the end of the experiment. (a) Normal smoldering. (b and c) Pulsating smoldering. (d) Extinguished smoldering. Triangles indicate peak temperatures for each pulse. Black horizontal lines indicate transition from synchronized pulsating to disordered combustion, squares indicate maximum temperatures during intense disordered combustion.

5.5.4. Pulse peaks: adiabatic model

In this section, an adiabatic model is used to illustrate the effect of heat losses on the maximum point temperature turnaround. When there are no heat losses, the heat production in the sample ($\dot{q}_{\mathrm{prod}}$, Eq. 5.17) equals the heat storage in the sample ($\dot{q}_{\mathrm{st,s}}$, Eq. 5.18).

$$\dot{q}_{\mathrm{prod}} = H_{\mathrm{c}} \, m_{\mathrm{s}} \, A_A \, e^{-(E/R\,T_{\mathrm{s,t_i}})} \tag{5.17}$$

$$\dot{q}_{\mathrm{st,s}} = \frac{T_{\mathrm{s,t_{i+1}}} - T_{\mathrm{s,t_i}}}{t_{i+1} - t_i} \, C_{\mathrm{p,s}} \, m_{\mathrm{s}} \tag{5.18}$$

Here H_{c} is the heat of combustion (set to 6 MJ/kg, see discussion in section 5.3.1), m_{s} the mass of the sample, A_A the pre-exponential factor, E the measured activation energy (91.4 kJ/mol), R the gas constant, $T_{\mathrm{s,t_i}}$ the average sample temperature at time t_i and $C_{\mathrm{p,s}}$ the specific heat capacity of the sample.

Adiabatic temperature profiles as shown in Fig. 5.13 can be built using Eq. 5.17 and Eq. 5.18 recursively. The rapid increase for adiabatic conditions is a consequence of the non-linear heat production combined with the linear term of heat storage. The curves in Fig. 5.13 were found by adapting the unknown parameters A_A and $C_{\mathrm{p,s}}$ to the first half of the temperature increase of each pulse in the experimental temperature data. The best fit of the adiabatic temperatures was set to when the adiabatic temperatures during the temperature rise was close to, but not intersecting the average temperature. The best fit for a constant $C_{\mathrm{p,s}}$ of 1.8 J/gK resulted in A_A in the range 35-150 s^{-1}. The best fit for a constant A_A of $80s^{-1}$ resulted in $C_{\mathrm{p,s}}$ range of 1.0-4.5 J/gK (shown in Fig. 5.13). For comparison, literature values of wood, wooden products and wood pellets have been reported in the range 1.2-2.8 J/gK [73, 75, 79]. The spread in the adaption range and the variation in curve shape between pulses are not unreasonable, considering the complex nature of smoldering.

The assumption of adiabatic conditions is acceptable as long as the measured temperatures are similar to the calculated adiabatic temperatures. After about 75% of the temperature rise of each pulse, the heat losses in the experimental results started to become prominent, as indicated by arrows in Fig. 5.13. At this point, the adiabatic temperatures were 15% higher than the measured sample temperatures. Here, the sum of heat losses were sufficiently prominent to cause the temperature rise to decrease. The maximum temperature of the pulse was thus reached.
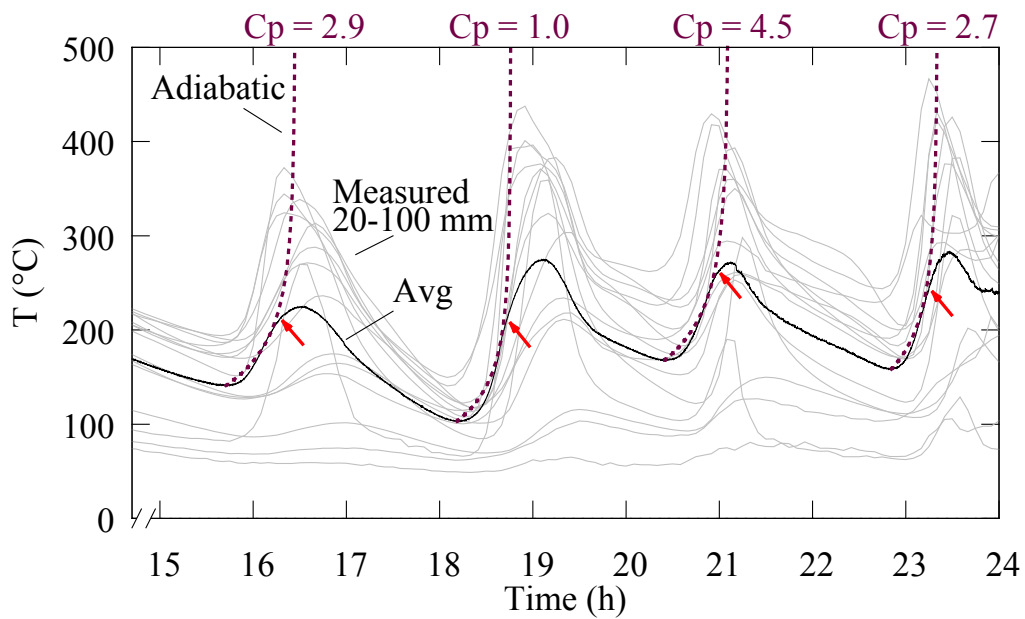
Figure 5.13.: Temperatures as functions of time, for the pulsating period of an example experiment. Measured sample temperatures (gray). Calculated adiabatic temperatures (dotted lines) are adapted to the average of sample temperatures (black) by varying A_A and C_p. Here, $A_A = 80$ s^{-1}, C_p is in the range 1.0-4.5 J/gK. Red arrows indicate the time when measured temperatures deviate from adiabatic by more than 15%. The figure is reused with permission from Mikalsen et.al. [80].

5.6. Discussion: Extinguishing smoldering by cooling

The results presented in this chapter are of interest both for fundamental understanding of smoldering and from an applied industrial point of view.

Small-scale proof-of-concept:
A proof-of-concept for cooling as an extinguishing method for self-sustained smoldering is provided. Firstly, it was shown that the heat losses to the cooling unit could prevent initiation of self-sustained smoldering, with significantly longer heating duration necessary to obtain smoldering. Second, when a longer heating duration was used and self-sustained smoldering was initiated, cooling could result in complete extinguishment.

Cause of extinguishment:
Extinguishment was obtained in 7 of 15 cases in scenario C. Even though the cooling did not represent the largest heat loss from the system (see section 5.3.5), the cooling unit must have caused extinguishment. The centrally located cooling unit was the only physical difference between the experiments with and without pulsations and extinguishment.

To identify how this relatively moderate heat loss could have caused extinguishment, the heat loss to the cooling unit was compared to the heat production from the combustion (section 5.3.6). The heat losses to the cooling unit was in the same range as the heat production in the sample. Within the same cooling scenario, there were only marginal differences in heating and cooling between extinguished and non-extinguished cases, indicating that the system was at a balance point between continued combustion and extinguishment.

Increased cooling - increased predictability:
For lower cooling levels (scenarios A and B), and with no cooling (Background scenario), extinguishment was never obtained. For the experiments that were not extinguished, the results indicate that increased cooling could still have an effect, with increased predictability and delayed intense combustion (see section 5.2). This can be advantageous from a risk perspective, as the delay could provide more time for alternative extinguishing efforts to be implemented.

The increased cooling from scenario A to B to C could have been expected to impact maximum temperatures in the fuel bed. In previous experiments with water mist extinguishment of smoldering dust beds, it was found that the extinguishing efforts in fact increased the fuel bed temperatures [44]. In our study, however, there was no statistically significant increase in the maximum fuel bed temperatures when increasing the cooling level. This does not contradict the suggested mechanism by

Göransson and Husted [44] that elevated temperatures were caused by increased air flow to the fuel bed, not by the additional cooling.

Practical applications:
For practical applications, cooling could be feasible as a measure to prevent self-heating in industrial storage units. For prevention of low-temperature escalation, the estimated water flow for a silo with fuel bed temperatures of 50 °C was around 50 L/min, see section 5.4. This is well within what can be an expected water supply capacity at an industrial site. For fuel bed temperatures of 400 °C, the estimated water flow of 550 L/min is also feasible. From these estimations using stationary condition, water cooling could be feasible as a large-scale preventive measure. A prerequisite is that a temperature gradient in the fuel bed must be established sufficiently early to prevent escalation, as will be discussed below. For implementation, the mechanical robustness of the cooling unit should be considered, since central location in a storage unit will cause severe mechanical strain.

An advantage of cooling as a method is that there is no fuel-water contact. Several common challenges of extinguishment efforts using water in industrial storage units is thus avoided. Firstly, swelling of compacted fuels upon water contact does not occur. Another industrial extinguishment challenge is water run-off. In small-scale experiments it has been found that 1-6 liters of water is needed per kilogram fuel for complete extinguishment of coal and peat samples [42, 43]. With the continuous water flow through the cooling unit in our study, the required total water volume is not smaller than in these studies. However, the closed system allows for water recycling. Thus, at a large scale, unfortunate environmental consequences of water and foam run-off to nearby rivers and lakes can be avoided.

A third challenge of direct application of water in an industrial storage unit is channeling, in which the water finds the path of least flow resistance through the fuel bed [1, 42]. The consequence is that the water will not necessarily reach the combustion zone. Water channeling is avoided using the cooling unit presented in this study. However, a similar challenge arises, namely that the cooling unit is stationary, and combustion can occur in other locations. As was shown in sections 5.1 and 5.2, starting the water flow through the cooling unit at a late stage, when the self-sustained smoldering was well-established, did not result in extinguishment. This indicates that a temperature gradient in the fuel bed must be established sufficiently early to prevent escalation. A numerical study on a similar, closed water cooling system, showed that inserting a cooled pipe into an underground coal fire had a very limited spacial impact on the smoldering fire [47]. The cooling unit method is therefore suggested as best suited for smoldering fires with a limited horizontal extension, such as in silos.

Another potential application area is to prevent underground smoldering from propagating from one area to another, using multiple cooling units as a barrier, provided a limited spacial extent of the barrier area. As described in section 2.5, this is currently attempted in an effort to hinder smoldering from propagating into a nuclear waste site of a landfill in St.Louis, USA [39, 40]. These potential application areas for up-scaling, combined with the small-scale experimental proof-of-concept provided in this study, represent important steps towards safer storage of biomass prone to smoldering.

Pulsating fire phenomena:
The phenomenon of pulsating smoldering presented in section 5.5 will be discussed in the following paragraphs. Pulsating temperature profiles over large spatial extension are regularly observed in flaming fires. Pulsating temperatures in flaming fires can be an effect of fresh fuel supply to the combustion, for instance by delamination of timber walls [81,82]. It can also be an effect of poor ventilation to flaming combustion in a compartment fire [83,84]. Unlike flaming, smoldering is slow and persistent [1]. It was therefore not expected to see long-lived pulsating temperatures in smoldering. The pulsations represent a form of synchronized behavior in which the whole system displays the same behavior, like soldiers marching in step. This occurs despite the very random underlying process, as smoldering fires normally are unpredictable. The pulsations are therefore not only relevant for the fire and combustion fields, but also for the physics of network synchronization [85, 86].

Macroscopic pulsations:
Previous studies have observed pulsating phenomena *locally* at the smoldering fronts, with oscillating temperatures and propagation velocities [87–90]. The observed time and length scales of the pulsations in these studies were milliseconds and micrometers. Our reported pulsating temperatures occur across the entire sample volume (1.8 l, 1.25 kg), not merely at a front. Each pulse had a period of about 2-4 h, reaching temperatures around 300-500 °C. Pulsating mode was maintained for up to 25 h. The time and length scales were thus orders of magnitude larger than in previous studies.

Predictability of stochastic systems:
The observed variation in pulsating duration and in the temperature profiles of each pulse (see section 5.5.1), despite having the same initial experimental conditions, reflects the inherent stochastic component in the dynamics of smoldering fires. In wildfires as well as in domestic fires, this stochastic behavior is cause of concern, as flare-ups may occur a long time after ignition [1]. Re-ignition after extinguishment efforts is also a regular challenge, both at industrial scale [8] and laboratory scale [41,43]. This is pronounced in our pulsating temperature profiles, with cold periods

of several hours, and turnaround temperatures as low as 94 °C, which can be seen after the first pulse in Fig. 5.10b.

The temperature and frequency of the pulsations increased as the system approached transition to non-pulsating, normal combustion. This indicates increasing activity in the fuel bed with time. Previous studies have reported that transition from pulsating to non-pulsating mode is facilitated by high combustion temperatures and that the transition depends on a material specific stability criterion [87, 91]. Although dimensionality and geometry are different in our system, the link between the reported transition prerequisite of high combustion temperatures and our increased activity in the fuel bed towards transition (both pulse temperature and frequency) is interesting. An estimated stability criterion for our pulsating period was found to be in the same range as that reported in literature (details are given in Mikalsen et.al. [80]).

Mechanisms of pulsations:
The suggested mechanisms causing pulsations will now be discussed. The synchronized temperature profiles had a near-exponential heat production term dominating the temperature increase, with linear heat loss terms becoming increasingly prominent. As presented in section 5.5.4, after about 75% of the temperature rise of a pulse, the heat losses were sufficiently prominent to cause the temperature rise to decrease. The temperature peak of a pulse was thus reached.

The high heat losses could have been expected to cause complete extinguishment, but this was not the case, as is apparent from the observed repetitive pulsating temperature profiles. To understand this unexpected behavior, consider the temperature slopes before and after a peak in Fig. 5.13, which resembled relaxation oscillations (see e.g. [92]). The temperature slope leading up to a peak followed a near-exponential curve, while the declining temperature slope was less steep, as is expected for cooling [93].

At the minimum temperature point, the mechanism causing temperatures to increase again is most likely linked to sample collapse. During a temperature peak, mass loss of the sample also peaked. Each pellet consists of compacted wood dusts. As the dried pellets undergo mass loss, each pellet becomes brittle and will eventually not retain its structural integrity, and disintegrate. This can cause small, local collapses of each pellet. Also, bridge formations within the fuel bed were commonly observed, structurally aided by sticky tar pyrolysis products. Upon significant mass loss, small or large bridge formations could collapse. This combination of gradual subsidence of each pellet, and local collapses of bridge formations can cause delivery of unburnt fuel to reaction zones. Collapse has previously been observed to cause local temperature

turnaround of smoldering in peat fuel beds [94]. Compacting of the fuel bed can also result in more insulated reaction zones, which also promote combustion.

The long duration of the low temperature troughs indicate that the suggested mechanisms of gradual compacting not only promoted combustion. Local, gradual compacting can also reduce oxygen supply to the reaction zones, promoting extinguishment. The low temperatures of the troughs also cause lower reaction rates of the fuel and reduced air convection, both promoting extinguishment.

At a balance point:
Pulsations were never observed without cooling, and were increasingly common as cooling was increased. The pulsations were also observed in the experiments resulting in extinguishment, with one or two pulsating temperatures before complete extinguishment. The pulsation mode therefore represents a balance point between heat loss, oxygen supply and heat production. At this balance point, the system was not static, but there was an increasing activity in the fuel bed. Pulsating smoldering combustion is proposed to be an intermediate step between persistent, normal smoldering and extinguishment.

6. Conclusions and outlook

This is a study of smoldering combustion in granular biomass. The study explores the conditions leading to initiation of self-sustained smoldering and parameters affecting combustion pattern. Heat extraction from smoldering is also explored, aiming at extinguishment.

Initiation of smoldering in wood pellets was found to be susceptible to alterations in several parameters. The duration of the external heating was the factor that had the largest impact, more important than fuel bed temperature at the switch off time for the external heating (cut-off temperature). Sample height was also found to be important, especially for low sample heights, where the free surface to volume ratio was highest. Pellet type was found to be near significant, while changes in the height of the sample container did not change the air flow sufficiently to affect the initiation of smoldering.

Logistic regression was used to quantify the transition region from non-smoldering to smoldering, and to determine which parameters significantly affected initiation. This method is not commonly used in the fire science community today, but the method can be recommended for use in experimental fire studies with binary outcome.

It was found that a change in the air supply to the bottom of the fuel bed caused a large shift in the smoldering pattern. Forward air flow resulted in a distinctly more intense smoldering with higher maximum temperatures reached at an earlier stage, with shorter time till burn-out and higher total mass loss, compared to opposed air flow. This shows the importance of convection for heat transfers in this granular fuel bed.

Heat extraction from the fuel bed was found to have a large impact on smoldering. Extinguishment of self-sustained smoldering was obtained by cooling the sample with a cooling unit located in the sample center. Cooling the sample resulted in extinguishment in 7 of 15 cases where water cooling was started at the same time as the heating. During the period before extinguishment, the heat production was around 0-60 W and the heat loss to the cooling unit was around 5-20 W. Starting the water cooling at a later stage, or using only the cooling unit without water, never resulted in extinguishment. The overall smoldering pattern was still affected

by a changed cooling level, in that the combustion became increasingly steady and predictable as cooling was increased.

An interesting phenomenon of pulsating smoldering combustion was also discovered during the heat extraction study. The pulsations consisted of a near-exponential temperature build-up, until the heat losses became too large, causing the maximum-point turnaround. For all extinguished cases, there were one or two such pulsations before extinguishment. The mechanism causing the following minimum-point turnaround is proposed to be linked to local collapses of brittle fuel or bridges in the fuel bed, giving fresh fuel supply and more insulated reaction zones. This could hinder complete extinguishment in some cases, enabling the combustion to get a foothold and resume a temperature build-up. Up to 9 consecutive pulses were observed, maintaining pulsating mode up to 25 h, after which the system spontaneously transitioned to intense, normal disordered combustion. The peak temperatures and frequency of the pulsations increased as the system with time when approaching transition from pulsating mode to disordered combustion. The pulsations reflect the balance point to which the cooling is pushing the system. Pulsating smoldering is proposed as an intermediate step between normal smoldering and extinguishment.

Future research: For practical applications, this heat extraction study represents the first step towards using cooling for smoldering prevention industrially. Future research should therefore include up-scaling and a variation of cooling unit geometries. An up-scaling should be supported by numerical work to limit the total number of experiments needed in large scale. More experimental research on the fundamentals of smoldering in granular biomass would also be beneficial, including a study of pellets with a larger variation in material properties than that included in this study, or other types of granular biofuels. Also, studies of the air flow patterns to and from the combustion zone and of the fuel composition as smoldering progresses, would be beneficial for the understanding of upward smoldering spread. The pulsating smoldering mode would also be of interest for future research, it would be particularly interesting to investigate if this pulsating mode can be observed using other fuels or in different experimental set-ups, for instance in larger fuel beds, or for horizontal smoldering propagation. Building a numerical model that could display and predict pulsating temperatures in a smoldering fuel bed would also be beneficial for the fundamental understanding of smoldering combustion.

To summarize, this study provides an elegant demonstration of the susceptibility of smoldering fires in granular biomass to a variety of external influences. The study provides a proof-of-concept for cooling as an extinguishment method for self-sustained smoldering fires, which could be used both for the fundamental understanding of smoldering, but also for practical applications.

Bibliography

[1] G. Rein, Smoldering Combustion, in: M. J. Hurley et al (Ed.), SFPE Handbook of Fire Protection Engineering, 5th Edition, Vol. 1, Springer, New York, 2016, pp. 581–603, Chapter 19.
URL https://doi.org/10.1007/978-1-4939-2565-0_19

[2] M. Ahrens, Home Structure Fires, Tech. Rep. NFPA No. USS12G, National Fire Protection Association, Quincy, MA, USA (2016).

[3] J. R. Hall Jr., The Smoking-Material Fire Problem, Tech. Rep. NFPA No. USS10, National Fire Protection Association (NFPA). Fire Analysis and Research Division, Quincy, MA, USA (2013).

[4] C. Sesseng, K. Storesund, A. Steen-Hansen, Analysis of fatal fires in Norway in the 2005 – 2014 period, RISE-report A17 20176:2, RISE Fire Research, Trondheim, Norway (Oct. 2017).
URL http://urn.kb.se/resolve?urn=urn:nbn:se:ri:diva-33292

[5] G. Rein, Smouldering Fires and Natural Fuels, in: C. Belcher (Ed.), Fire Phenomena and the Earth System- An interdisciplinary Approach to Fire Science, John Wiley & Sons, Oxford, 2013, pp. 15–34, Chapter 2, iSBN 978-0-470-65748-5.
URL https://dx.doi.org/10.1002/9781118529539.ch2

[6] B. Poulter, N. L. Christensen, P. N. Halpin, Carbon emissions from a temperate peat fire and its relevance to interannual variability of trace atmospheric greenhouse gases, Journal of Geophysical Research: Atmospheres 111 (D06301) (2006) D06301. doi:10.1029/2005JD006455.

[7] W. Stelte, A. R. Sanadi, L. Shang, J. K. Holm, J. Ahrenfeldt, U. B. Henriksen, Recent developments in biomass pelletization–A review, BioResources 7 (3) (2012) 4451–4490. doi:10.15376/biores.7.3.4451-4490.

[8] U. Krause, Fires in silos: hazards, prevention, and fire fighting, John Wiley & Sons, Germany, 2009, iSBN 978-3-527-31467-6.
URL https://doi.org/10.1002/9783527623822

[9] T. Ohlemiller, Modeling of smoldering combustion propagation, Progress in Energy and Combustion Science 11 (4) (1985) 277–310. doi:10.1016/0360-1285(85)90004-8.
URL http://www.scopus.com/inward/record.url?eid=2-s2.0-0022182332&partnerID=40&md5=3469a43114f004e9e6ea3dac3494b1bb

[10] V. Babrauskas, Information on specific materials and devices, in: Ignition handbook: principles and applications to fire safety engineering, fire investigation, risk management and forensic science, Fire Science Publishers, Issaquah, WA, 2003, pp. 675–1021, Chapter 14, iSBN 0-9728111-3-3.

[11] I. Larsson, A. Lönnermark, P. Blomqvist, H. Persson, H. Bohlén, Development of a screening test based on isothermal calorimetry for determination of self-heating potential of biomass pellets, Fire and Materials 41 (8) (2017) 940–952. doi:10.1002/fam.2427.

[12] D. Drysdale, Fire Science and Combustion, in: An Introduction to Fire Dynamics, John Wiley & Sons, Ltd, Chichester, UK, 2011, pp. 1–34, Chapter 1, iSBN 978-1-119-97546-5.
URL http://dx.doi.org/10.1002/9781119975465.ch1

[13] Drysdale, Smouldering Combustion, in: An Introduction to Fire Dynamics, Third Edition, John Wiley & Sons Ltd, Chichester, UK, 2011, pp. 331–347, Chapter 8, iSBN 978-1-119-97546-5.
URL http://dx.doi.org/10.1002/9781119975465.ch8

[14] V. Babrauskas, Ignition of Common Solids, in: Ignition handbook: principles and applications to fire safety engineering, fire investigation, risk management and forensic science, Fire Science Publishers, Issaquah, WA, 2003, pp. 234–351, Chapter 7, iSBN 0-9728111-3-3.

[15] T. Ohlemiller, Cellulosic Insulation Material III. Effects of Heat Flow Geometry on Smolder Initiation, Combustion Science and Technology 26 (3-4) (1981) 89–105. doi:https://doi.org/10.1080/00102208108946950.

[16] B. C. Hagen, V. Frette, G. Kleppe, B. J. Arntzen, Onset of smoldering in cotton: Effects of density, Fire Safety Journal 46 (3) (2011) 73–80. doi:10.1016/j.firesaf.2010.09.001.

[17] T. Ohlemiller, W. Shaub, Products of Wood Smolder and Their Relation-to Wood-Burning Stoves, Tech. Rep. NBSIR 88-3767, US Department of Commerce, National Bureau of Standards, Gaithersburg, MD, USA (1988).
URL http://fire.nist.gov/bfrlpubs/fire88/PDF/f88017.pdf

[18] G. Rein, Smouldering combustion phenomena in science and technology, International Review of Chemical Engineering 1 (2009) 3–18.
URL http://www.era.lib.ed.ac.uk/handle/1842/1152

[19] T. Ohlemiller, D. Lucca, An experimental comparison of forward and reverse smolder propagation in permeable fuel beds, Combustion and Flame 54 (1-3) (1983) 131–147. doi:https://doi.org/10.1016/0010-2180(83)90027-5.

[20] K. Palmer, Smouldering combustion in dusts and fibrous materials, Combustion and Flame 1 (2) (1957) 129–154. doi:10.1016/0010-2180(57)90041-X.

[21] J. Torero, A. Fernandez-Pello, Natural convection smolder of polyurethane foam, upward propagation, Fire Safety Journal 24 (1) (1995) 35–52. doi:10.1016/0379-7112(94)00030-J.

[22] X. Huang, G. Rein, Downward and Upward Spread of Smoldering Peat Fire, 10th U.S. National Combustion Meeting, Organized by the Eastern States Section of the Combustion Institute, College Park, Maryland, 2017, pp. 1595–1600, iSBN 978-1-5108-4238-0.
URL http://toc.proceedings.com/34904webtoc.pdf

[23] B. C. Hagen, V. Frette, G. Kleppe, B. J. Arntzen, Transition from smoldering to flaming fire in short cotton samples with asymmetrical boundary conditions, Fire Safety Journal 71 (2015) 69–78. doi:10.1016/j.firesaf.2014.11.004.

[24] R. K. Eckhoff, Dust explosions in the process industries: identification, assessment and control of dust hazards, 3rd Edition, Gulf professional publishing, USA, 2003, iSBN 0-7506-7602-7.
URL https://doi.org/10.1016/b978-0-7506-7602-1.x5000-8

[25] U. Krause, M. Schmidt, Propagation of smouldering in dust deposits caused by glowing nests or embedded hot bodies., Journal of Loss Prevention in the Process Industries 13 (2000) 319–326. doi:10.1016/S0950-4230(99)00031-5.

[26] B. C. Hagen, V. Frette, G. Kleppe, B. J. Arntzen, Effects of heat flux scenarios on smoldering in cotton, Fire Safety Journal 61 (2013) 144–159. doi:10.1016/j.firesaf.2013.08.001.

[27] J. Koppejan, A. Lönnermark, H. Persson, I. Larsson, P. Blomquist, Health and Safety Aspects of Solid Biomass Storage, Transportation and Feeding, Tech. Rep. Task 40, IEA Bioenergy (May 2013).
URL http://urn.kb.se/resolve?urn=urn:nbn:se:ri:diva-5595

[28] M. A. Pauner, H. Bygbjerg, Spontaneous ignition in storage and production lines: Investigation on wood pellets and protein powders, Fire and Materials 31 (8) (2007) 477–494. `doi:10.1002/fam.945`.

[29] I. Larsson, P. Blomquist, A. Lönnermark, H. Persson, Medium-scale reference tests and calculations of spontaneous ignition in wood pellets - the LUBA project, Tech. Rep. SP Report 2012:50, SP Technical Research Institute of Sweden, iSBN 978-91-87017-68-1 (2012).
URL `http://urn.kb.se/resolve?urn=urn:nbn:se:ri:diva-5073`

[30] I. Larsson, A. Lönnermark, P. Blomqvist, H. Persson, Measurement of self-heating potential of biomass pellets with isothermal calorimetry, Fire and Materials 41 (8) (2017) 1007–1015. `doi:10.1002/fam.2441`.

[31] W. Guo, K. Trischuk, X. Bi, C. J. Lim, S. Sokhansanj, Measurements of wood pellets self-heating kinetic parameters using isothermal calorimetry, Biomass and Bioenergy 63 (2014) 1–9. `doi:10.1016/j.biombioe.2014.02.022`.

[32] C. Serrano, E. Monedero, M. Lapuerta, H. Portero, Effect of moisture content, particle size and pine addition on quality parameters of barley straw pellets, Fuel Processing Technology 92 (3) (2011) 699–706. `doi:10.1016/j.fuproc.2010.11.031`.

[33] H. Li, X. Liu, R. Legros, X. T. Bi, C. J. Lim, S. Sokhansanj, Pelletization of torrefied sawdust and properties of torrefied pellets, Applied Energy 93 (2012) 680–685. `doi:10.1016/j.apenergy.2012.01.002`.

[34] P. Russo, A. De Rosa, M. Mazzaro, Silo explosion from smoldering combustion: A case study, The Canadian Journal of Chemical Engineering 95 (9) (2017) 1721–1729. `doi:10.1002/cjce.22815`.

[35] The year and place of the incident is obtained from personal e-mail correspondence with author of the case study- Prof. P. Russo (Jan. 2018).

[36] D. Botnen, Hallingdal trepellets 5.juli 2010 (in Norwegian) (2010).
URL `https://rib.msb.se/Filer/pdf/26258.pdf`

[37] R. K. Eckhoff, Case Hisories, in: Dust explosions in the process industries, 3rd Edition, Gulf professional publishing, USA, 2003, pp. 157–198, Chapter 2, iSBN 0-7506-7602-7.

[38] R. A. Ogle, S. E. Dillon, M. Fecke, Explosion from a smoldering silo fire, Process Safety Progress 33 (1) (2014) 94–103. `doi:10.1002/prs.11628`.

[39] M. Koerth-Baker, How Do You Put Out A Subterranean Fire Beneath A Mountain Of Trash? (May 2016).
URL http://fivethirtyeight.com/features/how-do-you-put-out-a-subterranean-fire-in-a-mountain-of-trash

[40] T. Sperling, A. R. Abedini, Report on subsurface self sustaining exothermic reaction incident at Bridgeton Landfill, with a focus on causes, suppression actions taken and future liabilities, Tech. Rep. LFCI – PRJ14-010, Landfill Fire Control Inc. (LFCI), British Colombia, Canada (Sep. 2015).
URL http://dnr.mo.gov/env/swmp/facilities/docs/lfci_report_bridgetonlf.pdf

[41] M. Tuomisaari, D. Baroudi, R. Latva, Extinguishing smouldering fires in silos, Brandforsk project 745-961, Tech. Rep. VTT publication 339, Technical Research Centre of Finland, Finland (1998).
URL http://www.vtt.fi/inf/pdf/publications/1998/P339.pdf

[42] R. Hadden, G. Rein, Burning and Water Suppression of Smoldering Coal Fires in Small-Scale Laboratory Experiments, in: Coal and Peat Fires: A Global Perspective, Vol. 1, Elsevier, Amsterdam, Netherlands, 2011, pp. 317–326, Chap 18, iSBN 978-0-444-52858-2.
URL 10.1016/B978-0-444-52858-2.00017-7

[43] M. L. Ramadhan, P. Palamba, F. A. Imran, E. A. Kosasih, Y. S. Nugroho, Experimental study of the effect of water spray on the spread of smoldering in Indonesian peat fires, Fire Safety Journal 91 (2017) 671–679. doi:10.1016/j.firesaf.2017.04.012.

[44] U. Göransson, B. Husted, Can water mist be used to extinguish deep-seated cellulose fibre smouldering fires? Experiments and calculations., Vol. 1, Interscience Communications, Interflam, Royal Holloway College, University of London, 2007, pp. 359–364.
URL http://lup.lub.lu.se/record/764594

[45] J. Seow, Fire fighting foams with perfluorochemicals - environmental review, Tech. rep., Hemming Information Services, Department of Environment and Conservation Western Australia, Australia (2013).
URL http://www.hemmingfire.com/news/get_file.php3/id/287/file/Seow_WA-DEC_PFCs_Firefighting_Foam_final_version_7June2013.pdf

[46] C. A. Moody, J. A. Field, Perfluorinated surfactants and the environmental implications of their use in fire-fighting foams, Environmental science & technology 34 (18) (2000) 3864–3870. doi:10.1021/es991359u.

[47] H. Krause, Wuda-Kohleflöz, Numerische Modellierung der Brandausbreitung infolge Selbstentzündung ohne und mit Heatpipes. Unpublished report- access granted by Prof. U. Krause at OvG University Magdeburg (2010).

[48] NS 3165, biofuel, Cylindrical pellets of pure wood, classification and requirements (in Norwegian), standard Norge, Oslo (1999).

[49] SS 187120 Biofuels and peat, Fuel pellets, Classification (in Swedish), swedish Standards Institute, Stockholm (1998).

[50] M. Schmidt, C. Wanke, U. Krause, Determination of Measurement Uncertainties in Adiabatic Hot-Storage Experiments for Reactive Dusts, Chemical Engineering & Technology 36 (10) (2013) 1764–1772. `doi:10.1002/ceat.201300068`.

[51] B. C. Hagen, Onset of smoldering and transition to flaming fire, PhD thesis, Bergen University, Bergen (Apr. 2013).
URL `http://hdl.handle.net/1956/6993`

[52] J. Torero, A. Fernandez-Pello, M. Kitano, Opposed forced flow smoldering of polyurethane foam, Combustion Science and Technology 91 (1-3) (1993) 95–117. `doi:10.1080/00102209308907635`.

[53] B. McCaffrey, G. Heskestad, A robust bidirectional low-velocity probe for flame and fire application, Combustion and Flame 26 (1976) 125–127. `doi:10.1016/0010-2180(76)90062-6`.

[54] S. S. Shapiro, M. B. Wilk, An analysis of variance test for normality (complete samples), Biometrika 52 (3/4) (1965) 591–611. `doi:10.2307/2333709`.

[55] H. B. Mann, D. R. Whitney, On a test of whether one of two random variables is stochastically larger than the other, The annals of mathematical statistics 18 (1) (1947) 50–60. `doi:10.1214/aoms/1177730491`.

[56] Dell Inc, Dell Statistica (data analysis software system) (2016).
URL `software.dell.com`

[57] H. Akaike, A new look at the statistical model identification, IEEE transactions on automatic control 19 (6) (1974) 716–723. `doi:10.1109/TAC.1974.1100705`.

[58] G. Schwarz, Estimating the dimension of a model, The annals of statistics 6 (2) (1978) 461–464. `doi:10.1214/aos/1176344136`.

[59] A. Lönnermark, H. Persson, P. Blomquist, I. Larsson, M. Rahm, J. Sjöström, Small scale methods for assessments of risk for self-heating of biomass pellets, Tech. Rep. SP Report 2012:49, SP Sveriges Tekniska Forskningsinstitut, iSBN 978-91-87017-67-4 (2012).
URL http://urn.kb.se/resolve?urn=urn:nbn:se:ri:diva-5072

[60] ASTM E2021-15, Standard Test Method for Hot-Surface Ignition Temperature of Dust Layers, aSTM International, West Conshohocken, PA, USA, DOI: 10.1520/E2021-15 (2015).
URL http://www.astm.org/cgi-bin/resolver.cgi?E2021

[61] E. Villacorta, I. Haraldseid, R. F. Mikalsen, B. C. Hagen, S. Erland, G. Kleppe, U. Krause, V. Frette, Onset of self-sustained smoldering fire in wood pellets: An experimental study (manuscript).

[62] D. Madsen, C. Wanke, R. F. Mikalsen, I. Haraldseid, E. Villacorta, B. C. Hagen, U. Krause, G. Kleppe, V. Frette, B. Husted, Emerging Risks in Smoldering Fires: Initial Results from the EMRIS Project, Vol. 2, Interscience Communications, Interflam, Windsor, UK, 2016, pp. 1345–1356.
URL https://www.researchgate.net/publication/306078503

[63] V. R. Valdés, Experimental study of smouldering fires in wood pellets, Master's thesis, Norwegian University of Science and Technology, Trondheim, Norway (2017).
URL http://hdl.handle.net/11250/2454929

[64] V. R. Valdés, R. F. Mikalsen, I. S. Ertesvåg, A. Steen-Hansen, Experimental study of forward and opposed smouldering in wood pellets (submitted manuscript).

[65] T. J. Ohlemiller, Smouldering Combustion Propagation on Solid Wood, Elsevier Applied Science, Edinburgh, Scotland, 1991, pp. 331–347. doi:10.3801/IAFSS.FSS.3-565.

[66] J. P. Valdivieso, J. D. Rivera, Effect of Wind on Smoldering Combustion Limits of Moist Pine Needle Beds, Fire Technology 50 (6) (2014) 1589–1605. doi:10.1007/s10694-013-0357-2.

[67] R. F. Mikalsen, B. C. Hagen, A. Steen Hansen, U. Krause, V. Frette, Extinguishing smoldering fires in wood pellets with water cooling- an experimental study (manuscript).

[68] R. F. Mikalsen, B. C. Hagen, A. Steen-Hansen, V. Frette, Extinguishing smoldering fires in wood pellets through cooling, 5th Magdeburg Fire and Explosions Days 2017,Otto-von-Guericke-University, Magdeburg, Germany, 2017. doi:10.978.300/0562013.

[69] Personal e-mail correspondence with Dr. Vytenis Babrauskas (Oct. 2016).

[70] V. Babrauskas, Engineering guidance for smoldering fires, unpublished report, vytob@doctorfire.com.

[71] J. G. Quintiere, M. Birky, F. Macdonald, G. Smith, An analysis of smoldering fires in closed compartments and their hazard due to carbon monoxide, Fire and Materials 6 (3-4) (1982) 99–110. doi:10.1002/fam.810060302.

[72] H. Hotta, Y. Oka, O. Sugawa, Interaction between hot layer and updraft from a smoldering fire source, Part I An experimental approach, Fire Science and Technology 7 (2) (1987) 17–25. doi:10.3210/fst.7.2_17.

[73] F. P. Incropera, D. P. Dewit, T. L. Bergman, A. S. Lavine, Appendix A, in: Foundations of heat transfer, 6th Edition, John Wiley & Sons, Singapore, 2013, pp. 899–924, iSBN 978-0-470-64616-8.

[74] J. R. Howell, R. Siegel, M. P. Menguc, Thermal radiation heat transfer, 5th Edition, CRC press, USA, 2010, iSBN 1-4398-0533-6.

[75] V. Babrauskas, Tables, in: Ignition handbook: principles and applications to fire safety engineering, fire investigation, risk management and forensic science, Fire Science Publishers, Issaquah, WA, 2003, pp. 1076–1077, Chapter 15, iSBN 0-9728111-3-3.

[76] H. Zhou, Y. Q. Long, A. H. Meng, Q. H. Li, Y. G. Zhang, Classification of municipal solid waste components for thermal conversion in waste-to-energy research, Fuel 145 (2015) 151–157. doi:10.1016/j.fuel.2014.12.015.

[77] J. P. Holman, Chapter 7, in: Heat Transfer, 10th Edition, McGraw-Hill, New York, USA, 2010, iSBN 978-0-07-352936-3.

[78] B. C. Hogan, H. Bocanegra, R. C. Alarcon, N. Yilmaz, A. B. Donaldson, W. Gill, Examination of the Bi-Directional Velocity Probe Used in Flames, Vol. 2, American Society of Mechanical Engineers, Colorado, USA, 2009, pp. 49–56. doi:10.1115/FEDSM2009-78560.

[79] W. Guo, C. J. Lim, X. Bi, S. Sokhansanj, S. Melin, Determination of effective thermal conductivity and specific heat capacity of wood pellets, Fuel 103 (Supplement C) (2013) 347–355. doi:10.1016/j.fuel.2012.08.037.

[80] R. F. Mikalsen, B. C. Hagen, V. Frette, Synchronized smoldering combustion, EPL 121 (5) (2018) 50002,p1–p6. `doi:10.1209/0295-5075/121/50002`.

[81] R. M. Hadden, A. I. Bartlett, J. P. Hidalgo, S. Santamaria, F. Wiesner, L. A. Bisby, S. Deeny, B. Lane, Effects of exposed cross laminated timber on compartment fire dynamics, Fire Safety Journal 91 (Fire Safety Science: Proceedings of the 12th International Symposium, Supplement C) (2017) 480–489. `doi:10.1016/j.firesaf.2017.03.074`.

[82] A. I. Bartlett, R. M. Hadden, J. P. Hidalgo, S. Santamaria, F. Wiesner, L. A. Bisby, S. Deeny, B. Lane, Auto-extinction of engineered timber: Application to compartment fires with exposed timber surfaces, Fire Safety Journal 91 (Fire Safety Science: Proceedings of the 12th International Symposium, Supplement C) (2017) 407–413. `doi:10.1016/j.firesaf.2017.03.050`.

[83] O. Sugawa, K. Kawagoe, Y. Oka, I. Ogahara, Burning behavior in a poorly-ventilated compartment fire-ghosting fire, Fire Science and Technology 9 (2) (1989) 2_5–2_14. `doi:10.3210/fst.9.2_5`.

[84] K. I. Kim, H. Ohtani, Y. Uehara, Experimental study on oscillating behaviour in a small-scale compartment fire, Fire safety journal 20 (4) (1993) 377–384. `doi:10.1016/0379-7112(93)90056-V`.

[85] C. I. del Genio, J. Gómez-Gardeñes, I. Bonamassa, S. Boccaletti, Synchronization in networks with multiple interaction layers, Science Advances 2 (11) (2016) e1601679. `doi:10.1126/sciadv.1601679`.

[86] T. Nishikawa, A. E. Motter, Symmetric states requiring system asymmetry, Physical review letters 117 (11) (2016) 114101. `doi:10.1103/PhysRevLett.117.114101`.

[87] A. Mukasyan, A. Rogachev, Discrete reaction waves: Gasless combustion of solid powder mixtures, Progress in Energy and Combustion Science 34 (3) (2008) 377–416. `doi:10.1016/j.pecs.2007.09.002`.

[88] S. Hwang, A. Mukasyan, A. Rogachev, A. Varma, Combustion wave microstructure in gas-solid reaction systems: experiments and theory, Combustion science and technology 123 (1-6) (1997) 165–184. `doi:10.1080/00102209708935626`.

[89] A. S. Mukasyan, A. S. Rogachev, A. Varma, Mechanisms of pulsating combustion during synthesis of advanced materials, AIChE journal, Materials, interfaces and electrochemical phenomena 45 (12) (1999) 2580–2585. `doi:10.1002/aic.690451214`.

[90] B. Matkowsky, G. Sivashinsky, Propagation of a pulsating reaction front in solid fuel combustion, SIAM Journal on Applied Mathematics 35 (3) (1978) 465–478. `doi:10.1137/0135038`.

[91] K. G. Shkadinskii, B. I. Khaikin, A. G. Merzhanov, Propagation of a pulsating exothermic reaction front in the condensed phase, Combustion, Explosion and Shock Waves 7 (1) (1971) 15–22. `doi:10.1007/BF00748907`.

[92] U. Rau, W. Clauss, A. Kittel, M. Lehr, M. Bayerbach, J. Parisi, J. Peinke, R. P. Huebener, Classification of spontaneous oscillations at the onset of avalanche breakdown in p-type germanium, Physical Review B 43 (3) (1991) 2255. `doi:10.1103/PhysRevB.43.2255`.

[93] D. Drysdale, Heat Transfer, in: An Introduction to Fire Dynamics, 3rd Edition, John Wiley & Sons, Chichester, UK, 2011, pp. 35–82, Chapter 2, iSBN 978-1-119-97546-5.
URL `http://dx.doi.org/10.1002/9781119975465.ch2`

[94] X. Huang, F. Restuccia, M. Gramola, G. Rein, Experimental study of the formation and collapse of an overhang in the lateral spread of smouldering peat fires, Combustion and Flame 168 (2016) 393–402. `doi:10.1016/j.combustflame.2016.01.017`.

A. Publications and conference contributions

A list of publications of parts of the dissertation is presented here, with manuscript status for unpublished papers.

Peer-reviewed papers:
Relevant for chapter 4:
Edmundo Villacorta, Ingunn Haraldseid, Ragni Fjellgaard Mikalsen, Bjarne Christian Hagen, Sveinung Erland, Gisle Kleppe, Ulrich Krause and Vidar Frette, Onset of self-sustained smoldering fire in wood pellets: An experimental study. (Manuscript draft)

Ingunn Haraldseid, Edmundo Villacorta, Ragni Fjellgaard Mikalsen, Bjarne Christian Hagen and Vidar Frette, Intensive combustion periods during smoldering: Scaling with sample size (Manuscript draft)

Virginia Rebaque-Valdés, Ivar S. Ertesvåg, Ragni Fjellgaard Mikalsen and Anne E. Steen-Hansen, Experimental study of forward and opposed smouldering in wood pellets (Submitted manuscript)

Relevant for chapter 5:
Ragni Fjellgaard Mikalsen, Bjarne Christian Hagen and Vidar Frette, Synchronized smoldering combustion, EPL 121 (5) (2018), 50002 p1-p6, doi: 10.1209/0295-5075/121/50002

Ragni Fjellgaard Mikalsen, Bjarne Christian Hagen, Anne Steen-Hansen, Ulrich Krause, Vidar Frette, Extinguishing smoldering fires in wood pellets with water cooling - an experimental study (Submitted manuscript)

Conference contributions:
Relevant for chapter 4:
Virginia Rebaque-Valdés, Ragni Fjellgaard Mikalsen and Anne Steen-Hansen, Smouldering fires in wood pellets: The effect of varying the airflow, presented at Nordic Fire & Safety Days, Copenhagen, 17-18 August 2017

Dan Madsen et.al, Emerging Risks in Smoldering Fires: Initial Results from the EMRIS Project, presented at 14th International Conference and Exhibition on Fire Science Interflam, Windsor, UK, 2016, vol 2, pp. 1345-1356

Relevant for chapter 5:

Ragni Fjellgaard Mikalsen et.al., Smoldering combustion- from pulsations to extinguishment, Poster, International Symposium on Fire Safety Science, 12-16 June 2017

Ragni Fjellgaard Mikalsen et.al., Extinguishing smoldering fires in wood pellets through cooling, presented at 5th Magdeburg Fire and Explosion Protection Days, Germany, 23-24 March 2017, ISBN 978-3-00-056201-3

B. Curriculum vitae

Personal data

Name	Ragni Fjellgaard Mikalsen
Date of birth	07.08.1987
Place of birth	Mo i Rana, Norway
Nationality	Norwegian

Professional background

2015 - present	PhD candidate, Otto von Guericke University Magdeburg, Germany
2013 - 2015	MSc at RISE Fire Research AS (formerly SP Fire Research, formerly SINTEF NBL), Trondheim, Norway

Education

2015 - present	PhD candidate, Otto von Guericke University Magdeburg, Germany
2011 - 2013	MSc, Dpt. of chemistry, Norwegian University of Science and Technology (NTNU), Trondheim, Norway
2012	Semester at Dpt. of materials, ETH Zürich
2008 - 2011	BSc, Dpt. of chemistry, NTNU
2007 - 2008	Swahili language, Dpt. of language and literature, NTNU
2003 - 2006	High School, Mo i Rana

Ragni Fjellgaard Mikalsen